FLOW INDUCED MORPHOLOGY OF POLYOLEFIN BLENDS

PATCHARAPOL SUPATHAM

A THESIS SUBMITTED IN PARTIAL FULFILLMENT
OF THE REQUIREMENTS FOR
THE DEGREE OF DOCTOR OF PHILOSOPHY
(POLYMER SCIENCE AND TECHNOLOGY)
FACULTY OF GRADUATE STUDIES
MAHIDOL UNIVERSITY
2004

ISBN 974-04-5053-9

FLOW INDUCED MORPHOLOGY OF POLYOLEFIN BLENDS

……
Mr. Patcharapol Supatham
Candidate

……
Assoc. Prof. Richard Venables, Ph.D
Major advisor

……
Assoc. Prof. Arunee Tabtiang, Ph.D.
Co-advisor

…….....
Miss Pasaree Laokijcharoen, Ph.D.
Co-advisor

……...
Assoc. Prof. Rassmidara Hoonsawat, Ph.D.
Dean.
Faculty of Graduate Studies

……
Assoc. Prof. Taweechai Amornsakchai, Ph.D.
Chair
Doctor of Programme
in Polymer Science and Technology

FLOW INDUCED MORPHOLOGY
OF POLYOLEFIN BLENDS

was submitted to the Faculty of Graduate Studies, Mahidol University for the degree of Doctor of Philosophy (Polymer Science and Technology)
on
July 19, 2004

……
Mr. Patcharapol Supatham
Candidate

……...
Assoc. Prof. Richard Venables, Ph.D
Chair

……
Assoc. Prof. Arunee Tabtiang, Ph.D.
Thesis Defence Committe

……...
Prof. James, N. Hay, Ph.D
Thesis Defence Committee

…….....
Miss Pasaree Laokijcharoen, Ph.D.
Thesis Defence Committee

……...
Assoc. Prof. Rassmidara Hoonsawat, Ph.D.
Dean
Faculty of Graduate Studies
Mahidol University

……
Prof. Prasert Sophon, Ph.D.
Dean
Faculty of Science
Mahidol University

ACKNOWLEDGEMENTS

First and foremost, I would like to express my most sincere thanks to my advisor, Dr. Richard A. Venables, and my co-advisor, Dr. Arunee Tabtiang, for their valuable guidance and helpful discussion throughout this research. I would like to thank my thesis committee members, Dr. Pasaree Laokijcharoen and Prof. James. N. Hay for their useful comments and suggestions.

Special words of thank go to Miss Phungphit Khompraphan, for DSC measurement, and the staff of the electron microscopy and cell biology laboratory at Mahidol University for the morphological characterisation. Thanks are due to Petroleum and Petrochemical College, Chulalongkorn University, in particular Mr. Bernd Jacob, for use of Collin extruder. I would also like to thank Mr. Frank Biddlestone at Birmingham University for his great assistance with the DSC, DMA and Minimat experiments.

Additionally, I would like to acknowledge the financial support of Young / New Scientist Development Scholarship, Faculty of Science Mahidol University and the Thailand Research Fund (TRF) through the Golden Jubilee Ph.D. Program (Grant No. PHD / 0179 / 2543)

My grateful thanks are also extended to all teachers, my friends Kittiporn, Noree, Benjamaporn, Bonloom, Pannee, Bootsara and other people, whose names are not mentioned here, for their help and kindness. My special thanks are also due to Arada Chaiyanurakkul and Jantagarn Guaysomboon, without whose kind words of support and encouragement, this would not have been possible. Finally, I would like to dedicate this thesis to my family and my parents for their constant inspiration, support, encouragement and all of the best things that always give to me.

Patcharapol Supatham

FLOW INDUCED MORPHOLOGY OF POLYOLEFIN BLENDS

PATCHARAPOL SUPATHAM 4136645 SCPO/D

Ph.D. (POLYMER SCIENCE AND TECHNOLOGY)

THESIS ADVISORS: RICHARD A. VENABLES, Ph.D. (POLYMER TECHNOLOGY), ARUNEE TABTIANG, Ph.D. (POLYMER TECHNOLOGY), PASAREE LAOKIJCHAROEN, Ph.D. (POLYMER ENGINEERING), JAMES N. HAY, Ph.D. (CHEMISTRY)

ABSTRACT

The effects of thermomechanical history upon the morphology evolution of selected polyolefin blends were investigated. A blend of polyethylene (PE) and an elastomeric poly(ethylene-co-1-octene) (EOC) resin, containing 7 mol% of octene and long chain branching, was phase separated in a melt under quiescent conditions. After melt flow, the blend had fine globular or interconnected phase morphologies that were interpreted as originating from the various stages of coarsening after liquid-liquid phase separation through spinodal decomposition. It was inferred that the miscibility of the blend was enhanced under melt flow. Upon cessation of flow, concurrent liquid-liquid and solid-liquid phase separation took place, resulting in the formation of an interpenetrating morphology. Processing history was found to have a marked effect upon the subsequent morphology formation, with higher processing temperatures leading to slower coarsening in subsequent operations.

The plane stress fracture toughness of extruded sheets of the PE / EOC blend samples showed that the presence of EOC did not affect the work of fracture, (energy needed to create a fracture), when crack propagation took place in the transverse direction of the extruded sheet, in comparison with pure PE. The branched copolymer increased the overall work of fracture for crack propagation in the machine direction due to an increase in the non-essential work of fracture, but had no significant effect upon the essential work of fracture. A blend of polyethylene (PE) and poly(ethylene-co-1-butene) (ECB) was also used to investigate the effect of the types of branched copolymer upon the fracture toughness of the PE / copolymer blend system. It was found that the PE / ECB blend system has a finer length-scale morphology, which is a consequence of a greater compatibility than the PE / EOC blend system; this results in enhanced plane stress fracture toughness in comparison with the EOC system.

KEY WORDS: POLYOLEFIN / MORPHOLOGY / FRACTURE TOUGHNESS / ORIENTATION / EXTRUSION

127 pp. ISBN 974-04-5053-9

โครงสร้างสัณฐานของพอลิออเลฟินส์ผสมที่เกิดจากการไหล
(FLOW INDUCED MORPHOLOGY OF POLYOLEFIN BLENDS)

พัชรพล ศุปธรรม 4136645 SCPO/D

ปร.ด. (วิทยาศาสตร์และเทคโนโลยีพอลิเมอร์)

คณะกรรมการควบคุมวิทยานิพนธ์: RICHARD A. VENABLES, Ph.D. (Polymer Technology), อรุณี ทับเที่ยง, Ph.D. (Polymer Technology),
ภาสรี เล้ากิจเจริญ, Ph.D. (Polymer Engineering), JAMES N. HAY, Ph.D. (Chemistry)

บทคัดย่อ

งานวิจัยนี้เป็นการศึกษาผลของความร้อนและงานกลที่มีต่อโครงสร้างสัณฐานที่เกิดขึ้นของพอลิออเลฟินส์ผสม โดยพอลิเมอร์ผสมที่ประกอบด้วยพอลิเอทธิลีนและพอลิเมอร์ร่วม เอทธิลีน-ออคทีน ซึ่งมีปริมาณ ออคทีนและสายโซ่ยาวอยู่ 7 mol% ได้แสดงลักษณะสองวัฏภาคภายใต้สภาวะปกติ และภายหลังจากสภาวะการไหลจะเกิดสัณฐานวัฏภาคที่มีลักษณะเป็นทรงกลมขนาดเล็ก หรือลักษณะเชื่อมต่อกัน ซึ่งแสดงให้เห็นว่าโครงสร้างสัณฐานที่เกิดขึ้นนี้เกิดผ่านกระบวนการ coarsening ภายหลังจากการเกิดหลังการเกิดการแยกวัฏภาคที่เกิดขึ้นในสภาวะของเหลวผ่านกระบวนการ spinodal decomposition จากการศึกษาดังกล่าวนี้ทำให้ทราบว่าความเข้ากันได้ของพอลิเมอร์ผสมได้เพิ่มขึ้นภายใต้สภาวะการไหล โดยที่เมื่อกระบวนการไหลหยุดลง กระบวนการเกิดการแยกวัฏภาคทั้งในสภาวะของเหลว และสภาวะของเหลวและของแข็งแยกจากกันนี้ เป็นผลให้เกิดโครงสร้างสัณฐานแบบ interpenetrating นอกจากนั้นจากการศึกษาพบว่ากระบวนการขึ้นรูปมีผลต่อโครงสร้างสัณฐานที่เกิดขึ้นด้วย โดยที่ยิ่งอุณหภูมิในการขึ้นรูปสูงขึ้นเป็นผลให้กระบวนการเกิด coarsening เกิดช้าลง

ความเหนียวที่เกิดจากการขาดของพอลิเมอร์ผสมของพอลิเอทธิลีน และพอลิเมอร์ร่วม เอทธิลีน-ออคทีนที่ขึ้นรูปแบบแผ่นนี้แสดงให้เห็นว่าพอลิเมอร์ร่วมไม่มีผลต่องานในการขาดเมื่อแนวในการขาดตั้งฉากกับแนวการขึ้นรูปของพอลิเมอร์ผสมนั้นเมื่อเทียบกับพอลิเอทธิลีน โดยพอลิเมอร์ร่วมจะมีผลให้งานรวมในการขาดในแนวเดียวกับการขึ้นรูปเพิ่มขึ้น เนื่องจากการเพิ่มขึ้นของงานที่ไม่จำเป็นในการขาด แต่ไม่มีผลสำคัญมากนักต่องานที่จำเป็นในการขาด นอกจากนี้ยังศึกษาถึงผลของชนิดพอลิเมอร์ร่วมที่มีผลต่อความเหนียว โดยในพอลิเมอร์ผสมที่ประกอบด้วยพอลิเอทธิลีน และพอลิเมอร์ร่วม เอทธิลีน-บิวทีน มีโครงสร้างสัณฐานที่เล็กกว่าเนื่องจากมีความเข้ากันได้มากกว่าพอลิเมอร์ร่วม เอทธิลีน-ออคทีน เป็นผลให้มีความเหนียวมากกว่าพอลิเมอร์ผสมของพอลิเอทธิลีน และพอลิเมอร์ร่วม เอทธิลีน-ออคทีน

127 หน้า. ISBN 974-04-5053-9

CONTENTS

CONTENTS (continued)

CONTENTS (continued)

CONTENTS (continued)

CONTENTS (continued)

LIST OF TABLES

LIST OF FIGURES

LIST OF FIGURES (continued)

LIST OF FIGURES (continued)

LIST OF FIGURES (continued)

LIST OF FIGURES (continued)

LIST OF ABBREVIATIONS

HDPE	=	High-density polyethylene
EOC	=	Poly(ethylene-co-1-octene)
ECB	=	Poly(ethylene-co-1-butene)
UCST	=	Upper critical solution temperature
LCST	=	Lower critical solution temperature
LLPS	=	Liquid-liquid phase separation
SANS	=	Small angle neutron scattering
SAXS	=	Small angle X-ray scattering
WAXS	=	Wide angle X-ray scattering
SEM	=	Scanning electron microscopy
TEM	=	Transmission electron microscopy
R_m	=	Maximum growth rate
MD	=	Machine direction
TD	=	Transverse direction
SS	=	Single screw extrusion
TS	=	Twin screw extrusion
EWF	=	Essential work of fracture method
COD	=	Crack opening displacement
CTOD	=	Crack tip opening displacement

CHAPTER 1
INTRODUCTION

Polyolefins, such as polyethylene (PE), polypropylene (PP), and ethylene / α-olefin copolymers, constitute the most extensive group of industrially important polymers; moreover, the manufacture and conversion of polyolefins is by far the largest sector of the Thai polymer industry. Polyolefins may be blended together to give a wide range of materials from tough plastics to elastomers. Their use is expanding due to their low cost and ease of processing, in particular into applications where the incumbent is poly(vinyl chloride), partly because of the environmental hazards associated with the latter. The end-use properties of polyolefin blends depend strongly upon the phase morphology of the solid state. Blend morphology is determined principally by the thermodynamics of interaction between polymer molecules with differing types and quantities of chain-branches that control liquid-liquid and solid-liquid phase separation.

Whilst phase separation in polyolefin blends in the melt-state has been suspected, and known in some cases, recent work on model systems has increased the basic understanding of the phenomenon [1,2]. Mechanical fracture studies, in combination with phase morphology characterisation, have begun to reveal how phase separation in the liquid state has a pronounced effect upon the solid state properties [3]. These studies were carried out upon statically annealed samples, and hence the phase morphologies differ from those found in processed materials where the polymers are subjected to melt flow followed by rapid cooling. Phase morphology is greatly affected by melt flow, and hence it is necessary to extend these basic studies to the understanding of phase morphology-processing relationships such that materials with controlled morphologies may be obtained under realistic processing conditions.

The thought that melt flow affects phase behaviour thermodynamically does not seem to be widely appreciated, rather it has been considered that only the thermodynamic quantities associated with the polymer architecture, such as the presence of specific interactions and combinatorial entropy, are important. This is illustrated by a quote from the widely cited text *'Polymer-Polymer Miscibility'* by Olabisi et al. [4]:

> *"…the driving forces for the transition from the one-phase (miscible) to the two-phase (immiscible) state are thermodynamic in origin and do not depend, for example, on the extent or intensity of mixing."*

The experimental work of [5], concerning polystyrene / poly(vinyl methyl ether) blends, and the theoretical analysis of [6], however, has shown that melt flow does contribute to the thermodynamics of mixing, most importantly through the contribution of stored elastic energy to the free energy of mixing. Our own recent studies, after collaboration with Prof. Takashi Inoue's group at the Tokyo Institute of Technology (TIT) in Japan, revealed that a linear polyethylene / elastomeric α-olefin copolymer blend exhibited extensive miscibility under melt-flow conditions and was essentially immiscible in the solid state. This was inferred from transmission electron microscopy results that revealed phase morphologies associated with liquid-liquid phase separation via the spinodal decomposition mechanism; thermal analysis confirmed that phase separation was complete in the solid state. Reports by Japanese polyolefin manufacturers have described similar effects in polypropylene-based blends [7]; moreover, it has been suggested that these compounds exhibit enhanced properties over commercial blends possessing dispersed phase morphologies. The results show that flow contributes significantly to the thermodynamics of phase mixing. additionally, [7] has shown that even very low levels of flow-induced miscibility may have significant effects upon end use properties.

Flow enhanced miscibility in polyolefin blends may prove to be an important mechanism to obtain novel morphologies and enhanced performance from these materials. Thus, a fuller understanding of this phenomenon and its effects under realistic processing conditions is needed. With this goal, a detailed study of the melt-flow / phase separation / morphology / property relationships was undertaken. It is envisaged that the work will elucidate the relationship between basic polymer architecture via melt processing to the final phase morphology in the solid state, and ultimately to the physical properties of the material. The insight gained is expected to aid in the development of new polyolefin blends with controlled morphologies and enhanced properties.

CHAPTER 2
OBJECTIVES

1.Study and characterisation of the solid state morphology in the linear polyethylene / ethylene-α-olefin copolymers blends over the practical range of the procession conditions used in fabrication, and comparison with the corresponding quiescent conditions.

2.Study the processing-morphology-property relationship and study microstructure-mechanical deformation of selected morphologies through a fracture mechanics approach.

CHAPTER 3
LITERATURE REVIEW

3.1 Polyolefins

Polyolefins are commercially important because of their relatively low cost and versatility. Recently, blending of polypropylene (PP) and polyethylene (PE) with elastomers has become of increasing interest as a way of increasing impact strength and improving low temperature toughness. Toughness can be improved by incorporating rubber into the plastic by melt-blending or by in-situ polymerization to form the rubbery component. Because of the high molar mass polymers, the entropy of mixing of two polymers is dramatically less than that for two low molecular mass compounds. The polymers are miscible in limited temperature and compositions ranges but are immiscible outside of these ranges. Recent studies in this area have primarily concentrated on theoretical and experimental studies of blend miscibility and the kinetics of phase separation in partially miscible blends under equilibrium conditions [8-10].

The effects of flow in the processing of blends where temperature gradients and high deformation rates are encountered, such as in melt extrusion or injection moulding have been studied. Flow was found to exert a marked influence on the phase behaviour of liquid-liquid mixtures and it is apparent that this effect must be taken into account, in particular, in understanding the state of polymer blends during processing [11-13]. Melt processing profoundly affects the morphology of polymer blends, particularly when the polymers approach the limits of miscibility [14].

3.1.1 Polyolefins types and properties

Polyolefin are the most important class of polymers in terms of volume usage and the simplest in terms of composition. They are long chain, aliphatic hydrocarbons consisting of polymers of alpha-olefins, with high molecular weight. They have

differences in the degree of chain branching, the frequency of (short) side chains, and in the regularity of the chain structure. These differences result from variations in reaction conditions, the type of catalyst used, and the particular olefin, or combination of olefins, used as monomer [15,16].

3.1.1.1 Low density polyethylene (LDPE)

LDPE is made by free-radical polymerization of ethylene under high pressure (15,000-40,000 psi) and high temperature (150-300 ^{0}C) in the presence of trace amounts of oxygen or peroxides as initiator. LDPE has a moderate degree of crystallinity (ca. 50%) because the molecular chain has numerous chain branches. It is a non-brittle plastic with easy processability, moderate hardness, and low softening temperature. Major uses of LDPE are in packaging film and laminates, paper and foil coating, blow moulded containers, wire insulation, and injection-moulded articles.

3.1.1.2 High density polyethylene (HDPE)

Polymerization processes using ionic catalysts make HDPE. The Ziegler type (typically titanium trichloride and aluminum alkyl) and Philips type (chromium oxide on silica) catalysts are active at relatively low temperatures (50-120 ^{0}C) and pressures (100-600 psi). Because it has little or no branching, or side chains, HDPE has higher crystallinity than LDPE and consequently, higher stiffness, strength, and melting point. The applications of HDPE are blow-moulded containers, extruded pipe, sheet and wire coating, packaging film, and injection-moulded articles such as containers, toys, and housewares.

3.1.1.3 Linear low density polyethylene (LLDPE)

LLDPE is made by copolymerizing ethylene at low pressure in the presence of catalysts with small amounts (4-8%) of α-olefin comonomers such as butene, hexene, or octene, which play the role of uniform short branches along a nearly linear backbone. LLDPE has a higher degree of crystallinity than LDPE and properties generally intermediate between conventional high- and low-density polyethylene. Because LLDPE has an attractive balance of properties, its consumption has grown

rapidly. Major applications are in film, injection moulded containers, wire and cable insulation, and extruded pipe and tubing.

3.1.1.4 Ultra high molecular weight polyethylene (UHMWPE)

It is possible to produce polyethylene of extremely high molecular weight at least ten times that of regular polyethylene, i.e., in the range 3 x 10^6 to 6 x 10^6 $gmol^{-1}$. The polymerization process leads to linear molecules associated with high density polyethylene, although reported densities (0.93-0.94 g/cm^3) correspond to the usual medium crystallinity range. UHMWPE has certain outstanding properties that probably qualify it as an engineering or specialty plastic. Its most cited outstanding property is its wear or abrasion resistance; it is associated with the chemical inertness, a very low coefficient of friction, excellent impact resistance, i.e., toughness and fatigue resistance. The growing use of UHMWPE in large scale materials handling equipment, as well as in many specialized applications such as pen tips, prosthetic wear surfaces, gears, etc.

3.1.1.5 Cross-linked polyethylene (XPE)

The introduction of chemical cross-links into polyethylene can be achieved by the addition of small amounts of organic peroxide, such as dicumyl peroxide, which must not cause significant cross-linking before the polymer has acquired its final shape in processing. A process such as rotational moulding is suited to this cross-linking method. Another method involves the irradiation of finished products in high-energy fields. It is used particularly for extruded products such as films, pipes, electrical wire, and cable insulation.

3.1.1.6 Polypropylene (PP)

Polypropylene is prepared under mild conditions (80^{o}C or less, with pressures of up to 600 psi), using catalyst systems similar to those employed for HDPE or LLDPE and operating in either bulk, solution, slurry, or the gas phase. Polypropylene can be produced in several forms that differ in their stereo-configuration. By far the most commercially important is the isotactic form, in which all of the methyl side groups are located on the same side of the polymer chain.

Isotactic polypropylene has a high degree of crystallinity owing to excellent packing of the polymer chains, which confers relatively high stiffness, strength, and melting point. This combination of properties enables the polymer to be oriented by drawing or stretching, making it useful for fibers and oriented films. Major applications for polypropylene are in fibers and filaments, moulded and extruded articles, and film.

3.1.1.7 Polybutylene (PBI)

Polybutylene is based on the butene-1-monomer and is also referred to as poly(butene-1). It may contain small amounts of comonomers. Its melting point is comparable to that of polyethylene, while its glass transition temperature is closer to that of polypropylene. The applications are primarily in the pipe and film areas.

3.1.1.8 Polymethylpentene (PMP)

Polymethylpentene (PMP) or, more specifically poly(4-methyl pentene-1), is somewhat of an oddity in that, in spite of the presence of rather bulky side groups in the repeat unit it crystallises to high degrees (40-60%) and unexpectedly remains highly transparent (90% transmission). Its mechanical properties are said to be generally comparable to those of polyolefins, such as polypropylene, but stable to higher temperatures up to about 200 ^{0}C. Creep resistance is claimed to be better than that of other polyolefins and it has a lower permeability to gases and vapors. It has good chemical resistance, but is sensitive to environmental stress-cracking, and not recommended for use in the presence of high energy radiation or sunlight (UV); it is quite flammable. PMP is primarily processed by injection and blow moulding. Because of the high transparency of the plastic, it is used in lighting elements, such as diffusers, lenses, and reflectors, or in liquid level and flow indicators. PMP is used in food packaging, processing, and service, and as cook-in containers, trays or bags.

3.1.1.9 Copolymers

Small amounts of higher olefins are often added in polyolefin manufacturing processes as co-monomers to moderate crystallinity and to improve certain polymer properties such as impact resistance, particularly at low temperature.

1-Butene, 1-hexene, 1-octene, and 4-methyl-1-pentene are copolymerized with ethylene in small amounts (4-8 %) in making various LLDPE grades. 1-Hexene, 1-butene, and propylene are copolymerized with ethylene in HDPE processes to reduce crystallinity and to improve stress-crack resistance. Propylene polymers that have incorporated from 2% to 4% ethylene have better clarity and toughness than propylene homopolymer.

A recently introduced novel copolymer of propylene and 1-octene is characterized by an unusual linear structure with long-chain branching. Produced by use of a homogenous transition metal catalyst, in contrast to Ziegler / Natta type catalysts, which are heterogeneous, this copolymer displays elastomeric properties, combined with easy processing characteristics. Target applications include packaging, medical products, wire coating and automotive components.

3.1.2 Ziegler-Natta based copolymers

It is also essential to understand the nature of the copolymers used in the current study and recognize the specific features that differentiate them from the remaining "polyethylenes". A brief review of the historical evolution of the different types of low density polyethylenes starting from the discovery of Ziegler-Natta type catalyst systems to that of the metallocene-based ones is presented in this section. The metallocene-based ethylene / α-olefin copolymers used in the present study are also compared with the other existing types of polyethylenes such as low density Polyethylene (LDPE), linear low density polyethylene (LLDPE), Ziegler-Natta based systems etc., with specific reference to the features that make them ideal for the present investigation.

The search for newer methods to synthesize polymeric materials, The search for newer methods to synthesize polymeric materials, in particular polyethylene, with exceptionally controlled molecular structure and desired properties has been ongoing for several decades. A major breakthrough in this area occurred with the discovery in 1953 by Ziegler and his co-workers [17] that a combination of transition metal halides with alkyl aluminums in an inert hydrocarbon could catalyze the polymerization of ethylene to produce highly linear and high molecular weight polymer. Several transition metal compounds such as those of nickel, zirconium, titanium, etc. were

utilized and were found to give similar results, with titanium being the most active. The commercial significance of this discovery was the fact that these polymerizations could be carried out under moderate conditions of temperature and pressure compared to the previously employed procedures. In an independent and concurrent investigation, Natta and co-workers established that the above catalyst system could also polymerize propylene to yield a polymer with a high degree of isotactic stereo regularity. They also extended their study to the polymerization of α-alkenes and successfully employed transition metal compounds in their lower valence states than those used by Ziegler et al. [10]. Independent research was carried out in several industrial laboratories in the United States at the same time. These investigations led to the discovery of a related class of silica-supported chromium trioxide catalysts by the Phillips Petroleum Company during the early 1950's. These catalysts constituted some of the earliest low-pressure catalyst systems for the production of linear high-density polyethylene.

These discoveries introduced a new class of catalysts as well as of polymers. They also enabled achieving a high degree of control in the synthesis of some of the most readily available and cheap monomers such as ethylene and propylene. In the case of ethylene, it had become possible to produce a more linear and high molecular weight polyethylene. Whereas in the case of propylene, it had become possible to synthesize linear and highly stereo regular molecules by exercising control on the propagation step. In recognition of the profound effect that these discoveries had on the field of synthetic polymer chemistry, Ziegler and Natta were awarded the Nobel Prize for Chemistry in 1963, and the catalyst system was appropriately named after them.

3.1.2.1 Linear low density polyethylenes (LLDPE)

This class of polymers are formed by the copolymerization of ethylene and α-alkene comonomers in the presence of Ziegler-Natta catalysts, resulting in side chains at the point of insertion of the alkene. The structure of these copolymers can be carefully manipulated by varying the manufacturing conditions according to the application desired. The branches in LLDPE not only lower the degree of crystallinity compared to high density polyethylene (HDPE) but also lower the density of the

material (similar to low density polyethylene-LDPE). However, LLDPE is superior to LDPE with respect to ease of processability, impact, tensile and tear strength as well as optical properties. Furthermore, LDPE consists of short chain as well as long chain branches that disrupt the crystal structure and affect desirable properties such as melt strength. LLDPE, on the other hand, is comprised only of branches of a constant length leading to potentially higher crystallinity and higher rigidity compared to a similar LDPE. These factors have contributed to the immense success of LLDPE over typical low density polyethylenes in the recent years.

3.1.2.2 Metallocene based copolymers

Several studies were carried out with the aim of understanding the polymerization mechanism using Ziegler-Natta catalysts. These studies led to the hypothesis that the propagation step involved the insertion of an activated monoalkene molecule into a transition metal-carbon [18] bond and that the high degree of "isotactic stereocontrol was associated with the chiral structure of the transition metal complex" [19]. These observations on the heterogeneous Ziegler-Natta catalyst systems suggested that it may be possible to carry out similar polymerizations using homogeneous transition metal organometallic derivatives if the active complex can be formed. Several attempts at finding such a soluble catalyst were made, culminating in the discovery in the early 1980's by Kaminsky and coworkers that metallocene complexes of transition metals, when activated with alkylalumoxanes, yielded highly active and soluble catalysts with similar catalytic activity as the heterogeneous Ziegler-Natta catalysts. The discovery of metallocene-based catalysts provided an alternative to the heterogeneous system of catalysts in general. In particular, it had become possible to synthesize isotactic, high molecular weight polypropylene (which was not feasible before the use of alkylalumoxanes).

The first commercial copolymers based on the metallocene-based catalysts were produced by Exxon in 1991 using an achiral single-site catalyst . In 1993, Dow Chemical began production of copolymers using a cyclopentadienyl amide titanium catalyst. The term "constrained geometry catalysts" is derived from the open and highly reactive nature of the metal atom resulting from the presence of a short dialkylsilyl bridging moiety.

3.1.2.3 Metallocene-based ethylene / α-olefin copolymers

This class of materials owes it origin to the recent developments in metallocene based catalyst chemistry and has spurred renewed interest in the effect of comonomer distribution on the morphology and physical properties of a polymer. These copolymers possess all the favorable characteristics of LLDPE's in addition to a high degree of control over the stereospecificity and the molecular weight distribution of the resulting materials. The single-site catalysts involved in the synthesis of such copolymers permit a uniform distribution of comonomers in the various polymer chains i.e., the distributions of comonomers in the different polymer chains are identical to each other, irrespective of chain length. This is in sharp contrast to the Ziegler-Natta based systems that yield a broad distribution of comonomers among the various polymer chains. Both the metallocene as well as the cyclopentadienyl amide catalysts result in random incorporation of ethylene and α-olefins without the use of excess comonomer. Furthermore, the randomness is achieved independent of chain length. It must however be noted that the cyclopentadienyl amide type catalysts yield copolymers with long chain branching as well. The metallocene-based copolymers may include a variety of branches such as ethyl, butyl, pentyl, hexyl, etc. Copolymers made by Dow Chemical using the single-site constrained geometry catalyst technology (CGCT) are employed in the present study.

3.2 Polymer Blends and Alloys

Blending processes can make up for the deficiency of one polymer by combining it with another that has a corresponding superior property. For example, blending may be used to reduce the cost of an expensive engineering thermoplastic, to improve the processibility of high temperature or heat-sensitive thermoplastic, or to improve impact resistance. Another reason for blending may be for the use for recycled plastics to avoid the expensive process of separating mixed feed stocks into the constituent resins.

3.2.1 Terminology in polymer blending

Polymer blends can show miscibility, partially miscibility, or complete immiscibility. Most of the commercially useful polymer blends have compatibility even though they do not have thermodynamic miscibility. In fact, they usually form multiphase morphologies that produce a synergistic advantage in the balance of properties. There are several types of polymer blend systems that may be defined [20,21]:

(i) Polymer blend: two or more polymer or copolymers combined to from one material.

(ii) Miscible blend: the blends, which are homogeneous at a molecular level

a) Homologous miscible blend: combinations of different fractions of the same polymer.

b) Heterogeneous miscible blend: two or more polymers that are thermodynamically miscible.

(iii) Immiscible blend: the blends that are thermodynamically immiscible that are formed from a blend with two or more phases.

a) Compatible blend: the mechanically processable blends which resist gross phase segregation and / or give desirable properties, and may consist of two or more phases.

b) Polymer alloy: a polymer blend with a morphology controlled by compatibilisation (the term compatibilisation refers to any physical or chemical method employed to stabiles the blend morphology).

3.2.2 Miscibility of polymer blends

Whether polymer blends will be homogeneous or phase separated will depend upon many factors, such as the kinetics of the mixing process, the processing temperature, and the presence of solvent or other additive.

3.2.2.1 Thermodynamics miscibility

The primary consideration for determining miscibility of two polymer the thermodynamics that are governed by the relationship between the Gibbs free energy change during mixing (ΔG_m), the enthalpy change (ΔH_m), and the entropy change (ΔS_m) of mixing for a reversible system. This is given as:

$$\Delta G_m = \Delta H_m - T\Delta S_m \quad (3.1)$$

Enthalpy (ΔH_m) depends on the attraction / repulsion between the two polymer and the volume change of mixing. Since the attraction between like molecule is greater than the attraction between unlike molecules, ΔH_m is generally positive. Entropy (ΔS_m) results from the randomization, which occurs upon mixing. Since the mixing of small solvent molecules produces great randomization, many solvents are miscible, whereas for polymers each repeat unit is connected together, and hence the randomization is relatively low and the entropy change is small. Thus, the higher the molecular weight of the polymer in the blend, the less likely the blend will be miscible.

From the fundamental thermodynamic equation it can be seen that an increase in temperature will favour mixing. At higher temperature the kinetic energy will increase and the exothermic specific interactions will be weakened, thereby reducing the ΔH_m term. Moreover, differences in free volume of the constituent polymers may become important at high temperature. Thus, a blend may be miscible at one temperature and immiscible at a higher or lower temperature.

3.2.2.2 Kinetic effects

Thermodynamics can be used to describe the miscibility at equilibrium, but due to the high viscosity and the slow diffusion rates in polymer blends the speed to reach equilibrium is slow; i.e., there is a kinetic control of the blending process. There may not be sufficient time for miscibility to occur.

3.3 Polyolefin Blends

There are many objectives for blending polyolefins including toughness and processability enhancement through blending with thermoplastic elastomers such as ethylene-α-olefin copolymer type polymers. Beyond the principle thermodynamic equation, several factors may favour thermodynamic miscibility. These may be discussed with particular reference to polyolefins.

(a) *Polarity:* The two polymers have very similar polarities, randomization (ΔS) may then favour thermodynamic miscibility.

(b) *Molecular weight:* The randomization (ΔS) is inversely related to the molecular weight. Therefore, the lower molecular weight polymers tend to be more thermodynamically miscible.

(c) *Co-crystallisation:* Whilst crystallisable polymers may be thermodynamically miscible and truly miscible in the melt, when cooled each polymer usually separates and forms its own unique crystal structure. Co-crystallisation is the important behaviour in several polyolefin blends. If two polymers have such similar isomorphous crystal structures that both can enter the same crystal lattice and co-crystallise, a single homogeneous solid product may be formed. For example, in the blends of LDPE with HDPE, a large increase in the crystallisation temperature of LDPE when blended with HDPE was indicative of co-crystallisation between the components when blends were rapidly cooled from the melt [22].

3.3.1 Phase separation of polyolefin blends

The miscibility in the liquid state of saturated hydrocarbon polymers having different chemical microstructures based on repeat units represented by $-CH_2CR_1R_2-$ where R_1 and R_2 are either hydrogen (H) or alkyl groups has been studied. Polyolefins have the overall chemical composition CH_2 , but relative numbers and placements of methyl ($–CH_3$), methylene ($–CH_2–$), methine (–CH) and quaternary carbons (–C–) vary from polymer to polymer. Interest in miscibility, phase separation, and compatibility is driven by the development of blends with enhanced properties and by growing pressures to manage waste streams that contain significant amounts of

polyolefins [23]. Polyolefin blends, in which specific interactions are absent or minimal, are furthermore relatively tractable systems for condensed matter theories.

The distinction between one or more phases in a molten blend of polyolefins is often blurred by similar component properties, particularly refractive index. Nevertheless, it has been known for some time that blends of isotactic polypropylene and random ethylene-propylene copolymers, similar to impact-modified polypropylene, are immiscible in the liquid state [24,25]. With phase contrast enhanced by deuteration of one component, a blend of polyethylene and polypropylene was shown by small-angle neutron scattering to have two melt phases [26]. Relatively indirect evidence was used to infer liquid–liquid phase separation (LLPS) in certain mixtures of linear and lightly branched polyethylenes [27]. Two coexisting liquid phases were reported in random or statistical copolymers of ethylene and 1-butene [28] or 1-octene [29]. Those materials, prepared with heterogeneous catalysts, are known to be multicomponent mixtures of chains having different amounts of comonomer or short-chain branching [28].

The energetics of a blend of two (monodisperse) polymers are usually treated in terms of the Flory-Huggins lattice theory where the free energy of mixing per monomer, ΔG_m, is written as:

$$\frac{\Delta G_m}{\upsilon_o kT} = \frac{\phi_1 \ln \phi_1}{\upsilon_1 N_1} + \frac{\phi_2 \ln \phi_2}{\upsilon_2 N_2} + \frac{\phi_1 \phi_2 \chi}{\upsilon_0} \quad (3.2)$$

The lattice has a cell or reference volume ν_0, ϕ_i, Ni and ν_I, i are volume fraction, degree of polymerization, and monomer volume of polymers 1 and 2. Thermal energy is given by kT, and χ is the Flory-Huggins interaction parameter which represents energetic repulsion ($\chi > 0$) or, more rarely, attraction ($\chi < 0$) between monomers of the two polymers. χ contains all non-ideal (noncombinatorial) contributions to the free energy of mixing, reckoned per lattice site and normalized by kT. For the general case when monomer volumes are not equal, the reference volume is defined as $\nu_0 = (\nu_1 \nu_2)^{1/2}$. With the usual assumptions that χ is independent of blend

concentration .{ϕ_1, ϕ_2} and degree of polymerization {N_1 , N_2}, it is straightforward to construct a binary phase diagram from equation (3.2). Three regions are identified in Figure 3.1: stable, metastable, and unstable. Any one-phase binary blend is unstable when $\chi \geq \chi_s$, where χ_s is the spinodal value of χ:

$$\chi_s = \frac{\upsilon_0}{2}\left[\frac{1}{\upsilon_1 N_1 \phi_1} + \frac{1}{\upsilon_2 N_2 \phi_2}\right] \tag{3.3}$$

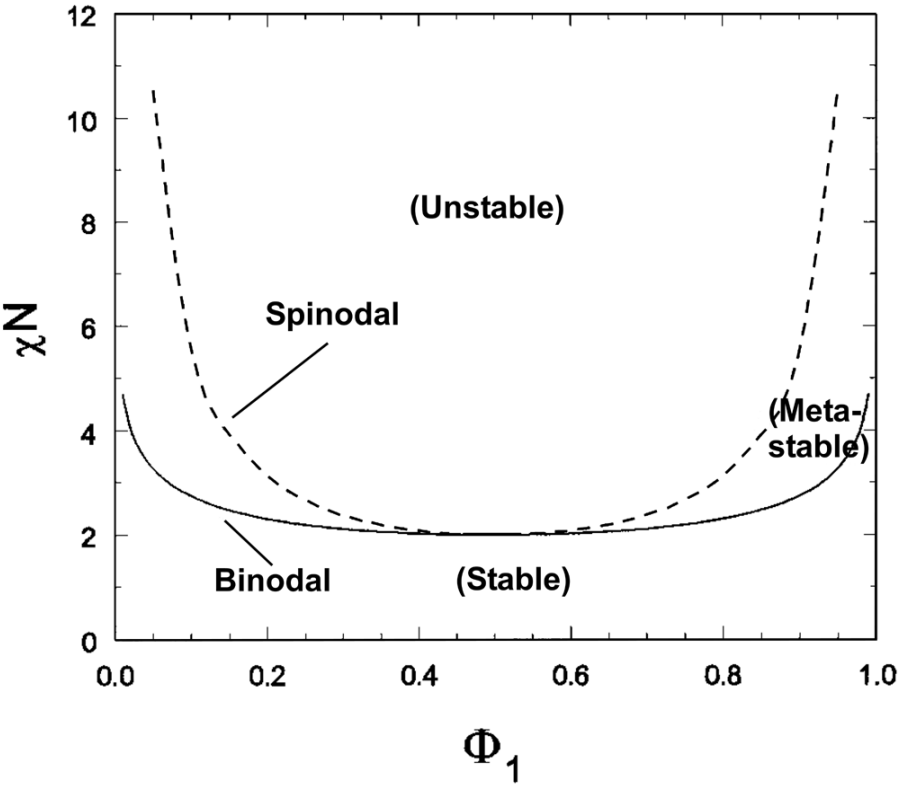

Figure 3.1 Phase diagrams for a symmetric polymer blend showing binodal and spinodal boundaries as a function of χN and concentration ϕ_1.

The coexistence or binodal curve is established by equating chemical potentials for the two components (1 and 2) in two phases (α and β). The metastable regions of the phase diagram between the binodal and spinodal curves are indicated in Figure 3.1.

Altering the temperature of a binary blend changes the size of the Flory-Huggins interaction parameter χ. The most common situation is when χ is positive and decrease with increasing temperature:

$$\chi(T) = A + \frac{B}{T} \tag{3.4}$$

Here the constant B is greater than zero. Lowering the absolute temperature T enhances χ, the magnitude of repulsive interactions relative to thermal energy, to the point where the system crosses from the stable region into either a metastable or unstable region; subsequent heating will return the system to one phase at a large enough value of T. This situation is represented in Figure 3.2 with the assumption that A = 0 in equation (3.4) and B chosen to give phase transitions near room temperature when N = 1000.

The binodal and spinodal lines are common in Figure 3.1 at the critical point defined by a critical concentration (of component 1) ϕ_{1C} and a critical value of the interaction parameter χ_C:

$$\phi_{1C} = \frac{1}{1 + (\upsilon_1 N_1 / \upsilon_2 N_2)^2} \tag{3.5}$$

$$\chi_C = \frac{\upsilon_0}{2}\left[\frac{1}{(\upsilon_1 N_1)^{1/2}} + \frac{1}{(\upsilon_2 N_2)^{1/2}}\right]^2 \tag{3.6}$$

For the symmetric case ($N_1 = N_2 = N$ and $\nu_1 = \nu_2$) represented in Figure 3.2, the critical points is given by $\phi_{1C} = ½$ and $\chi_C = 2/N$. Changing the temperature of a blend having the critical concentration ϕ_{1C} will assure that liquid-liquid phase separation occurs when $\chi \geq \chi_C$ at a temperature very near the critical temperature T_C where $\chi(T_C) = \chi_C$. For the usual case when χ becomes smaller on heating (B > 0 in equation (3.4)) T_C is the upper critical solution temperature or UCST; this situation is depicted by the vertical line labeled ‘C’ (critical) in Figure 3.2. Also shown in Figure 3.2 is a

temperature range for an off-critical (OC) blend, which is cooled through the metastable range before entering the spinodal region. If χ has a positive temperature dependence (B < 0), phase separation occurs on heating at the lower critical solution temperature or LCST.

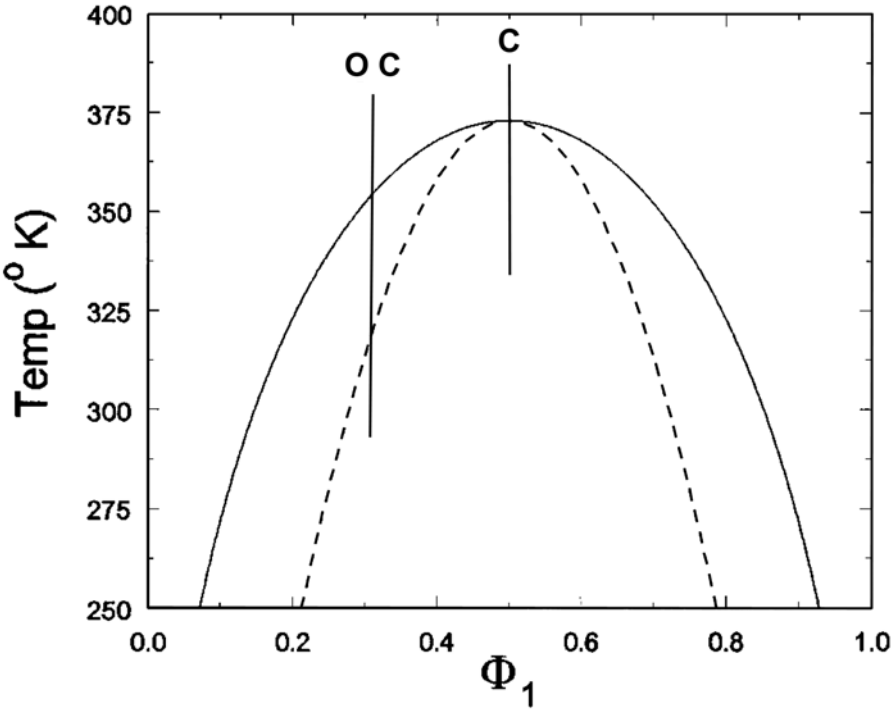

Figure 3.2 Phase diagrams for a symmetric polymer blend showing binodal and spinodal boundaries as a function of χN and concentration ϕ_1 for N = 1,000 and $\chi(T) = B/T$. Vertical lines are for blends with critical (C) and off-critical (OC) concentrations.

A stable single phase is assured for a binary polymer system at all concentrations if $\chi \leq \chi_C \approx 2/N$. Consider a representative degree of polymerization N = 1000 for which complete miscibility corresponds to $\chi < 2 \times 10^3$. Recalling that χ is the excess free energy of mixing divided by kT, this is equivalent to an enthalpy of mixing of only 6.2 J/mol (1.5cal/mol) at T = 373K (100°C). The immediate conclusion is that polymer-polymer blends are miscible only when intermolecular interactions are

exquisitely balances so that χ is very small. One quite practical method for controlling the magnitude of χ is to employ random copolymers as one or both blend components. Consider two *AB* random copolymers differing in the amount of comonomer designated by the mole fraction y of monomer *B*. The simplest thermodynamic analysis leads to the prediction that the effective χ for random copolymers 1 and 2 having compositions y_1 and y_2 is given by

$$\chi = \chi_{AB}(y_1 - y_2)^2 \tag{3.7}$$

Here χ_{AB} represents the interactions between *A* and *B* monomers, and is the value of χ for a blend of homopolymer *A* with homopolymer *B*. χ in equation. (3.7) can be made arbitrarily small by having y_1 approach y_2. Only the difference in comonomer composition is important; a blend with components having $y_1 = 0.1$, $y_2 = 0.2$ should have the same χ as a blend of copolymers having $y_1 = 0.8$, $y_2 = 0.9$, etc. Equation (3.7) is in principle applicable to homopolymer or alternating copolymer chains, but diblock copolymers, etc. are not amenable to this mean field approach.

The interaction parameter χ can be interpreted in terms of the difference in solubility parameters (square root of cohesive energy density) of repeat units constituting polymers 1 and 2.

$$\chi_s = \frac{\upsilon_0}{kT}\left(\delta_1^2 - \delta_1^2\right)^2 \tag{3.8}$$

For a blend of two random copolymers the solubility parameter δ_1 and δ_2 can be estimated from group addivity schemes with contributions from monomers A and B scaled according to y_1 and y_2. Interactions formulated by equation (3.8) are always repulsive ($\chi \geq 0$) and, assuming (δ_1 - δ_2) is independent of temperature, $\chi(T) \propto T$. Krishnamootri et al. measure $\delta_{1,2}$ from the thermal expansion coefficient α and the isothermal compressibility β of polyolefins. Subject to certain approximations, the solubility parameter for, e.g., component 1 can be written as:

$$\delta_1 = \left[T \frac{\alpha_1(T)}{\beta_1(T)} \right]^2 \tag{3.9}$$

With this formalism the temperature dependence of χ in equation (3.8) derives from the temperature dependence of $\delta_1 - \delta_2$; while χ must be positive, it may increase or decrease with T in any manner.

It will be shown that χ for a particular polyolefin blend or χ_{AB} for a particular pair of repeat units) may be negative and may have a temperature dependence different from $\chi(T) \propto T$ in equation (3.4). An interesting case is when χ is positive but displays a maximum with respect to temperature; here the phase diagram may be a closed loop defining the two-phase region with the single phase being stable at both high and low temperature.

3.3.2 Conformations of polyolefin chains

A polymer chain in dilute solution can be pictured as a coil, continuously changing its shape under the action of random thermal motions. Therefore, the volume occupied by a chain in solution could differ from that occupied by it neighbours, and these size differences are describe by the fact that each sample will contain a variety of chain lengths.

In polyolefins, rotation around the backbone single bonds can generate an enormous number of possible geometrical structures of chains. Two factors are used to describe the conformation of polymer chains in solution: the root mean square distance between the chain ends $(\overline{r^2})^{1/2}$ and $(\overline{R_g^2})^{1/2}$ which is the average distance of the chain elements from the center of gravity of the coil. The relation between the two factors in the absence of excluded volume effects for simple chains is [30]:

$$(\overline{r^2})^{1/2} = 6(\overline{R_g^2})^{1/2} \tag{3.10}$$

The conformational asymmetry theory developed by Fredrickson et al. [31] is an alternative approach to the description of non-ideal mixing in polyolefin blends. In this treatment, a correlation is established between differences in statistical segment length

and the excess free energy of mixing. The statistical segment length (b) is related to the radius of gyration of a polymer by

$$R_g = b(N/6)^{1/2} \quad (3.11)$$

where N is the number of statistical segments.

Bates et al. [32] reported the correlation between the magnitude of interaction paramenter (χ) and the asymmetry in the statistical segment length of binary polyolefin blends. Four model polyolefins were considered in this study: polyethylene (PE), poly(ethylenepropylene) (PEP), poly(ethylene / ethylethylene) (PE / PEE, a random copolymer) and poly(ethylethylene) (PEE). They found that χ tends to increase with increasing Δb (the difference in statistical segment lengths of the constituent polymers).

3.3.3 Effect of structure on the miscibility, compatibility and properties of polyolefin blends

Polyolefins play an important role in research, development and application of polymers. Each of their daily life applications relies on a unique combination of molecular structure or chain microstructure and the processing conditions. It also depends on the conditions of crystallisation , not only through the usual effects of crystallisation temperature on crystallite size, but also, depending on the comonomer, through partial incorporation of co-units to form defects in the crystallites themselves. To control and influence the final properties of polymers, a good knowledge of the relations between the chain microstructure, the crystallisation conditions, the morphology and the resulting properties is important.

The miscibilities of polyolefin blends are strongly affected by the extents of short and long chain branching in each polymer, which are controlled by the types and quantities of comonomer and chemical reaction. Carriere et al. [33] have shown that the compatibility of polypropylene / poly(ethylene-co-α-olefin) elastomer (PP / POE) blends was related with the octene content and comonomer type via measurement of the interfacial tension. The interfacial tensions decreased when the comonomer type was changed from propylene to octene; i.e., when the length of the side chain was

increased. This indicated that PP / POE blends where the POE is the ethylene-octene type should be more compatible than those made with either ethylene-butene or ethylene-propylene at the composition studied. Moreover, the interfacial tension was found to decrease when increasing octene content. Yamaguchi et al. [34] investigated rheological properties in the melt and solid states of binary blends of isotactic polypropylene (i-PP) and an ethylene-1-hexene (EHR) in which two types of EHR were used, i.e., ethylene rich and 1-hexene rich EHR. The dynamic viscoelastic properties were obtained by using a cone and plate type rheometer. The blends of i-PP and the ethylene rich shows a very long relaxation time due to the phase separation in the molten-state. The blend showed two separate glass relaxation processes associated with those of the pure components, indicating that the blends showed phase separated morphology in the solid-state. It was found that the dynamic moduli for the binary blends of i-PP and the 1-hexene rich EHR are intermediate between those of the pure components in the molten state. The time temperature superposition principle was applicable to the frequency dependence of the dynamic moduli for the blends, suggesting that the molecular aggregation state in the higher temperatures is stable over the entire frequency or temperature regions. The apparent activation energy of the blends is constant and is identical with those of i-PP and the EHR. The blend showed a single glass transition process between those of pure components indicating that the 1-hexene rich EHR chains are incorporated into the amorphous region of i-PP in the solid-state. It was concluded that the polymer miscibility in the molten state for the polyolefin blends directly affects the morphology in the solid state. Another study by the same author [35] also investigated the compatibility of the binary blends of i-PP with ethylene α-olefin copolymers such as EPR, ethylene-1-butene copolymers (EBR) EHR. It was found that the EPR component was incompatible with i-PP component, irrespective of propylene content in copolymer. The i-PP / EBR and i-PP / EHR blends were miscible. The EBR and EHR were dissolved in the amorphous region of i-PP. The results suggested that morphology can be controlled by changing the α-olefin content in EBR or EHR copolymer. Chen et al. [36] investigated the miscibility and phase separation behaviour in blends of i-PP and ethylene-propylene diene terpolymer (EPDM, ethylene content 70%). It was found that the i-PP / EPDM blends were immiscible, except in a limited temperature gap bound by the crystallisation

temperature and the crystal melting temperature. A lower critical solution temperature (LCST) was observed above the crystallisation temperature, but below the melting temperature. The phase behaviour and morphology development in a melted blend of i-PP and hydrogenated poly(styrene-co-butadiene) (hSBR) was studied by Inoue et al. [37]. A hSBR was found to be miscible with i-PP above the melting point of i-PP. The mixture was phase separated at lower temperatures, i.e. the i-PP / hSBR blend exhibited UCST phase behaviour. The UCST phase behaviour was determined by time-resolved light scattering analysis. In the quench 50 / 50 blend, a microphase separated structure of hSBR domains, having a diameter of 20 nm, dispersed quite regularly in an i-PP matrix was observed by transmission electron microscopy. The microphase-separated structure seems to originate from spinodal decomposition below the UCST during the quenching process. The formation of large and ordered lamellar crystallites was suppressed to yield fine PP crystallites. This may be caused by the presence of the hSBR. In a further study by the same authors [38] it was found that the blend showed good strain recovery after large deformation. The presence of rubbery (hSBR-rich) domains may provide a favorable contribution to the good strain recovery mechanism. The strain recovery mechanism may also originate from the characteristic morphology of i-PP crystallites in the matrix; i.e., rather fragmented crystallites formed by crystallisation in the presence of polymer impurity (hSBR). Lee et al. [39] studied the morphology development in i-PP and a partially hydrogenated oligo(styrene-co-indene) (HSI). It was found that the blends are miscible above the melting temperature of i-PP. The author used time-resolved light scattering to study on the spherulite formation at various crystallisation temperatures. The results were assessed by transmission electron microscopy. The light scattering and transmission electron microscopy analyses revealed that the new morphologies are available by adding miscible impurity and controlling crystallisation temperature. At high crystallisation temperature, both the population of crosshatch lamellae and the ordering of radial lamellae in the blend are higher than in neat i-PP. At low crystallisation temperature, no crosshatch lamellae are formed but the fragmented lamellae develop in the blend. The fragmented lamellae are arranged parallel with each other in a radial direction.

Mader et al. [40] studied the influence of comonomer on morphology and the properties of the melt blends of i-PP with random ethylene-co-1-butene copolymers which differ in 1-butene concentrations. It was found that the compatibility between i-PP and ethylene-co-1-butene copolymers increased with increasing 1-butene contents in ethylene-co-1-butene copolymers and a single phase blends are formed at 1-butene contents exceeding 82 wt%. The system was investigated by using atomic force microscopy and transmission microscopy. The improved compatibility accounted for enhanced ethylene-co-1-butene copolymers dispersion and interfacial tension. Yamaguchi et al. [41] investigated the effect of molecular structure in branched PE which is LLDPE and low density polyethylene on the adhesion properties of polypropylene. It was found that the adhesive strength of LLDPE / PP is much higher than that of LDPE / PP. The viscoelastic measurements in the molten state for the binary blends composed of branched PE and PP were also carried out, and the interfacial tension between two polymers was estimated using a rheological model. It was found that the interfacial tension was found to be 1.0 Nm^{-1} for LLDPE / PP and 2.1 Nm^{-1} for LDPE / PP, suggesting that the interfacial thickness of LLDPE / PP is about twice that of LDPE / PP. These results demonstrate that entanglements between branched PE and PP have significant effects on the adhesive strength in this study. Furthermore, ethyl and butyl branches in branched PE will be responsible for the adhesion strength with PP. Morgan et al. [42] studied the liquid-liquid phase separation in ternary blends of linear polyethylene with two ethylene-butene copolymers. It was found that the length of the branches is of secondary importance in determining phase behaviour. In blends of linear polyethylenes with lightly branched copolymer it is the number of branches that is the most important factor influencing the extent of phase separation. Graessley et al. [43] investigated the effect of deuterium labeling on the thermodynamic interactions in blends of labeled and unlabeled saturated hydrocarbon polymers, in this experiment used polybutadienes. Small angle neutron scattering (SANS) was used to evaluated the interaction parameter χ at several temperatures and compositions. It was found that deuterium labeling changes χ relative to the value for hydrogenous components and that the direction of the change depends on which of the two components is labeled. For blends of hydrogenated polybutadienes, χ always increases when the more branched

component in labeled. Rhee and Crist [44] studied the interaction parameter (χ) and the phase separation of the binary blends of linear polyethylene (PE) and the series of hydrogenated polybutadiene (HPB) in which the polymer chains differ in ethyl branched C_4H_8 units. The phase separation was studied by annealing the blend samples at 150^oC and varying the time permitted for phase separation to occur and quench the samples and studying the phase morphology by SEM. It was found that the domain sizes increase with increasing the time permitted for phase separation and the interaction between linear and branched copolymer has the relationship where χ is proportional to the square of the branch content of the copolymers.

The effect of comonomer contents on the ethylene-1-octene copolymers has been studied by Mathot et al. [45]. The comonomer contents covering a wide range of 0 to 44 mol%. With increasing the comonomer content, the crystallisation and melting occur at lower temperatures approaching the glass transition and lower crystallinities were observed. These observations reflect dimension distributions of increasingly small or imperfect crystalline structures with low thermal stability at higher comonomer contents or longer branch lengths. When comparing homogeneous ethylene copolymers of different short chain branch lengths, all effects associated with increasing comonomer content appear to be stronger at higher side branch lengths. For instance, the crystallisation and melting temperatures decrease more sharply with increasing comonomer content at higher branch lengths, irrespective of the determination methods. The effect of comonomer content was also investigated by Chum et al. [46]. Ethylene-octene copolymers varied in comonomer content and density were used in their study. A copolymer of higher comonomer content than the target was blended with the appropriate amount of a lower comonomer content copolymer to obtain the target level of crystallinity. Thermal analysis indicated that the components crystallised separately in all the blends. The non-crystalline regions were immiscible when the branch concentration of the blended copolymers was too different.

3.3.4 Effect of flow on the mixing, demixing, and phase morphology of polyolefin blends

Theoretical and experimental studies upon the miscibility of polymer blends, particularly in field of kinetics of phase separation in partially miscible blends, have been carried out under equilibrium conditions. The behaviour of a polymer during flow is not easily predicted because polymer compounds are normally much more complex than pure homopolymers and the limiting condition for flow, e.g., melt fracture; However, phase behaviour and phase transitions may be induced by flow.

The miscibility of blends has been observed to increase by the application of shear flow due to the contribution of elastic free energy of the system, as a result of the flow, to the free energy change to mixing. The elastic energy is defined as [47].

$$\Delta G_{elastic} = \frac{3KT}{2}\left(\frac{\sum V_i\left(r^2 - r_o^2\right)}{r_{oi}^2}\right) = \frac{N_1}{2} \qquad (3.12)$$

Where K is the Boltzmann constant, T the temperature, V_i the chemical potential of chains of the components i, r and r_o are the mean radii of gyration of chains in their stretched and relaxed states, respectively, and N_1 is the first normal stress difference.

Incorporation of equation (3.12) into the spinodal condition for phase separation gives:

$$\frac{\partial^2 \Delta G_m}{\partial \phi_2^2} + \frac{1}{2}\frac{\partial^2 N_1}{\partial \phi_2^2} = 0 \qquad (3.13)$$

In the homogeneous state the first term in equation (3.13) is positive and goes to zero at the spinodal and becomes negative in the phase-separated region. The second term, however, is always positive which helps to improve the phase miscibility under shear.

There are many experimental studies on the phase behaviour of partially miscible blends under flow. The influence of shear flow on the cloud point curves for three different binary polymer blends, namely polystyrene (PS) / poly(vinyl methyl ether)

(PVME), poly(ethylene-co-vinyl acetate) (EVA) / solution chlorinated polyethylene (SCPE), and SCPE / poly(butyl acrylate) blends which have LCST behaviour, has been studied by Hindawi et al.[48]. It was found that cloud point curves were shifted to lower temperatures at low shear rates, indicating that flow induced phase separation. Above a critical shear rate, the cloud point curves increased in temperature, indicating flow induced phase mixing. A rheooptical apparatus was used in the study of the phase behaviour of EVA / SCPE blends by Hindawi et al [49]. It was found that the phase boundary of the polymer mixture that exhibited a lower critical solution temperature was shifted upward in temperature due to the application of stress. Madbouly et al. [50] studied the effect of shear flow on the phase behaviour of PS / PVME blend with an LCST-type phase diagram. They found that the shear effect was composition dependent and that the values of the cloud points corresponding to shear induced mixing or demixing were greatly affected by rotation speed. The phase behaviour of binary blends of SAN, with 29.5 wt% acrylonitrile content (SAN-29.5), and PMMA with different molecular weights under simple shear flow applied by parallel plates was investigated [51]. Shear-induced mixing was observed for all samples. The magnitudes of the elevation of the cloud points with shear rate were found to be molecular weight of PMMA dependent. The molecular weight of PMMA that showed a maximum elevation of cloud point was consistent with one at which the viscosity ratio (η_{PMMA}/η_{SAN}) is almost unity. This indicated that the phase behaviour of the polymer blend under shear is strongly affected by viscoelastic properties of constituent polymers. Katsaros et al. [52] reported an increase in the cloud point of the PS / PVME blend in a planar stagnation flow by as much as 12, the magnitude depends on the extension rate, strain and blend composition . They also found flow induced miscibility in the shear flow between two parallel plates. On the other hand, at lower temperatures as much as 30K below the quiescent cloud point, the flow induced phase separation was observed in both shear flow and extensional flow.

The effect of shear fields on the structure development in a polymer blend during melt processing; i.e., through extrusion and injection moulding, was investigated. Okamoto et al. [53] reported that, a blend of 50 / 50 poly(butylene terepthalate) (PBT) / polycarbonate (PC) using twin screw extruder had a bicontinuous two-phase structure with unique periodicity and phase connectivity. This structure was the result

of dissolution, under high shear rate that caused LCST elevation, and then spinodal decomposition under zero shear rate when the extruded melt was quickly quenched in ice-water. The blend of polycarbonate (PC) / poly(styrene-co-acrylonitrile) [54] had a similar structure to the PC / PBT blend after it was injection moulded. Sano et al. [55] studied the phase separated structure in an injection moulded blend of i-PP / HDPE. A 60 / 40 PP / HDPE blend was made through injection moulding sheet of 2 mm thickness. The maximum shear rate was estimated by the author was 2.12×10^3 s^{-1}. The blends of HDPE with i-PP are known to be immiscible in the quiescent state but from the TEM micrograph results, the author observed the regular structure and proposed it to be formed through spinodal decomposition from a single phase mixture attained in the high shear field in the injection moulder. The area of the i-PP rich region and the HDPE rich region obtained from the TEM micrograph showed that the HDPE rich regions were wider than those of the i-PP rich regions for the 60 / 40 i-PP / HDPE blend. This suggest that the PE rich region for the should contain a significant amount of i-PP. The i-PP may reside in an amorphous region between PE lamellar. Furthermore, the thick lamellae could be seen in the bright regions. The development of PE lamellae in the i-PP rich region strongly suggests that PE chains had existed in the i-PP rich melt after the spinodal decomposition, and that they then segregated in the i-PP rich region. The results imply that the periodic structure is fixed by the crystallisation at a relatively early stage of spinodal decomposition. The mechanism was also supported by microscopic observation of the structure development during isothermal annealing above the melting point of i-PP because a bicontinuous structure with regularlity developed and grew up self-similarly.

The effect of orientation on the morphology development in a polymer blend during the melt processing was investigated. Yu and Wilkes [56] studied the orientation determination and morphology of HDPE in the blown film process. Two HDPE resins with different molecular weight distributions were used in this study. A fibril nucleated morphology was observed in the melt-extruded films by transmission electron microscopy (TEM). The broader molecular weight samples possessed fibril nuclei that were not evident in the narrower molecular weight distribution films. The existence of the fibril nuclei was further confirmed from wide angle X-ray scattering (WAXS) by the intense sharp spots superimposed on the

equatorial (110), (200) and (020) reflection planes. The origin of this pronounced fibril nucleation was clearly believed to be due to the longer relaxation time behaviour of the broader molecular weight HDPE. The amorphous phase orientation and form birefringence for all films were found to be very small and the observed birefringence arose almost exclusively from the crystalline phase. David et al. [57] investigated the processing-structure-property relationship of HDPE blown films. A series of blown films were prepared using two high density polyethylene resins of differing molecular weight and molecular weight distribution, using a high stalk process. Both the resins were processed at three frost line heights (FLHs) and three draw down ratios to determine the effect of processing parameters and resin characteristics on final film morphology and mechanical properties. By changing the FLH and the time to initiate transverse direction (TD) expansion, the relative number of lamellae stacked both perpendicular and parallel to the machine direction (MD) could be controlled for a constant blow up ratio (BUR) of 4:1. It was determined that the proportion of lamellae stacked parallel to the MD increased with increasing FLH. This effect was found to be related to the relaxation behaviour of the melt and bubble shape. Increasing the stress in the stalk region was observed to lead to a reduction in stalk diameter just prior to bubble expansion, resulting in a greater effective BUR. Film morphology was observed to strongly influence end mechanical properties. Elmendorf tear resistance was found to increase in the MD and decreased in the TD with increasing FLH. The tear properties were observed to be a strong function of the molecular anisotropy of the films.

3.3.5 Effect of annealing time on dispersed domain size

Phase separation will occur when the blend becomes unstable either by spinodal decomposition, or process of nucleation and growth. After separation the system composed of small domains of one phase dispersed in a matrix of the other. The domain size increase with time progresses, this phenomenon of coarsening or ripening was originally described by Ostwald. The process of Ostwald ripening consists of the growth of larger domains at the expense of smaller domains to reduce the total surface energy in a demixed system. Several authors have examined the problem and have from their different perspectives, come up with similar results

concerning the rate of growth of the domains, and the overall shape of the distribution of domain sizes.

The growth of the larger domains at the expense of smaller domains to reduce the total surface energy in a demixed system has been studied by several authors. A review of this theory and modern developments has been carried out by Voorhees [104,105]. The growth rate of the domains may be written in the from:

$$\bar{r}_{(t)}^3 = \bar{r}_{(0)}^3 + Kt \qquad (3.14)$$

where $\bar{r}_{(t)}$ and $\bar{r}_{(0)}$ are the number average domain radii at times t and t=0 (where zero time is defined as the time when the measurement of long term coarsening begins) and K is a constant which is independent of the volume fraction of the coarsening phase.

The phenomenon of ripening of phase separated regions in polyolefin blends has been studied by Mirabella et al. [58,59]. The influence of phase separation upon the blend system of hydrogenated polybutadiene (HPB) with HDPE and impact polypropylene copolymers system with 17.6wt% ethylene-propylene rubber (EPR) shown that the average volume (mean size) of the phase separated domains obtained from Scanning Electron Microscopy (SEM) was found to increase with the cube root of storage time in the melt that agree with Ostwald ripening theory.

Hill and Barham [60] have studied the coarsening of phase-separated domains in a molten blend of two ethylene-octene copolymers. The blends containing 10% of the 2 mol% octene copolymer with 90% of the 8 mol% octene copolymer were held in the melt for various times at the temperature of 180^{o}C at which phase separation was known to take place and then rapidly quenched. Transmission electron microscopy (TEM) was used to measure the diameters of the region rich in 2mol% copolymer; the diameters linearly increased with the cube root of time in the melt. The results showed that phase separation occured in melts of a system containing two octene copolymers of differing octene content. The phase-separated domains in the system coarsen during storage in the phase-separated region of the phase diagram. The coarsening mechanism has also been found in commercial block propylene ethylene block

copolymer by Hay and Feng [61]. They found that the size of the discrete domains of the ethylene-propylene rubber, within the copolymer, increased with storage time in the melt followed the Ostwald ripening mechanism.

3.4 Characterisation of Polyolefin Blends

In a practical sense, miscibility means that the systems appears to be homogeneous in the type of test applied in the study, i.e. it is defined in terms of degree of dispersion. There are many methods use to study miscibility. The length-scales over which experimental techniques are used to study polymer blends are shown in Figure 3.3.

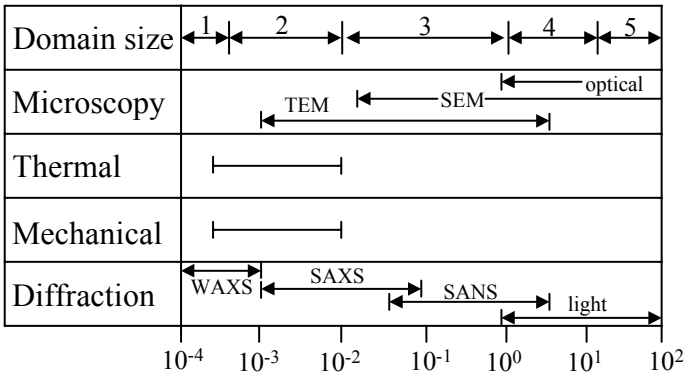

Figure 3.3 Approximate length-scale ranges of experimental techniques used to study blend morphology and structure: (1) inter-atomic; (2) molecular, spherulites; (3) filler aggregates, compatibilized blends; (4) reinforcements, noncompatible blends; (5) voids.

3.4.1 Scattering methods

These methods have been used to determine the miscibility of polymer blends [62-64]. The phase separation temperature and the "cloud point" temperature at which light scattering intensity increases, indicates the onset of liquid-liquid phase separation (LLPS). For polyolefins, the sizes of refractive index fluctuations caused by phase separation of chemically similar saturated hydrocarbons is small, and therefore the

cloud point technique has been employed less successfully with polyolefin blends than for other systems.

3.4.1.1 SAXS and SANS

Small angle X-ray scattering (SAXS) and small angle neutron scattering (SANS) has been used with increasing frequency to study polymer blend structure. The principles of SAXS and SANS are similar to that of light scattering but X-ray and neutrons are used, respectively, as the radiation sources. Light, X-ray, and neutron scattering depend on differences in refractive indices, electron densities, and atomic number, respectively. These techniques complement each other; e.g., SAXS and SANS have been used to investigate the solid-state morphology of HDPE / LDPE blends. The authors concluded that the blends are homogeneous in the melt as demonstrated by SANS using the contrast obtained by deuterating the linear polymer and heterogeneous in the solid-state due to the formation of separate HDPE and LDPE lamellae, as indicated by two-peak SAXS curves [65].

3.4.2 Measurement of the polymer / polymer interaction parameter, χ_{ij}

SANS and SAXS has been used to determine χ_{ij} and have already been discussed. χ_{ij} can be determined from the melting point depression (T_m). T_m depends on the crystalline type and size; χ_{ij} is also a function of the independent variables: temperature (T), pressure (P), and mole fraction (ϕ). T_m depression is taken as one of the signs of "compatibility" as shown in Table 3.1.

3.4.3 Indirect methods

Methods for determination of polymer / polymer miscibility will be divided into three parts: 1.Glass transition temperature, 2. Spectroscopy, and 3. Microscopy.

3.4.3.1 Glass transition temperature (T_g)

In polymers, the glass transition is related to cooperative segmental motion. A traditional method sometimes applied to polyolefin blends is the determination of the glass transition temperature, T_g. Two-phase blends have two T_g's while

completely miscible systems have a single, intermediate T_g. There are many techniques that may be employed to find T_g such as calorimetry or dynamic mechanical analysis (DMA).

Table 3.1 Melting point depression in polymer blends [20]

No.	Polymer 1	Polymer 2	T(^{0}C)	Observation
1	Polybutylene terephthalate	Aromatic polyester,CP-350 Styrene copolymer	218-226	Miscible
2	Polyethylene oxide	Styrene copolymer	50-58	Miscibility decreases With concentration of OH in copolymer.
3	Polyamide	Epoxy	140-153	Three phases
4	Polyvinylchloride and Poly(35%vinylchloride-co-vinylidene chloride),35% vinylchloride (Saran)	Poly(acrylonitrile-co-buta- diene) 30 and 40% of acrylonitrile, AN	140-152	Miscible ternary blends containing 40% AN; partially miscible for 30% AN
5	Poly-ε-carpolactone	Poly(styrene-co-acrylonitrile)	55,64	Miscible for 8.45 AN(wt%) 29.6
6	Polyethylene (low density, LDPE)	Polystyrene, PS	71,101	Two melting peak located at temperatures dependent on mixing method immiscible
7	Polyethylene oxide	Poly(vinylacetate)	39-68	χ_{12} = -0.18 at 65 ^{0}C limited miscibility
8	Polyethylene (low density and linera low density, or LDPE and LLDPE, respectively)	Polyethylene (high density, HDPE)	109-134	Blend HDPE / LLDPE compatible, that with LDPE incompatible
9	Aromatic polyether-ester-amide	Poly(ε-carpolactam)	215-220	Miscible, strong mutual effects of these polymers on kinetics of crystallisation
10	Aromatic polyesters	Chlorinated polymer	125-268	Miscibility window in terms or the chlorine content vs. number of CH_2-per-COO-group was defined

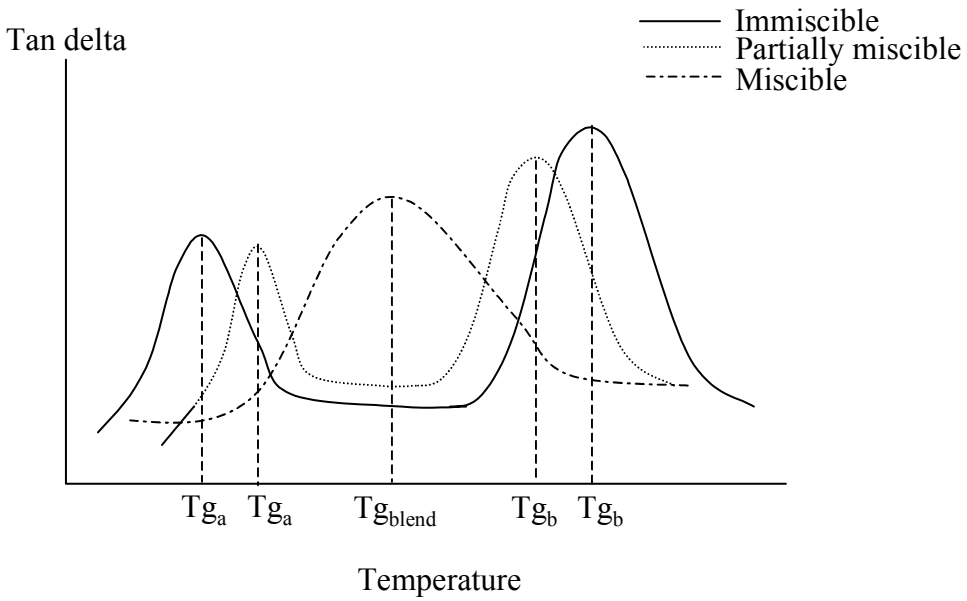

Figure 3.4 Dynamic mechanical analysis (DMA) traces for three types of polymer blend.

3.4.3.2 Nuclear magnetic resonance (NMR)

Spectroscopic methods are important for the study of interactions in polymer blends. Mirabella et al. [66] used NMR to analyse a blend of PP and EPR. Resonance intensities were reported to be proportional to the phase volume fractions, and chemical shift differences were said to be sensitive to domain size differences.

3.4.3.3 Microscopy

In polymer blends, microscopy has been applied with other techniques to determined the miscibility from and observation the blend morphology. The microscopy methods can be divided into two categories: optical or light microscopy (OM), and scanning electron microscopy (SEM) and transmission electron microscopy (TEM). Before samples can be observed, specific sample preparations must be carried out: viz., staining, swelling, sectioning, fracturing, or etching.

Table 3.2 Microscopy methods

No.	Parameter	Units	Optical Microscopy (OM)	Scanning Microscopy (SEM)	Transmission Microscopy (TEM)
1	Magnification	(time)×	1 to 500	5 to 10	10^2 to 5.10^6
2	Resolution	nm	500 to 1000	5 to 10	0.1 to 0.2
3	Field depth	μm	~ 1 (at high magn.)	10 to 100	~ 100
4	Field size	μm	10^3 to 10^5	1 to 10^4	0.1 to 100
5	Specimen	---	solid or liquid	solid	solid

The coarsening in polyethylene / hydrogenated polybutadiene blends could be observed using an optical microscope. It was found that optical contrast was very weak in the liquid state, though it was possible to resolve fairly large spherical domains comprising HPB droplets, which were unchanged by cooling to crystallise the PE matrix [67].

SEM is the most popular method used to observe the phase morphology of polymer blends, because of the rapidity of sample preparation and the range of readily accessible magnifications. In the study of the phase separation in melt blends of polyethylene and copolymers, SEM was used to observe the morphology of quenched and etched sample [68, 69].

TEM has higher resolution than the other microscopy techniques, but sample preparation is more tedious and exacting. The specimens have to be stained with electron dense atoms such as those found in OsO_4 and RuO_4 to enhanced phase contrast. TEM was used to study the miscibility of polymer blends combined with other methods such as scattering techniques [53-55].

3.5 Introduction of General Fracture Mechanics

The basic concept of the fracture mechanics is the imbalance between the energy needed to continue enlargement of a crack and the energy available from the work of external forces and internal elastic strain energy. This basic concept and related

equations were developed by Griffith [70], with some amendments three years later. Griffith only considered materials which behaved in a linear-elastic manner up to or almost up to the point of fracture. Later workers modified Griffith's theory to deal with more ductile materials, which nevertheless behaved elastically except when very close to the growing crack. Within this limitation, the subject was referred to as linear elastic fracture mechanics (LEFM). When dealing with more ductile materials, such as many polymers, the basic criteria have to be modified, and at a later stage the methods of elastoplastic fracture mechanics were developed.

A crack in a solid can be deformed in more than one way. Three modes of deformation can be distinguished. The cracks that is loaded in the normal direction is referred to as Mode I. Shear within the plane of the material gives the Mode II or sliding mode, while out of plane shear gives Mode III or shearing modes. Mode I is the only one that will be considered in this thesis.

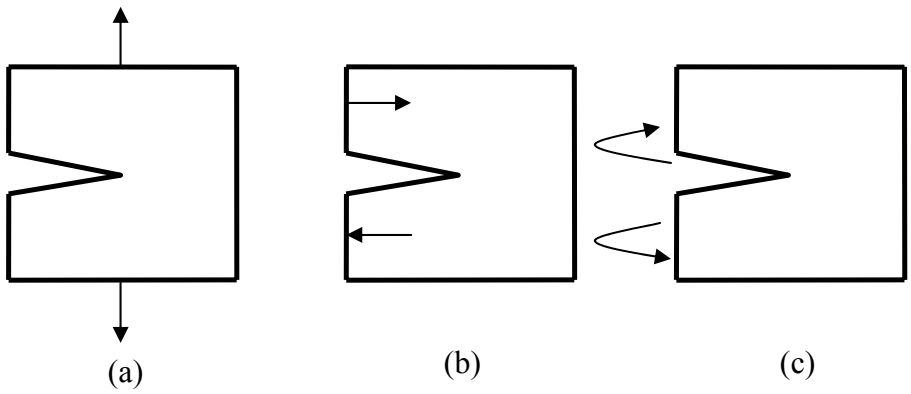

Figure 3.5 Three crack opening modes can be distinguished. Mode I, tensile mode (a), Mode II, sliding mode (b) and Mode III, shearing mode (c). The arrows represent load direction.

3.5.1 Linear elastic fracture mechanics (LEFM)

Consider a sheet of materials that behaves in linear elastic manner and contains a crack of length 2a extends right through an infinite elastic flat plate of small thickness b. [Figure 3.6] The plate is loaded by a uniform tensile stress, σ, normal to the crack. From equilibrium, take an origin at one crack tip with x and y axes parrallel and

perpendicular to the plane of the crack and within the plane of the sheet [Figure 3.6]. Any position in the sheet can be described in terms of its polar co-ordinates r and θ and the stresses on a small element at that point are normal stresses σ_x and σ_y and shear stress τ_{xy}.

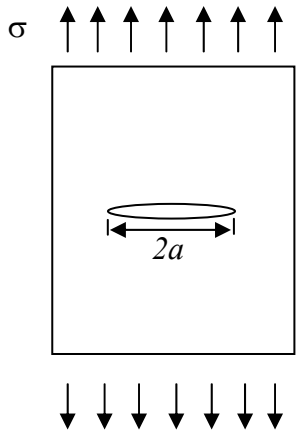

Figure 3.6 Sheet of material that has finite width and contains a crack of length 2a.

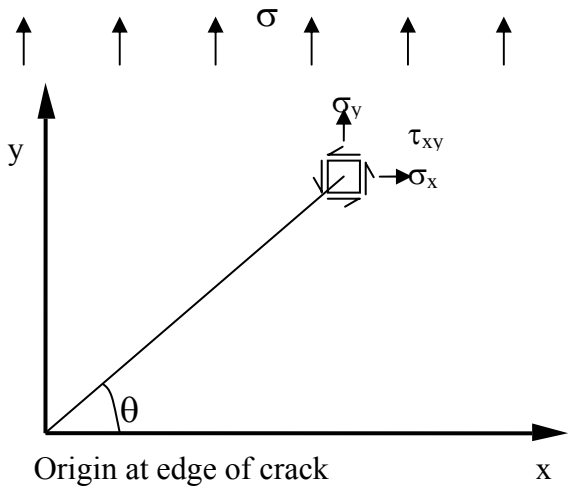

Figure 3.7 Co-ordinate system in vicinity of crack tip.

The stress distribution has been solved

$$\sigma_x = \sigma\sqrt{\frac{h}{2r}}\cos\frac{\theta}{2}\left(1-\sin\frac{\theta}{2}\sin\frac{3\theta}{2}\right)$$

$$\sigma_y = \sigma\sqrt{\frac{h}{2r}}\cos\frac{\theta}{2}\left(1+\sin\frac{\theta}{2}\sin\frac{3\theta}{2}\right)$$

$$\tau_{xy} = \sigma\sqrt{\frac{h}{2r}}\sin\frac{\theta}{2}\cos\frac{\theta}{2}\cos\frac{3\theta}{2} \qquad (3.15)$$

The stress components (equation (3.15)) are of the general form :

stress component = constant (K) × function of element location (r, θ)

The constant is termed the stress intensity factor and embodies the geometry is denoted by K_I. The subscripts refers to the Mode I loading conditions. The stress intensity factor is a measure of the stress singularlity at the crack tip, i.e., it characterizes the stress distribution near the tip. The dimensions of K are stress × length $^{1/2}$. Also its value depends upon both crack size and the general stress level.

3.5.2 Plane stress and plane strain conditions

In a thin sheet there will be plane stress conditions, while in a thick sheet the condition approximates to plain strain. The ratio of stress to strain for elastic behaviour, i.e., the apparent modulus, is greater in plane strain than in plane stress, given by

$$E' = E/(1-\nu^2) \qquad (3.16)$$

where E is Young's modulus and ν is Poisson's ratio.

Typically, in a thin sheet, failure occurs by shear through the materials on 45^o plane. Even if a crack starts perpendicular to the plane of the sheet, it tends to rotate to the 45^o configuration and fail by Mode III shearing. The force per unit length of crack to cause failure must have a component in the plane of the crack equal to the shear stress of the material times the width of crack surface. The strain failure is also the width of crack surface. Hence, the work done to extend the crack by unit length will be

proportional to the square of the thickness, or the work per unit length per unit thickness is proportional to thickness. Hence the apparent value of K_c should increase with increasing sheet thickness.

As thicker plates are considered, the plain strain region will occupy a progressively greater fraction of the total thickness. In this region, the plastic zone is smaller in extent and the fracture surface remains perpendicular to the plane of the plate. In the plain strain region, less plastic flow occurs and therefore, less plastic work is expended in forming the crack surface. K_c, which initially rises in a linear manner with thickness and will increase at a decreasing rate as the plate thickness is increased pass through a maximum and then fall asymptotically to the plain strain fracture toughness K_{Ic}. Therefore K_c is a function of material and plate thickness, K_{Ic} is a material property.

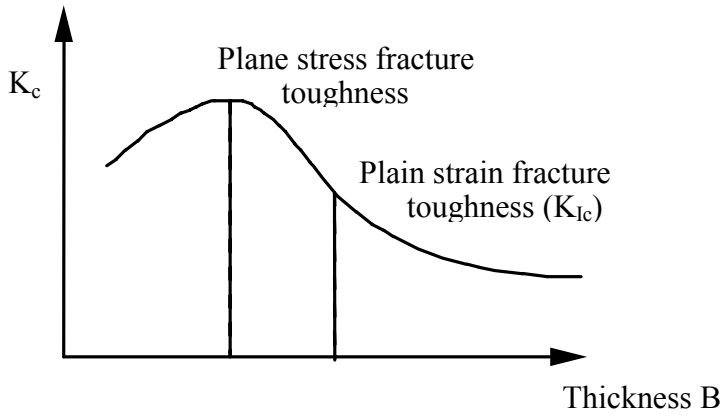

Figure 3.8 Typical variation of K_c with materials thickness.

3.5.3 Crack tip opening displacement

In cases where linear elastic fracture mechanics is not applicable and significant plasticity occurs, the fracture process is controlled primarily by the extent of plastic deformation close to the crack tip and the separation of the crack faces is presumably a measure of this deformation. If the material has a high fracture toughness, the stress that would be predicted to cause fracture may be greater than the yield stress, and

general yielding will occur before fracture can take place, so that no measurement of K_{Ic} is possible.

Consider a plate specimen of width W containing an internal crack of length 2h. As the load is increased, plastic flow will spread from the crack tip across the entire remaining section before fracture starts. The net stress on the uncracked portion will be

$$\sigma_{net} = \frac{W}{W - 2h}\sigma > \sigma_{ys} \tag{3.17}$$

A measure of the plastic strain at the crack tip is known as the crack tip opening displacement (CTOD). Wells [71] proposed that once a critical CTOD is exceeded, fracture will occur. It can be calculated that under linear elastic conditions.

$$CTOD = \frac{4}{\pi}\frac{K_I^2}{E\sigma_{ys}} \tag{3.18}$$

In the case of LEFM, fracture occurs if K_I equals K_{Ic} which implies a constant value for the critical CTOD.

For a simpler analysis, if the crack opens by a distance δ before failure, then to a first approximation the work done will be $\sigma_{ys}\delta$ per unit area of crack surface. Wells [71] pointed out, therefore

$$G_r = \sigma_{ys}\delta \tag{3.19}$$

whereas from equation (3.18)

$$G_r = \frac{\pi}{4}\sigma_{ys}\delta \tag{3.20}$$

More refined models give values for the numerical factor which differ slightly.

$$CTOD = \frac{G_I}{\lambda_p \sigma_{ys}} = \frac{K_I^2}{E\lambda_p \sigma_{ys}} \tag{3.21}$$

In general it can be shown that

$$CTOD = \frac{K_I^2\left(1-\nu^2\right)}{E\lambda_p \sigma_{ys}} \tag{3.22}$$

The value of the constant λ_p depends upon the plastic constraint at the crack tip. Various authors give values between 1 and 2.3. Careful experimental measurements give values near unity.

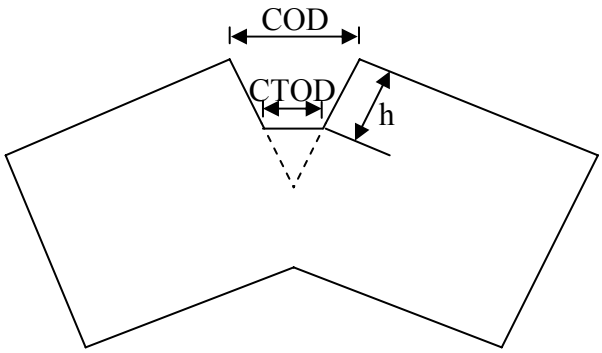

Figure 3.9 Schematic sketch illustrating the determination of COD and CTOD.

3.5.4 Essential work of fracture method (EWF)

The EWF is a methodology to characterize the fracture toughness of polymers films, ductile metals, paper sheets and fibrous composites under plane stress conditions [72-74]. The simplicity of the EWF approach is the main reason why the method has gained so much popularity in recent years for evaluation of fracture toughness of ductile polymers as a simpler alternative to J-integral analysis. The experimental measurement of the EWF is fairly easy since it simply consists of

the determination of the total fracture energy of several samples differing in initial ligament length, and the linear regression of these data.

It is of interest in many cases to characterize the fracture toughness under plane strain conditions and to extend the EWF methodology to conditions other than plane stress. This topic has been extensively studied during recent years with results published on the applicability of the EWF to the plane stress / plane strain transition and pure plane strain regimes [75,76] and high-rate impact testing [77,78]. The EWF methodology can be applied to conditions other than pure plane stress, provided the specimen ligament is fully yielded at initiation in geometrically similar specimens. Under these conditions, the specific EWF is a material constant and independent of the specimen geometry, but not necessarily independent of thickness. However, whether the requirements have been completely satisfied has not always been strictly demonstrated.

3.5.4.1 The essential work of fracture methodology

The EWF method was originally suggested by Broberg [73] in order to characterise the fracture behaviour of ductile materials, and then developed by Mai and Cotterell [79] for ductile metals. It has been used recently to evaluate the fracture parameters of different polymers by many authors [106-115], but some aspects of this technique still remain controversial, such as the thickness influence on the fracture properties.

According to Broberg, when a ductile material, which contains a crack is loaded, the total work of fracture (W_f) may be divided into two terms: the essential work of fracture (W_e) (or fracture process zone) and the nonessential (or plastic zone) work of fracture (W_p). The former corresponds to the instability in the crack tip - the real fracture process region - and the latter to the yielding in the surrounding region. Thus, the total work of fracture can be written in the following way:

$$W_f = W_e + W_p = w_e l t + w_p \beta l^2 t \qquad (3.23)$$

where w_e is the specific essential work of fracture (per ligament area unit),

w_p is the specific nonessential work of fracture (per volume unit),

l is the ligament length, t is the specimen thickness

and β is a dimensionless factor that describes the plastic zone size.

The specific work of fracture, i.e. the work of fracture per unit ligament area, is:

$$w_f = W_f/lt = w_e + \beta w_p l \tag{3.24}$$

Assuming that w_e is a material parameter and that w_p and β are independent of l, when w_f is plotted as a function of l, according to equation (3.24). There should be a linear relationship between w_f and l. By extrapolating this straight line to a ligament length (l) equal to zero, w_e can be determined by the intersection of the straight line and the Y axis. The slope of this straight line yields βw_p. However, if β changes with the geometry of the fracture process zone and with the initial crack length, a linear relation between w_f and l can only be achieved if the geometrical similarity is maintained for all the ligament lengths.

Application of the EWF method to determine fracture toughness using the above equations depends on four assumptions:

1. Before the crack begins, the ligament must be totally yielded.
2. For (w_e) and (βw_p) to remain constant and independent of the ligament length, the equations apply in theory to the biaxial condition (plane stress). Thus, the linear relation between w_f and l may be invalid if the fracture occurs in a biaxial / triaxial transition region (plane stress / plane strain).
3. There must be a geometrical similarity among test specimens with different ligament lengths during crack propagation, as illustrated in the load vs. elongation diagrams.
4. The fracture process zone volume involving the ligament must be proportional to the square of the length of the ligament l. The β parameter relative to the shape of the fracture process zone may be $\pi/4$ (circular). $\pi h/4l$ (elliptical) or $h/2l$ (diamond-shaped) ,according to the ESIS protocal for EWF measures.

There have been a number of reports in the literature concerning the fracture toughness of polyolefins, while fewer published studies have described fracture in polyolefin blends. Swei et al. [80] investigated the fracture toughness of polyethylene using J-integral analysis in thick sections. It was reported that for samples with lower toughness levels, crack propagation involved crazing ahead of the advancing crack and that toughness was also imparted by the formation of shear bands near the notch tip. In the toughest materials, response to crack propagation was by general yielding and blunting of the notch tip. Wu and Mai [73] reported that while the J-integral method could not be used for testing a thin, ductile polymer film, it was shown that the specific essential work of fracture is a material constant, independent of sample geometry, and equivalent to the J-integral method. Casellas et al. [81] used the essential work of fracture method to characterise fracture in compression-moulded sheets of low and linear-low-density polyethylene. The crystallinity, molecular weight, degree of structural continuity and β-relaxation process were found to affect toughness. Pegoretti et al. [82] and Yokoyama and Ricco [83] studied the fracture toughness of rubber toughened polypropylene vacuum formings and injection moulded plaques using the essential work of fracture method. The materials were oriented through the vacuum forming process. It was found that the fracture resistance for cracks propagating along the drawing direction was reduced by the presence of dispersed rubber particles in comparison with the unblended polypropylene. For cracks running in the transverse direction to the drawing direction, the elastomer domains increased the fracture toughness. Rhee and Crist [84] investigated the relationship between phase behaviour, morphology, and fracture toughness in polyethylene-copolymer blends. Binary blends of polyethylene PE and 5-10% of HPB were used. It was reported that slowly cooled samples of melt miscible-blends were tougher than unblended PE and blends with dispersed amorphous domains. Enhanced toughness is associated with nonuniform morphology formed on slow cooling one phase melts composed of chain with different amounts of branching. Tensile properties were relatively unaffected by blending under the conditions investigated.

CHAPTER 4
MATERIALS AND METHODS

The preparation and characterisation techniques employed in this work are outlined in this chapter.

4.1 Chemical Reagents and Materials

The chemical reagents and materials used for this study are given in Table 4.1

Table 4.1 The chemical reagents and materials used for this study

Chemical reagents / Materials	**Trade name / Grade**	**Suppliers**
Polyethylene	H5814J	TPE Co., Ltd
Poly(ethylene-co-1-octene)	Engage8150	Dow-Chemicals
Poly(ethylene-co-1-butene)	Catalogue No. 43,469-8	Aldrich Chemicals
Potassium permanganate	Analytical Reagent	Fluka
Sulfuric acid (conc.)	Analytical Reagent	Merck
Orthophosphoric acid	Analytical Reagent	Merck
Hydrogen peroxide (30%)	Analytical Reagent	Merck
Rhuthenium oxide hydrate	Analytical Reagent	Fluka
Sodium periodate	Analytical Reagent	Fluka

4.2 Instruments

The instruments and manufacturers of the instruments that were used for this study are shown in Table 4.2.

Table 4.2 Instrument and manufacturers of instruments used in the present study

Instrument	Manufacturer and Model
Co-rotating twin screw extruder	Prism TSE 16TC
Injection moulder	DR. Boy 22S
Compression moulder	Wabash Genesis Series Hydraulic Press Model G 30 H
Ultramicrotome	RMC MT-7
Scanning electron microscope	Hitachi S-2500, Jeol JSM 5410
Transmission electron microscope	Hitachi H-300
Differential scanning calorimeter	Perkin Elmer DSC2, DSC7
Dynamic mechanical thermal analysis	A Polymer Laboratories Ltd. Dynamic Mechanical Thermal Analyser MK II
Microscope tensile tester	A Polymer Laboratories Ltd. Miniaturized material testing apparatus (MiniMat)
Charpy impact tester	Zwick 5102

4.3 Characterisation Methods

4.3.1 Dynamic mechanical analysis (DMA)

The samples were sectioned from the skins of the injection mouldings using a microtome. Analyses were carried out in tensile mode with a frequency of 10 Hz and heating rate of 5°C/min using a DMTA mkII thermal analyser from Polymer Laboratories Ltd.

4.3.2 Differential scanning calorimetry (DSC)

Differential scanning calorimetry (DSC) data were obtained with a Perkin Elmer DSC7 instrument: specimens (10 mg ± 0.1 mg) were cut from the central core of the mouldings and dipped in silicone oil to ensure rapid heat transfer to the specimens. Fusion endotherms were obtained at a heating rate of 30°C/min, to limit annealing during heating, under a nitrogen atmosphere.

4.3.3 Transmission electron microscopy (TEM)

TEM micrographs were obtained from material at the skin and cores of the mouldings. The samples were flattened using an RMC Ultramicrotome at –100°C and then stained in sealed tubes above a RuO_4 solution at 60°C for 1 h. The staining procedure was repeated three times using fresh reagent. Finally, sections of around 70 nm thickness were obtained from the stained samples through ultramicrotomy at room temperature. Sections were floated onto copper grids and were observed using an Hitachi H-300 microscope.

4.3.4 Scanning electron microscopy (SEM)

Surfaces of the samples were flattened using the ultramicrotome at –100°C were etched by immersion in permanganic acid for 24 h at 30°C, coated with platinum-palladium alloy, and viewed using an Hitachi S-2360N scanning electron microscope to obtain the number of spherulites per unit area in the cross-section.

4.4 Part 1: Melt Flow Induced Phase Morphology of PE / EOC Blends

4.4.1 Sample preparation

The PE used was obtained from the Thai Polyethylene Co., Ltd., Thailand. It had a melt flow index of 18 g/10min. The EOC, manufactured by Dow-Dupont Elastomers using a single site catalyst, had a melt flow index of 0.5 g/10min, melting point ≈ 50°C; it contained 7 mol% of octene and long chain branching. PE / EOC blends (72:28 wt%) were prepared either through melt blending using a Prism 16 mm twin screw extruder, employing a barrel temperature of 180°C and screw speed of 175 rpm, or through solvent blending. In the latter case, the resins were dissolved in boiling toluene under nitrogen and then precipitated by pouring into excess methanol. The BS 2782: Part 3, method 320A tensile specimens were prepared from the melt-blends using a Dr Boy 22S injection moulder, with barrel temperatures of 170 or 230°C; the screw speed was 100 min^{-1}, the back pressure was zero, and the cycle time was

approximately 30 s. Selected mouldings and the solution blends were annealed in an oil bath, after wrapping in aluminium foil, for 15 min and 6 hr, respectively; the temperatures used were 170 and 230°C. Specimens, ≈ 15 μm in thickness, for dynamic mechanical analysis (DMA) were sectioned from the skins of the injection mouldings using a microtome**.**

4.5 Part 2: Effect of Phase Morphology Upon the Toughness Properties of PE / EOC Blends

4.5.1 Sample preparation

The resins used were PE possessing a melt flow index of 14 g/10min and EOC with a melt flow index of 0.5 g/10min. The samples were prepared using a Prism 16 mm twin-screw extruder at a barrel temperature of 180°C and screw speed of 175 rpm. Volume and weight fraction concentrations were inter-converted based upon the resin densities at 25°C, shown in Table 5.1. Specimens of varying composition were annealed in an oil bath, after wrapping in aluminium foil, for 6 hrs at temperatures in the range 150 to 250°C. For higher temperatures, the specimens were heated in a tube furnace under nitrogen flow for 1 hr. A thermocouple was inserted in the sample to monitor the temperature. Compression mouldings were prepared by firstly forming the specimens in an injection mould at 170 or 230°C followed by annealing for 5 min under atmospheric pressure on a compression platen at the same temperature. Finally, the mould was rapidly transferred to a water-cooled press at approximately 30°C and 150 psi.

4.6 Part 3: The Influence of Orientation During Processing Upon the Fracture Toughness of PE / EOC Blends

4.6.1 Sample preparation

The PE had a melt flow index of 14 g/10min, weight average molecular weight, M_w, 48,000 g/mol, and nominal density of 0.962 g/cc. The copolymer used, EOC, had

a melt flow index of 0.5 g/10min, M_w = 162,700, M_w/M_n = 2, and density 0.868 g/cc; it contained 7 mol% octene.

PE / EOC blends, containing 0, 5, and 10 vol% of EOC, were prepared with a Prism 16 mm twin screw extruder at a barrel temperature in all zones of 170°C and screw speed of 175 rpm. Sheets, nominally 400 μm in thickness, were prepared using a Collin 35 mm single screw extruder fitted with a coat-hanger die. The temperature profile was 170°C, die, 170°C, adapter, and 170, 170, 165, and 145°C in the barrel zones 4 to 1, respectively. Barrel zones were cooled with blown air. The screw speed was 90 rpm and the chill roller, set at 50°C, was operated at 4.4 rpm.

4.6.1.1.Double edge notched specimens

Double edge notched specimens (length 200 mm and width 50 mm) were prepared from the sheets for fracture toughness testing as shown in figure 4.1 , where TD and MD refer to the transverse and the machine direction, respectively. Results from tests upon these specimens will be referred to by the direction of travel of the crack propagation. That is, for specimen type-A the crack propagates in the machine direction; with specimen type-B, the crack propagates in the transverse direction.

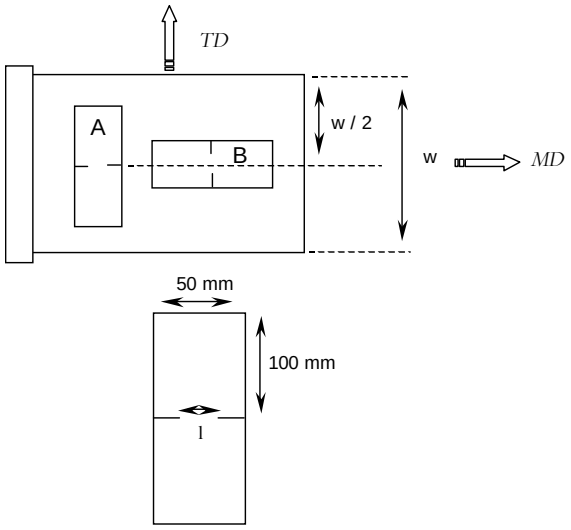

Figure 4.1 Fracture toughness specimens from the sheet extrusion material; A and B are the fracture toughness specimens, l is the ligament length, and w is the sheet width.

4.6.2 Characterisation

4.6.2.1 X-ray analysis

Wide-angle X-ray diffraction measurements were made using nickel-filtered CuK_α radiation using a Bruker powder X-ray diffractometer (model D8 advance) operated at 40 kV and 40 mA. All scans were recorded using the transmission mode. The azimuthal scans of (200) and (020) plane reflections (diffraction angle $°2\theta = 23.9$ and 36.3°, respectively) for poly(ethylene-co-1-octene) and polyethylene blends were carried out at a scan speed of $3°min^{-1}$.

4.6.2.2 Differential scanning calorimetry (DSC)

Differential scanning calorimetry (DSC) data were obtained with a Perkin Elmer DSC7 instrument: specimens (5 mg ± 0.1 mg) were cut from the sheet samples dipped in silicone oil to ensure rapid heat transfer to the specimens. Fusion endotherms were obtained at a heating rate of 10°C/min under a nitrogen atmosphere.

4.6.3 Testing

4.6.3.1 Fracture toughness test

Fracture toughness tests were conducted at room temperature (nominally 25°C) using an Instron 4301 tensile tester at an extension rate of 5 mm/min. All samples were notched using a razor on both sides of the sample in the centre of the sample length). The notches were made perpendicular to the tensile direction, obtaining 20 specimens of each sample set with ligament lengths in the range 15 to 23 mm. Load-displacement curves were recorded and the absorbed energy was calculated from the weight of loads-displacement papers.

4.6.3.2 Tensile test

Tensile tests were carried out using an Instron 4301 tensile tester at an extension rate of 5 mm/min upon dumbbell samples punch in the MD and TD of the sheet.

4.7 Part 4: The Effect of Compounding Upon Fracture Toughness of PE / ECB and PE / EOC Blends

4.7.1 Sample preparation

PE, supplied from Thai Polyethylene Co. (product code H5814J) was compounded with 15% by weight of EOC from Dow Chemical (product code Engage 8150) using two different methods. First, by single screw extruder at processing temperatures of 170 and 220^{o}C and a screw speed of 20 rpm. Other samples were compounded using twin screw extrusion at screw speed 100 rpm and then single screw extrusion at 170 and 220^{o}C and screw speed of 20 rpm. The blend samples of PE and 15% by weight of poly(ethylene-co-1-butene) (ECB) from Aldrich chemical (catalogue number; 43,469-8) were prepared under the same conditions. After compounding, the extrudates were annealed by compression moulding at 170^{o}C for 3 and 15 minutes and then cooled by water to produce the polymer blend sheet samples.

4.7.2 Characterisation

4.7.2.1 Scanning electron microscopy (SEM)

A Jeol JSM 5410 scanning electron microscope was used to observe the morphology of polymer samples. The polymer samples were prepared by cutting the surface with a cryo-ultramicrotome at a temperature of -80^{o}C to give a flat surface and then etched by permanganic acid for 18 hours. A coating of gold was applied by using a Polaron E500 vapour deposition device to prevent charging of polymer samples within the electron beam.

4.7.2.2 Differential scanning calorimetry (DSC)

Differential scanning calorimetry (DSC) data were obtained with a Perkin Elmer DSC2 instrument: specimens (5 mg ± 0.1 mg) were cut from the sheet samples. Fusion endotherms were obtained at a heating rate of 5°C/min,. The calorimetry was operated under a nitrogen flow 20 cm^3 min^{-1}. The temperature of the calorimeter was calibrated

from the observed melting points of ultra-pure materials-stearic acid, indium and tin at the heating rates of 10, 5 and 2.5 K min^{-1} and then extrapolated to zero heating rate to correct for thermal lag.

4.7.3 Testing

4.7.3.1 Microscope tensile test

A Polymer Laboratories Ltd. Miniaturized material testing apparatus, referred to as the minimat. The operations of the minimat were controlled by a PC computer. The television camera, JVC TK1085E was used to take images of the polymer specimens for looking at the crack behaviour of polymer samples; images were recorded to a VHS video recorder, Panasonic NVF 590B. The tests were divided into two parts. First, the polymer samples in rectangular shape 1 cm × 4 cm were notched at the centre by 3mm and vary the notch length by varied 2, 3, 4, 5, 6, 7 and 8 mm at an extension rate of 10 mm/min.

4.7.3.2 Dynamic mechanical analysis (DMA)

The samples were cut from the compression moulded samples in rectangular shape 1 cm × 4 cm. Analyses were carried out in bending mode with a frequency of 1 Hz and heating rate of 2°C/min using a DMTA mkII thermal analyser from Polymer Laboratories Ltd.

CHAPTER 5
RESULTS AND DISCUSSION

5.1 Part 1: Melt Flow Induced Phase Morphology of PE / EOC Blends

5.1.1 Solution blends

Figure 5.1 shows light micrographs of the solution blends after annealing at 170 and 230°C for 6 hr under quiescent conditions. At both temperatures, distinct large phase domains were visible. Banded spherulites are seen in one phase identifying it as being PE-rich.

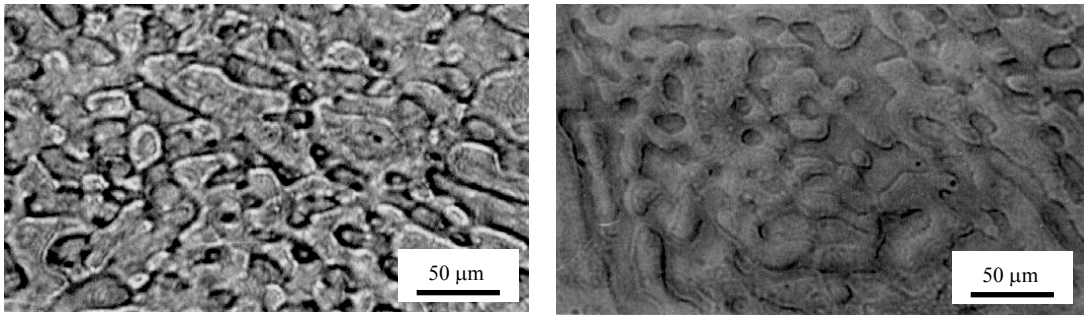

(a) (b)

Figure 5.1 Light micrographs of solution blends after annealing at (a) 170°C and (b) 230°C for 6 h.

Einstein's diffusion equation relates diffusion distance, x, to the diffusion rate, D_{app}, and the time for diffusion, t: $\overline{x^2} = 2D_{app}t$. If D_{app} is 1.1 x 10^{-10} cm^2s^{-1}, then x = 0.3 μm for a 5 s diffusion time. Given the rapid quenching, within 5 s, after annealing the morphology is too coarse for it to result from phase separation during cooling, and hence it is inferred that the melt was biphasic.

Direct observation of phase separation in the melt was not achieved, however, due to the closeness of the refractive indexes of the EOC and PE melts. In the solid state, the difference in density between the crystalline PE and the amorphous EOC provides contrast between the two phases. The area fraction of the EOC-rich phase is greater than that expected from the 28 wt%, or 30 vol% at 25°C, EOC composition of the blend. Moreover, there is connectivity between the phase domains, rather than discretely dispersed droplets. A probable explanation is that a fraction of the PE dissolves into the EOC phase thereby increasing its effective volume fraction resulting in droplet coalescence, and hence domain connectivity. These observations suggest some limited miscibility in the melt at both 170 and 230°C. The extensive branching in the EOC precludes its co-crystallisation with the PE, and therefore solid-liquid phase separation will occur as the PE crystallises, leading to heterogeneity within the phase domains observed in Figure 5.1.

5.1.2 Melt flow

An estimate of the flow history in the injection moulder was obtained through the following analysis. The power dissipated per unit volume during plasticisation, P, was taken as [85]

$$P = \eta^* (\dot{\gamma}_c)^2 \tag{5.1}$$

where η* is the complex viscosity at angular frequency, ω. It was assumed that ω = $\dot{\gamma}_c$, i.e. the steady shear rate in the channel of the screw in the metering zone: [86]

$$\dot{\gamma}_c = \pi(D - 2h)N/h \tag{5.2}$$

where D is the internal barrel diameter (24 mm), N the screw speed (100 min^{-1}), and h the screw channel depth (2 mm); thus, $\dot{\gamma}_c$ = 52 s^{-1}. For the blend, η* = 1,296 and 585 Pa.s at 170 and 230°C, respectively. Specific mechanical energy input during plasticisation, S_e, was calculated $S_e = Pt_p$, where t_p is the plasticisation time (5 s);

S_e = 17.5 MJm^{-3} at 170°C and S_e = 7.9 MJm^{-3} at 230°C. The shear rate at the wall of the nozzle, $\dot{\gamma}_N$, was estimated from [87]

$$\dot{\gamma}_N = \left(4Q/\pi r^3\right)\left(3n+1\right)/4n \tag{5.3}$$

where $n = d\lg\tau/d\lg\dot{\gamma}$, $Q = v_{T,P}m/t_I$, Q is the melt injection rate, m the shot weight (15 g), $v_{T,P}$ is the specific volume of the melt at temperature, T, and injection pressure, P (3.4 MPa), t_I is the injection time (2 s), r is the radius of the nozzle orifice (1.25 mm), τ is the shear stress at the wall, and n is the non-Newtonian exponent. Both at 230°C and 170°C, $\dot{\gamma}_N \approx$ 6,500 s^{-1}, assuming specific melt volumes of 1.27 and 1.33 cm^{3}g^{-1} for melts at 170°C and 230°C, respectively, under 3.4 MPa of pressure [88]. A description of the cooling process in the injection mouldings may be obtained using the Fourier equation for non-steady heat flow in one dimension:

$$\partial T/\partial t = \alpha\left(\partial^2 T/\partial x^2\right) \tag{5.4}$$

where T is the temperature, t is time, α is the thermal diffusivity, and x is the distance between the part of the moulding in question and the mould surface. The thermal diffusivity is related to k, the thermal conductivity, ρ, the density, and C_P, the specific heat capacity: $\alpha = k/\rho C_P$; data are given in Table 5.1.

If the cooling of the melt at the mould surface may be described by the one-sided heat conduction into a semi-infinite body and that α is constant over the temperature change, an estimate of the cooling rate may be made. Two-sided heat transfer was used to describe cooling of the core. The dimensionless Fourier parameter, F_0, is calculated $F_0 = \alpha t / x^2$. In the core, x is half the moulding thickness (x = 3.2 mm / 2); in the skin region, x is the distance from the mould surface to where the TEM sections were obtained (0.1 mm).

Table 5.1 Polymer characteristics

Parameter		Polymer			Blend
		Polyethylene (PE)	Poly(1-octene) (P1O)	Poly(ethylene-co-1-octene) (EOC)	(70/30 v_{PE}/v_{EOC})
C_∞		7.00[a]	9.10[a]	7.53[b]	-
b	(nm)	0.815	0.929	0.845	-
M_w	($gmol^{-1}$)	45,000	-	162,700	-
M_0	($gmol^{-1}$)	28.054	112.216	49.095	-
n		3,207	-	6,627	-
n_s		802	-	1,657	-
R_g	(nm)	9.4	-	14.0	12.1
r	(nm)	23.1	-	34.4	29.6
L	(nm)	-	-	-	17.1
$V_{25°C}$	(cm^3mol^{-1})	33.1[c]	130.8[c]	57.5	-
$\rho_{25°C}$	(gcm^{-3})	0.962[d]	-	0.868[d]	-
α	(m^2s^{-1}) x 10^7	1.57[e]	-	1.17[e]	1.46[f]
$D_{170°C}$	(cm^2s^{-1}) x 10^{10}	1.28	-	0.22	0.36
$D_{230°C}$	(cm^2s^{-1}) x 10^{10}	2.82	-	0.71	1.10

[a]reference; [89]

[b]data for EOC calculated from the copolymer composition weighted average of the values for PE and P1O;

[c]reference [90];

[d]typical density at 25°C;

[e]reference [91], assuming that α for EOC is equal to that of LDPE;

[f]calculated from the mass fraction weighted average of the values for PE and EOC.

A plot of the temperature gradient, ΔT, where

$$\Delta T = \left(T_{x,t} - T_{ms}\right)/\left(T_0 - T_{ms}\right) \tag{5.5}$$

against F_0 for a flat sheet was used to find F_0 at ΔT, and hence the time to reach $T_{x,t}$ may be found; [95] T_{ms} is the mould surface temperature (30°C), T_0 is the initial melt temperature (230°C or 170°C), $T_{x,t}$ is the temperature at x after time t. $T_{x,t}$ was taken as

the estimated temperature where the crystal growth rate of polyethylene is a maximum. This is [96] 5,000 μmmin^{-1} at 112°C, that is 30°C below the equilibrium melting point of 142°C. Thus, $T_{x,t}$ = 112°C, and hence for a melt temperature of 230°C, $\Delta T = 0.41$, $F_0 = 0.46$, and the time taken to reach 112°C is 8.1 s in the core and 0.03 s at the skin. For the 170°C melt temperature, the corresponding values are: $\Delta T = 0.59$, $F_0 = 0.31$, and the cooling times in the core and skin are 5.4 and 0.02 s, respectively. The crystallisation process in the core was assumed to be zeroth order three-dimensional spherulite growth. The number of spherulite nuclei in the cross-section of the core, N_A, was 1.06 x 10^{-2} μm^{-2}. This value was determined by point counting the spherulite centres in the SEM micrographs of permanganic acid etched surfaces. The number average spherulite diameter in the cross-section, D_{nA}, was 10.6 μm. The number average diameter in volume, D_{nV}, was [97]

$$D_{nV} = (4/\pi) D_{nA} \tag{5.6}$$

The number of spherulite nuclei per unit volume, N_V, was

$$N_V = N_A / D_{nV} \tag{5.7}$$

N_v = 7.9 x 10^{-4} μm^{-3}. To reach a maximum random packing fraction at impingement of the spherulites, ϕ_{max}, of $\phi_{max} \approx 0.7$, from [98]

$$\phi_{\max} = N_V \pi D_{nV}^3 / 6 \tag{5.8}$$

at a spherulite growth rate of 83 μms^{-1} the time taken was 0.07 s after 112°C was reached. The time taken for the melt to solidify is the sum of the cooling time and crystallisation time; at the end of this period, the morphology is effectively frozen-in. For the melt at 230°C, the solidification time was 8.2 s in the core and 0.10 s at the skin. The corresponding values for the 170°C melt were 5.5 and 0.09 s, respectively.

5.1.3 Flow induced morphology

Figure 5.2 displays TEM micrographs of the core regions of the as-moulded blends, prepared at 170 and 230°C, together with images of the original PE resin processed under comparable conditions.

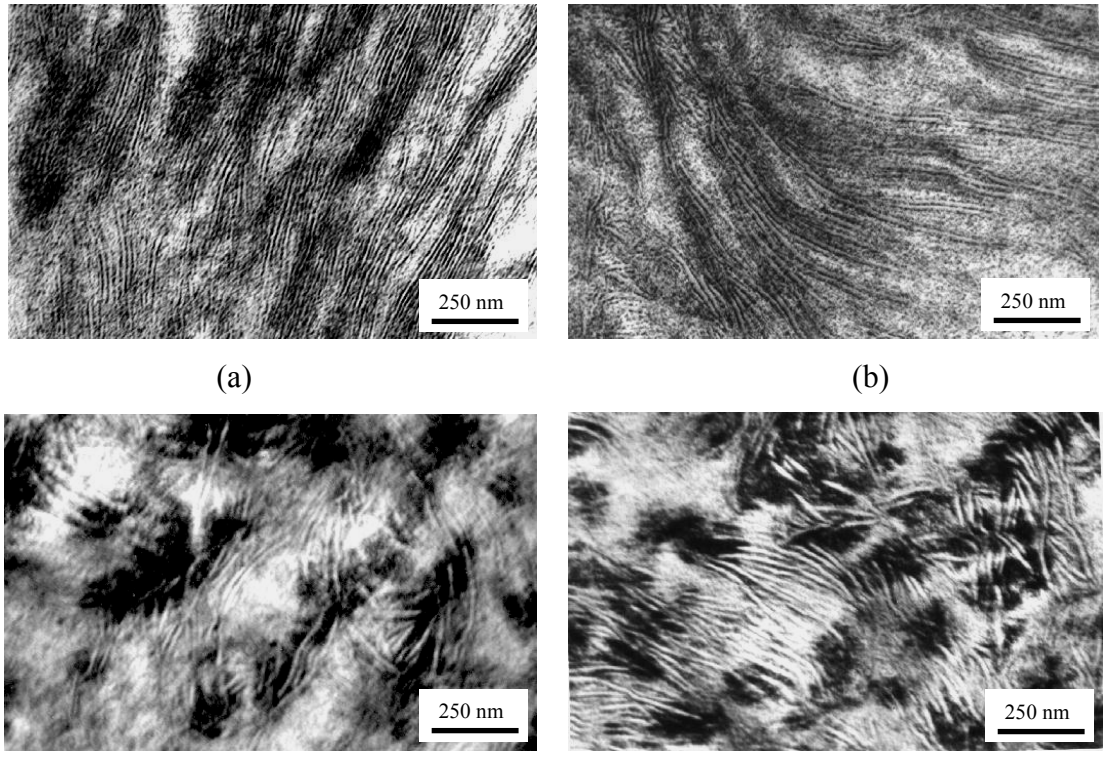

Figure 5.2 TEM micrographs of the as-moulded specimens in the core region, prepared at two temperatures: PE at (a) 170°C and (b) 230°C and the PE / EOC blend at (c) 170°C and (d) 230°C.

The near amorphous EOC constitutes the most heavily stained domains, whilst amorphous PE is more lightly stained; the PE lamellae are unstained. DMA traces of the PE resin, EOC, and the skin of a blend moulding prepared at 230°C are shown in Figure 5.3. The blend exhibits loss maxima at -115°C and -32°C that may be assigned to the glass transitions of PE and EOC, respectively. Whilst the T_g of the original PE and the PE in the blends were essentially the same, for all injection moulded blends, T_g of the EOC was 5 to 7°C higher than that of the original EOC, i.e. -37°C; moreover, the relaxation peaks were slightly broader. In some locations in the blend, the EOC is

pinned between neighbouring PE lamellae and consequently this may hinder its mobility, giving rise to the slight increase in T_g of the EOC. The peak broadening may result from the EOC being located both between the lamellae and in less confined domains that result in a distribution of local environments, each possessing different relaxation characteristics. The solid state phase domains largely comprise pure amorphous PE, pure EOC, and crystalline PE.

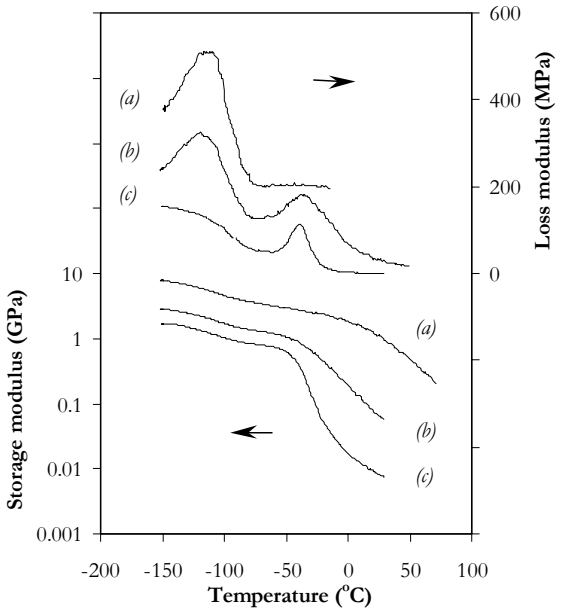

Figure 5.3 Typical DMA traces for (a) PE, (b) PE / EOC blend, and (c) EOC. The specimens were microtomed from the skins of the injection mouldings; the loss modulus curves of the blend and PE are offset from the EOC curve by +50 MPa for clarity.

In the injection-moulded blends, the EOC appears as an interconnected arrangement of globules that is intertwined with swathes of PE lamellae. The PE lamellae penetrate extensively into the EOC domains, indicating that crystals grew from, or into, a mixed phase containing both EOC and PE.

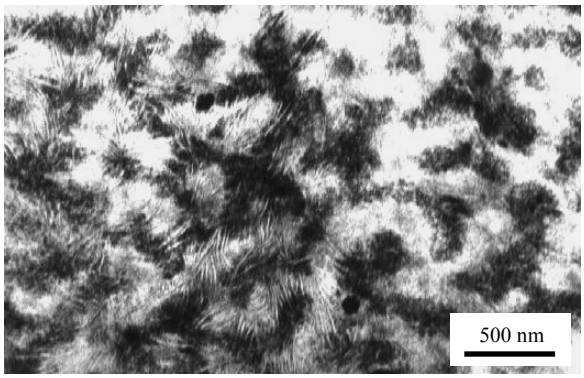

Figure 5.4 Overview of the EOC domain morphology in the core region of a blend moulded at 170°C.

The length-scale of the EOC phase domains is very fine, with an average periodic distance in the EOC-rich areas of 154 nm. This morphology is unlikely to result simply from the mechanical work of dispersive mixing, since the dynamic equilibrium of droplet break-up and coalescence confers a lower mean particle size limit for physical dispersive mixing in polymer blends of around 0.5 μm, although smaller domain are possible in reactive systems. Thus, it is inferred that the fine morphology is the product of concurrent liquid-liquid and solid-liquid phase separation from a mixed, or partially mixed melt, and hence that the flow during injection moulding enhances the miscibility of the blend. Bi-continuous morphologies are evident in the image of the core of a moulding prepared at 170°C, displayed in Figure 5.4.

The effects of the local cooling conditions in the mould are illustrated by the differences in the skin and core morphologies of the blend moulded at 230°C, shown in Figure 5.5.

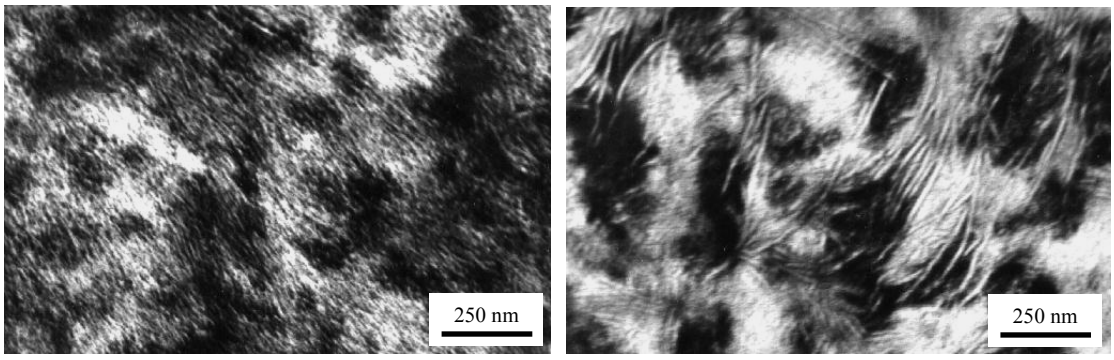

(a) (b)

Figure 5.5 TEM micrographs of (a) skin and (b) core areas of a blend moulded at 230°C.

At the skin, the EOC is more evenly distributed, whilst in the core the EOC domains are larger and more distinct from the PE-rich areas. Moreover, the PE lamellae are thinner and less well defined in the skin.

A description of the morphology evolution may be obtained through the following discussion. The statistical segment length, b, is given by

$$b = \left(C_\infty n L^2 / n_s\right)^{1/2} \tag{5.9}$$

where n is the number of backbone carbons, $n = \left(2M_w/M_0\right) - 1$, n_s is the number of statistical segments, based upon a four carbon unit, $n_s = \left(M_w/2M_0\right)$, M_w is the weight average molecular weight, M_0 is the molecular weight of the polymer repeat unit, and L is the C-C bond length (0.154 nm), and C_∞ is the characteristic ratio. R_g and r are the root mean square radius of gyration and root mean square end-to-end distance of the polymer chain: [99] $R_g = b\left(n_s/6\right)^{1/2}$ and $r = b\left(n_s\right)^{1/2}$ or $r = 6^{1/2} R_g$. These data are summarised in Table 5.1; data for the EOC were calculated from the mole-fraction weighted averages of the experimental data obtained for PE and poly(1-octene) (P1O). The radius of gyration for a mixture of polymer 1 and 2, where polymer 1 is PE and polymer 2 is EOC, is given as follows: [100]

$$R_g = \left(\frac{n_{s(1)} n_{s(2)} \left(\phi_2 b_1^2 + \phi_1 b_2^2 \right)}{6\left(\phi_1 n_{s(1)} + \phi_2 n_{s(2)} \right)} \right)^{1/2} \tag{5.10}$$

where ϕ_j is the volume fraction of polymer j. The polymer-polymer interaction length, L, is determined $L = r/3^{1/2}$; the kinetically favoured length-scale for demixing, λ_m, is related to the demixing temperature, T, and the temperature at the spinodal, T_s, from [101]

$$\lambda_m / L = 2\pi \left(3|T - T_s|/T_s \right)^{-1/2} \tag{5.11}$$

The 70:30 v_{PE}:v_{EOC} blend was found to be two-phase in the quiescent melt at all temperatures investigated, that is in the range 150 to 350°C. Limited miscibility for EOC contents of 10 vol% and lower were found at 350°C. The critical point, ϕ_2^c is

$$\phi_2^c = \left(1 + \left(\nu_2 n_2 / \nu_1 n_1 \right)^{1/2} \right)^{-1} = 0.35 \tag{5.12}$$

where v_j is the monomer volume of component j. Extrapolation of the 'cloud-point curve' to ϕ_2^c gave an approximate T_s of 400°C, the corresponding λ_m values for demixing at 230°C and 170°C would be 95 and 82 nm, respectively; that is λ_m decreases with increasing quench depth in a system with an upper critical solution temperature. The observed value of λ in the blend prepared at 230°C was 154 nm. The growth rate of fluctuations, $R_{q(t)}$, at scattering vector, q, is included in the following expression:

$$I_{q(t)} = I_{q(t=0)} \exp R_{q(t)} \tag{5.13}$$

where $q_m = 2\pi/\lambda_m$ and $I_{q(t)}$ is the Fourier component, or scattering intensity, at q and time, t. The maximum growth rate, R_m, is

$$R_m = q_m^2 D_{app} / 2 \tag{5.14}$$

The mutual diffusion coefficient, D_{app}, is found:

$$D_{app} = \frac{D_1 D_2 \left(\phi_1 n_{s(1)} + \phi_2 n_{s(2)}\right)}{\phi_1 n_{s(1)} D_1 + \phi_2 n_{s(2)} D_2} f \tag{5.15}$$

where D_j is the self-diffusion coefficient of polymer j, $D_j = k_j M_{(j)}^{-2}$, M is molecular weight, and f is a factor that describes the slowing of diffusion as the spinodal temperature is approached. In the specimens described herein, the quench is relatively deep; i.e., $\left|T_s - T\right| \geq 200°C$, and consequently no slowing is considered. The temperature dependence of D_j is

$$D_j / T = A e^{-E_{D/T}/RT} \tag{5.16}$$

For linear PE, [102] $E_{D/T}$ = 24 kJmol^{-1} and k = 0.26 cm^{2}g^{2}mol^{-2}s^{-1}. These values are not known for EOC, thus values were estimated from the data of Bartels et al. [103] for poly(ethylene-co-1-butene). The calculated growth rates at 230 and 170°C are 23.9 and 10.6 s^{-1}, respectively. The growth exponent is the product of R_m and the time allowed for growth, t; in this case t was taken as the solidification time of the moulding. R_mt at the skin and core for the melt at 230°C are 2.4 and 196, respectively; at 170°C the corresponding values are 1.0 and 58. The early stages of coarsening may be considered as $R_m t \leq 1.1$.

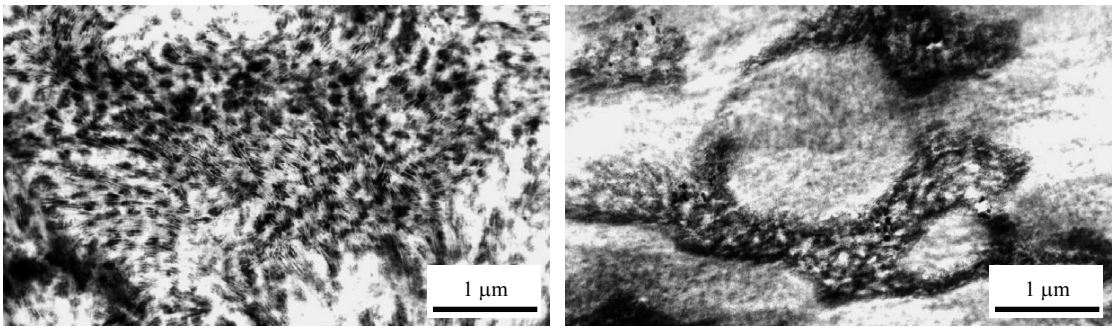

(a) (b)

Figure 5.6 Core region of a blend moulded at 230°C: (a) as-moulded and (b) after annealing at 230°C for 15 min.

Thus, the morphology observed in the core region may have coarsened beyond the early stage, and hence q decreases below q_m, and λ is greater than λ_m, whereas at the skin, the texture may be a consequence of the freezing-in of the early stage of phase separation.

Figure 5.6 shows the globular core morphology of the 230°C as-moulded melt-blend, alongside the same moulding after annealing at 230°C for 15 min. In the melt under quiescent conditions, the EOC domains coalesce and occlude some of the PE-rich phase, suggesting that this fraction of the PE does not re-dissolve into the EOC under static conditions. Detail of the domains in the blend moulded at 170°C and annealed at 170°C for 15 min, are displayed in Figure 5.7. PE lamellae can be seen penetrating into the EOC domain, from which it is inferred that some PE was mixed with the EOC under quiescent conditions in the melt.

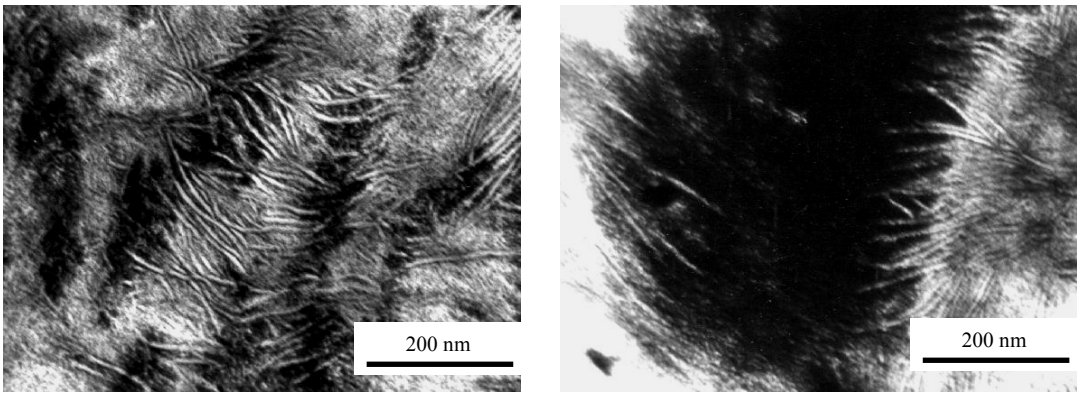

(a) (b)

Figure 5.7 Detail of the phase domains of a blend moulded at 170°C: (a) as-moulded and (b) after annealing at 170°C for 15 min.

The extent of interpenetration is considerably less than that seen in the melt-blend, however, and hence it is concluded that the melt flow in the injection moulder drives the blend towards miscibility. The spinodal boundary, which may be an upper or lower critical solution temperature type, may be shifted due to the melt flow. Upon cessation of flow and cooling, phase separation occurred rapidly and was complete within the cooling stage of the moulding cycle. From the connectivity of the minor phase and the rapidity of the moulding cycle, phase separation is likely to have occurred through spinodal decomposition. Moreover, the shape and arrangement of the EOC domains are consistent with this mechanism. The length-scales of the observed morphologies are of the order of magnitude expected from phase separation, based upon estimates of the molecular dimensions.

5.1.4 Lamellar morphology

In the moulded blends, the PE lamellae penetrate the EOC-rich areas and extend into the PE-rich phase. Moreover, the highly stained regions at the edges of the lamellae show strong contrast with the unstained crystalline material due to the concentration of the EOC at these locations. The extensive chain branching in the EOC precludes its incorporation into the PE lamellae, and consequently as the PE crystallises from the mixed phase the EOC collects at the edges of the lamellae.

This is further evidence that the polymers were mixed in the melt. The presence of EOC between the PE lamellae results in a distribution of the long period values, ranging from around 18 nm in PE-rich areas to 27 nm in EOC-rich regions, although there is little change in the average lamellae thickness between the blend and the original PE prepared at the same moulding temperature. This indicates that the melt was not homogeneous at the onset of crystallisation, with the more closely packed lamellae forming from PE-rich regions and the thicker inter-lamellar regions the product of crystallisation from areas with higher EOC concentrations. As the melt cools from above 200°C through the spinodal boundary, liquid-liquid phase separation will begin and will continue unperturbed until PE crystallisation begins at temperatures below about 120°C. At this point, PE lamellae grow rapidly from both EOC-rich and PE-rich areas. With close inspection of the PE lamellae in the melt-blends, in Figure 5.2, it is evident that the lamellae are not as straight as those seen in the original PE mouldings, with some exhibiting an abrupt kink, whilst others have a more gentle wave conformation. This may be caused by the presence of EOC impurity in the PE melt during crystallisation. The overall crystallinity of the PE, as determined by DSC, was significantly affected neither by moulding temperature nor by liquid-liquid phase separation, since all determinations fell in the range 62.4 to 62.8%.

5.2 Part 2: Effect of Phase Morphology Upon the Toughness Properties of PE / EOC Blends

5.2.1 Melt state phase behaviour

The direct observation of morphology development in the melts of polyolefin blends is hampered by the small refractive index differences between the polymers. In this work, the samples appeared to be uniform at all conditions through direct observation of the melt. Upon rapid crystallisation of the PE, the melt phase morphology could be partially frozen-in, however. The length-scale of the features seen may be used to infer the state of the melt from the following reasoning.

The self-diffusion distance, x, of a molecule diffusing in a melt of similar material may be estimated from $x^2 = 2D\Delta t$ and $D = 14 \times 10^{-6} M^{-2}$, where M is the molecular weight and t is time. From this analysis, the order of magnitude of the size of the phase dimensions expected during a 5 second quench from a homogeneous melt would be around 100 nm. Thus, an apparent state of the melt may be inferred. The true thermodynamic stability is not necessarily determined, however, only the homgeneity of the morphology is obtained.

Figure 5.8 shows micrographs of the samples that were annealed for six hours, quenched, microtomed, and then etched with permanganic acid. In Figure 5.8 (a), large circular holes up to 5 μm in diameter; i.e. an order of magnitude larger than that expected through quenching from a homogeneous melt, have been etched into the surface. The locations of the holes show the distribution of the EOC-rich phase. Moreover, the domains increased in size upon annealing for longer times, and hence from these observations it may be inferred that the blend was a two-phase state, at the annealing condition.

Figure 5.8 (b) shows a fine dispersed phase morphology, comprising holes with mean diameter of 0.33 μm left by etched domains of low crystallinity material; they are distributed in a continuous PE-rich phase that exhibits a banded spherulitic texture. The area fraction of the holes in the cross-section of the sample is 3.2%. If the area fraction is approximately equal to the volume fraction of the dispersed domains in the melt, the observed volume fraction is considerably lower than the 16.4 $vol\%_{(25°C)}$ total EOC content in the blend. In the melt-sate, the component polymers must have been partially mixed, forming a PE-rich majority α-phase and a minority EOC-rich β-phase. Using the 'lever rule', i.e.

$$\frac{\phi_\alpha}{\phi_\beta} = \frac{l}{l'} \qquad \text{or} \qquad \phi_\beta = \left(\frac{l}{l'+l}\right) \tag{5.17}$$

where ϕ_i is the volume fraction of phase i and l is the length of tie-line in the phase diagram, it may be concluded that this condition must be close to the binodal locus.

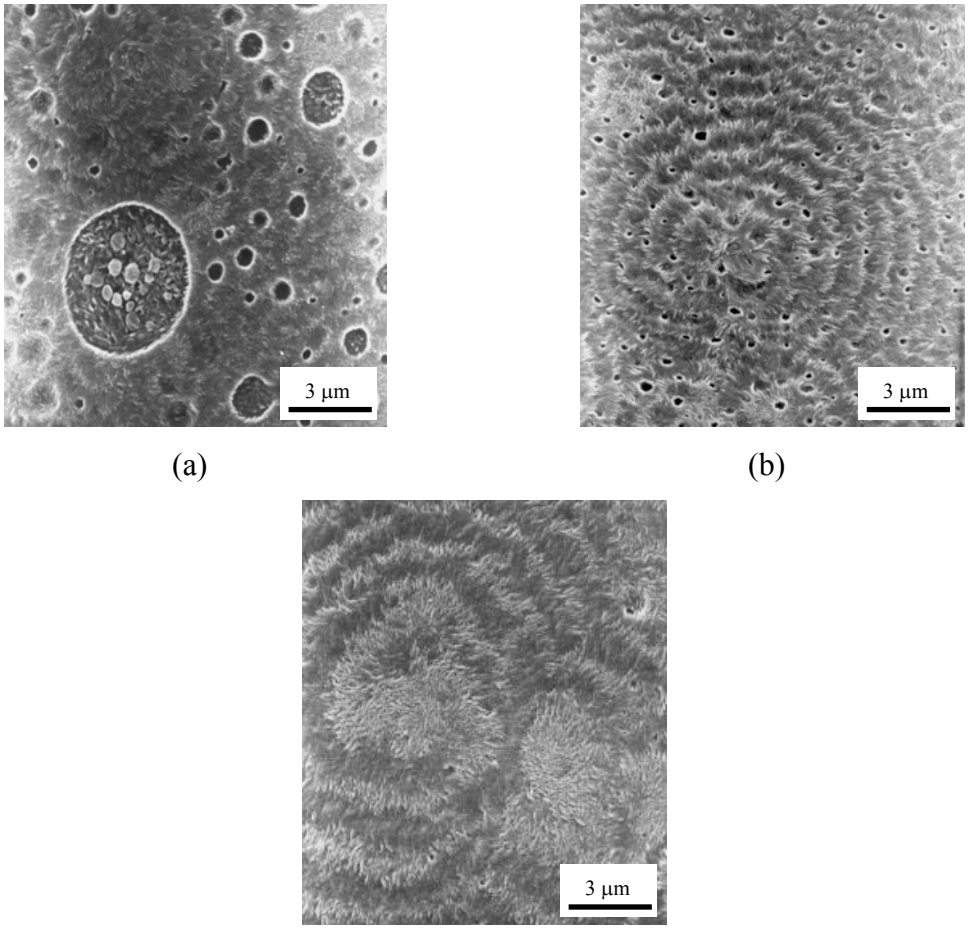

(a) (b)

(c)

Figure 5.8 SEM micrographs of permanganic acid etched, microtomed surfaces. Samples were annealed in the melt for six hours at 230°C and then quenched: (a) 80:20 w/w; (b) 85:15 w/w, and (c) 90:10 w/w PE / EOC blend.

Moreover, the measured area fraction of the sample containing 21.7 vol% of elastomer annealed at 230°C was 11.8%. Near the cloud point, the volume fraction of the β-phase, ϕ_β, is low and the thermodynamic driving force to coarsen the morphology is weak, and hence the rate of coalescence of the droplets to form large domains is slow. Consequently, the observed domains are small. The morphology in Figure 5.8 (c) is essentially the same as that of the pure PE. No holes left by etched EOC-rich domains are discernible at this magnification. Inspection at higher magnifications revealed the presence of very small, etched domains, typically 150 nm

in diameter, intertwined with the PE crystalline fibrils. The width of the fibrils lie in the range 150 to 200 nm and consequently must consist of 10 to 12 lamellae that are around 17 nm (from TEM) across the fold surface. The dimensions of the etched domains are consistent with the suggestion that the EOC-rich domains were formed through phase separation from a melt that was homogeneous before quenching. Homogeneity may be concluded at least at the microscopic level, although not necessarily at the molecular level. The spherulitic morphology of the PE is little affected by the presence of the dissolved elastomer, since spherulites with diameters in the range 5 to 7 μm comprising up to five bands are obtained regardless of the presence of elastomer. For samples with EOC contents of 20 vol% and higher the spherulitic texture is obscured by the holes in the etched samples, phase contrast optical microscopy showed that the overall semi-crystalline texture was comparable with the samples containing lower EOC concentrations.

The intermixing of the two polymers in the melt-state may be further illustrated through consideration of the analysis of the TEM images in Figure 5.9.

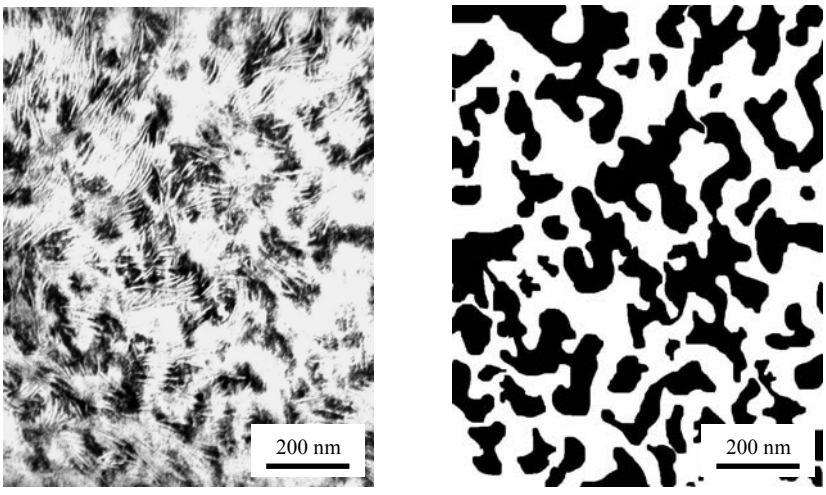

(a) (b)

Figure 5.9 Images of a 70/30 w/w PE / EOC blend injection moulded at 230°C: (a) original TEM micrograph and (b) image after outlining of the EOC domains; area fraction is 0.47.

Figure 5.9 (a) shows a TEM photomicrograph of a PE / EOC sample injection moulded at 230°C. Figure 5.9 (b) is the same image, except that the EOC-rich regions have been filled in black and the PE-rich regions filled in white to produce a binary image of the TEM micrograph. The area fractions of the two regions were then determined using Image analysis. The area fraction of the EOC regions was found to be 47%, and hence the PE-rich areas constitute 53%. The content of EOC in the blend was 30%. Apparently, the location of the PE lamellae crystals in the EOC-rich domains increases the effective area fraction of EOC. It is inferred from this observation that a fraction of the PE was dissolved in the EOC at the onset of crystallisation.

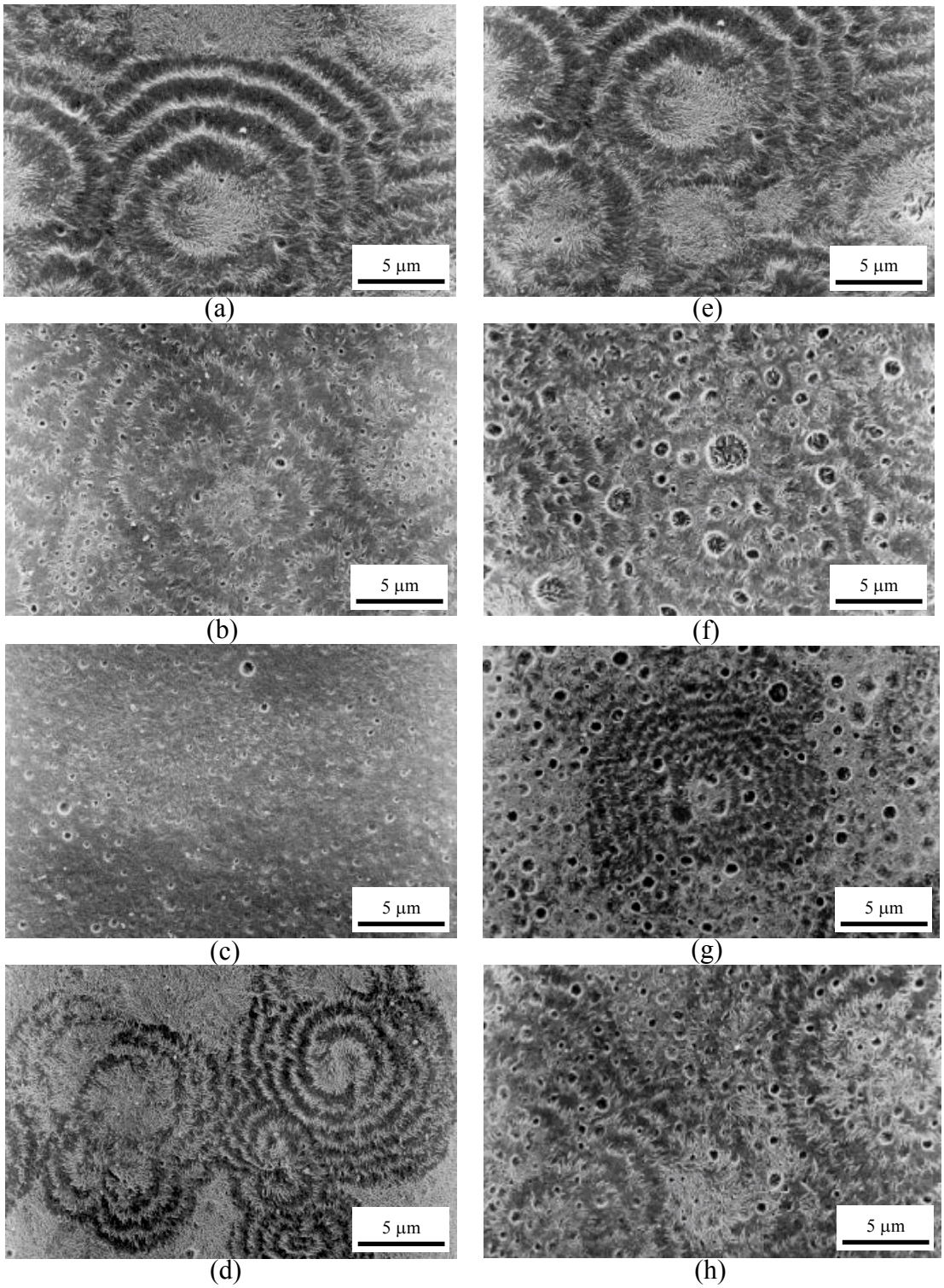

Figure 5.10 SEM micrographs of permanganic acid etched of quenched specimens: (a) and (e) PE resin; PE / EOC 80:20 w/w blend injection moulded at 230°C then annealed at (b) 285, (c) 300, and (d) 320°C, and moulded at 170°C then annealed at (f) 285, (g) 300, and (h) 320°C.

Figure 5.10 shows the phase morphology of the annealed samples at various temperature. The morphology observations of the annealed samples prepared at 170 and 230°C and annealed at various temperatures are summarised in the diagram in Figure 5.11, where the samples have been classified according to the observed length-scale of the etched domains.

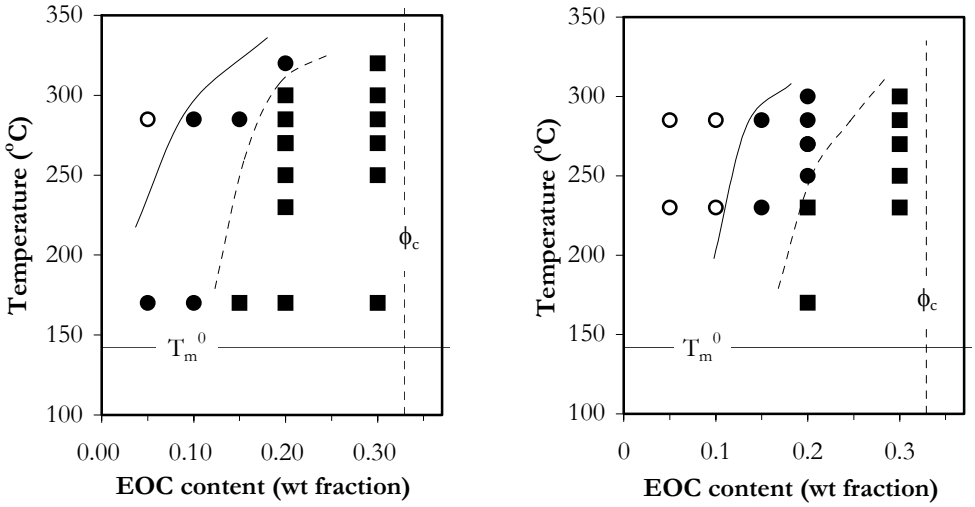

(a) (b)

Figure 5.11 'Morphology map' of the annealed samples based upon mean domain size, D_n: (■) 1 μm < D_n < 30 μm; (●) 200 nm < D_n < 1 μm, and (○) D_n < 200 nm. T_m and T_c were determined through DSC analysis; boundary curves were drawn arbitrarily. Samples prepared at (a) 170 and (b) 230°C.

The critical composition, ϕ_c, was calculated from the Flory-Huggins lattice theory, employing the data in Table 5.1:

$$\phi_{Min}^{c} = \left(1 + \left(\frac{v_{Min} x_{wMin}}{v_{Maj} x_{wMaj}} \right)^{1/2} \right)^{-1} \tag{5.18}$$

where x_{wi} and v_i are the degree of polymerisation and molar volume, respectively, of species i. v_{EOC} was calculated from the mole fraction weighted average of the values for PE and poly(1-octene).

From Figure 5.11 it can be seen that for both the samples prepared at 170 and 230°C the EOC-rich domains become smaller as the content of EOC decreases and as the temperature increases. The former observation is due to the reduction in the rate of coalescence as a consequence of fewer domain contacts as the quantity of EOC decreases. The reduced domain size at elevated temperatures shows that the greater thermal energy enhances the compatibility of the blend components. Increased thermal energy reduces the melt viscosity. This alone would increase the domain size due to accelerated rates of coalescence, and therefore the enhancement in compatibility overrides the effect of reduced viscosity. Comparison of the morphology map of the samples prepared at 170 and 230°C shows that for every temperature and composition the samples processed at 230°C have a finer morphology than the equivalent formulation prepared at 170°C. This shows that even after annealing period of six hours, the processing history still has a pronounced effect upon the morphology that is subsequently formed. The enhanced compatibility that results from melt-processing at high temperature is maintained during subsequent thermal processing.

The length scales and area fractions of the domain morphologies reflect the partial miscibility of the blend that is enhanced at elevated temperature and suggest the underlying phase behaviour, although not necessarily the equilibrium condition. Extrapolation of the arbitrarily drawn boundary lines to the critical volume fraction suggest a critical point that is higher than 350°C, that is some way above the melt-processing window and into the region of rapid degradation of the polyethylene. Thus, the morphology diagram suggests upper critical solution temperature-type phase behaviour, although an hourglass shaped binodal locus extending to very high temperatures where the polymer degrades is also possible.

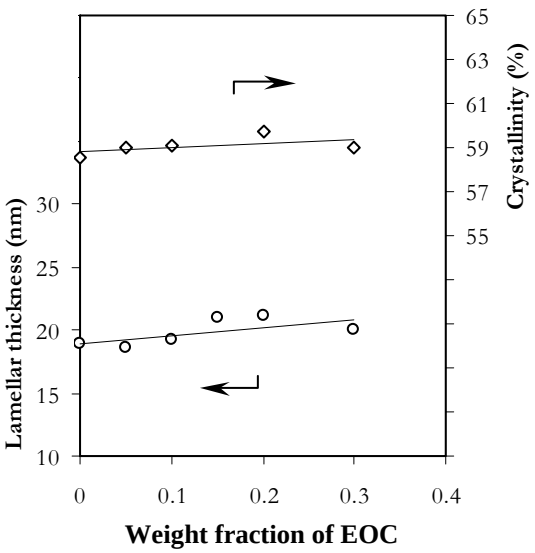

Figure 5.12 Crystallinity (◇) and lamellar thickness (o) calculated from DSC data for the samples prepared at 230°C; data for the samples prepared at 170°C showed essentially the same result.

Crystalline characteristics, determined from DSC analyses, are represented in Figure 5.12; lamellar thickness, L_c, was calculated using the Thompson-Gibbs equation:

$$T_m = T_m^0\left(1-\frac{2\sigma}{L_c\rho\Delta H^0}\right) \tag{5.19}$$

where T_m is the melting point, T_m^0 is the equilibrium melting point, ΔH^0 is the heat of fusion, ρ is the crystal density, and σ is surface energy. The melt state phase behaviour does not greatly affect the PE crystallinity or lamellar thickness, under the conditions of sample preparation, within the experimental error of the DSC analyses, as shown in Figure 5.12. Typical lamellar thickness, calculated from the Thompson-Gibbs equation, of around 20 nm was slightly higher than the 17 nm value obtained through TEM observations of stained sections.

5.2.2 Correlation of phase morphology with impact properties

The impact specimens were compression moulded in regions A and B of the morphology map, as shown in Figure 5.13 (a).

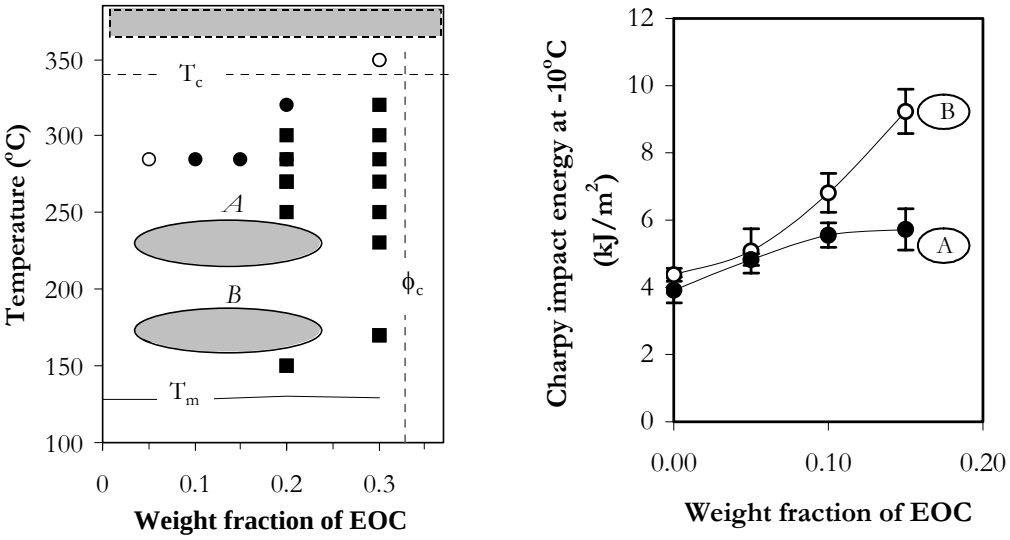

(a) (b)

Figure 5.13 Relationship between (a) the phase morphologies under quiescent melt conditions (same symbols as Figure 5.11) and (b) the impact energy at –10°C of the specimens compression moulded at (○) 170°C and (●) 230°C; error bars are the mean ± one standard deviation.

The corresponding impact energies, at –10°C, of these specimens are shown in Figure 5.13 (b); samples containing 20 wt% and higher EOC contents failed by hinging due to crack arrest. It is apparent that upon moving further into the immiscible region of the morphology diagram, either by reducing temperature or by increasing the EOC content, there are increases in the impact toughness of the blends. Representative morphologies of microtomed and permanganic acid etched specimens, moulded at condition A and B, are shown in Figure 5.14. The mean EOC-rich domain size of the etched impact specimens is plotted as a function of EOC content in Figure 5.15 (a); the impact energies are plotted against EOC-rich mean domain size in Figure 5.15 (b). Both higher EOC contents and lower temperature lead to a coarsening of the EOC-rich

domains in the melt state. Higher quantities of elastomer lead to an increased frequency of droplet contact and coalescence, whereas lower temperatures confer a greater thermodynamic driving force, although lower kinetic mobility, to coarsen the morphology.

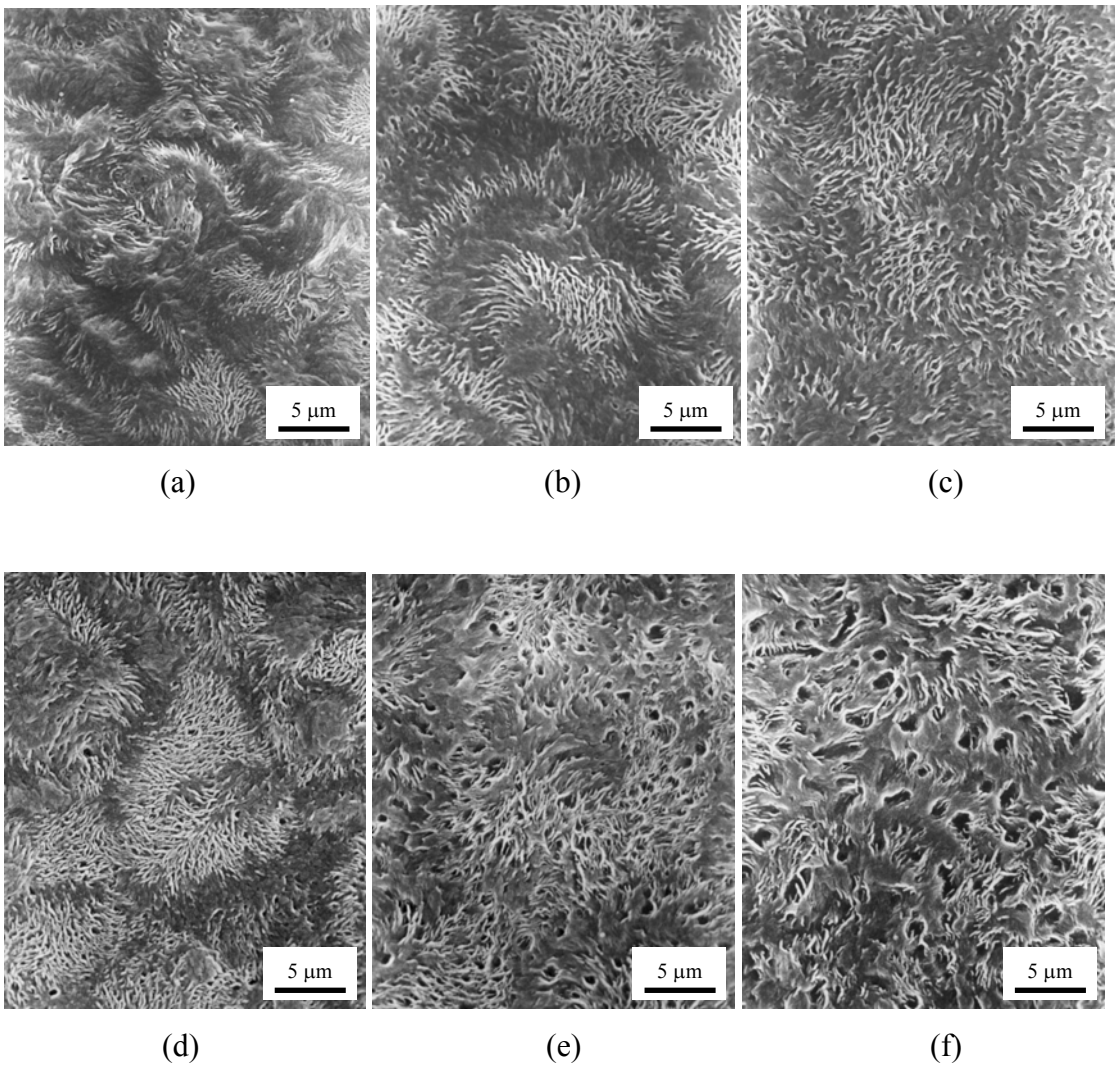

Figure 5.14. SEM micrographs showing the morphologies of the compression moulded impact specimens containing 10, 15, and 20 wt% EOC moulded at (a), (b), and (c) 230°C and (d), (e), and (f) 170°C for 5 min. Surfaces were prepared through microtomy followed by permanganic acid etching.

When plotted against EOC-rich mean domain size, or average inter-particle distance, I_{dn}, from:

$$I_{dn} = D_n / \left[\left(\frac{\pi}{6\phi_{EOC}} \right)^{1/3} - 1 \right] \tag{5.20}$$

the impact data do not fall on a single mastercurve, as is sometimes observed for rubber toughened matrices; a distinct curve is obtained for each moulding temperature. The impact toughness is affected not only by the domain size but also by the dispersed phase composition and volume fraction; all three factors are influenced by moulding temperature and total elastomer content. Samples moulded near to the binodal condition have low volume fractions of the EOC-rich phase, although these may not be the equilibrium values due to the processing time of 5 minutes.

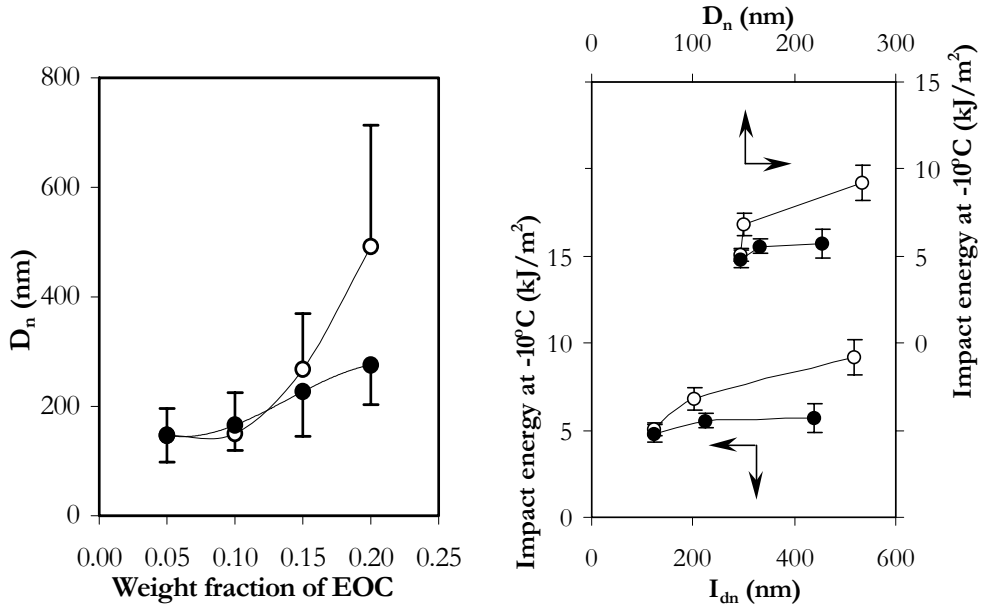

(a) (b)

Figure 5.15 (a) Mean elastomer-rich domain diameters, D_n, in the compression moulded impact specimens moulded at (○) 170°C and (●) 230°C; error bars are the standard deviations of particle size distributions. (b) Impact energy as a function of EOC-rich mean domain diameter and average inter-particle distance.

Consequently, the larger fraction of the elastomer is dissolved in the PE-rich phase. Upon cooling, the system moves deeper into the spinodal region and the elastomer further separates from the PE in the melt state. Due to the extensive branching in the EOC, upon crystallisation of the PE it is excluded from the rapidly growing lamellae and collects in 150 nm domains in the inter-fibrillar regions of the PE spherulites. DMA showed that there was a slight increase in the T_g of EOC in the blends cooled rapidly from the melt, in comparison with the original EOC. This 5 to 7°C change was insensitive to melt temperature or blend composition, however. If the T_g of linear PE were taken as -20°C [although this value is not universally accepted], this result would be consistent with the presence of an EOC-rich phase in the solid-state containing a small amount of amorphous polyethylene. Linear polyethylene does not show a clear transition at -20°C, and so the T_g of the conjugate PE-rich phase could not be determined. Thus, in the solid-state, the blend components largely exist in separate domains of amorphous PE, crystalline PE, and amorphous elastomer. Apparently, the very fine EOC-rich domains that are formed during quenching from microscopically homogeneous melts or near cloud point conditions are less effective at toughening the PE, at –10°C under Charpy impact conditions, than the coarser morphologies produced in the more strongly immiscible conditions.

5.3 Part 3: The Influence of Orientation During Processing Upon the Fracture Toughness of PE / EOC Blends

Figure 5.16 shows TEM micrographs displaying typical solid-state morphologies of the pure PE and a PE / EOC blend, both processed at 170°C. As was discussed in part 5.1 of this report, the white lines are PE lamellae of around 17 nm thick.

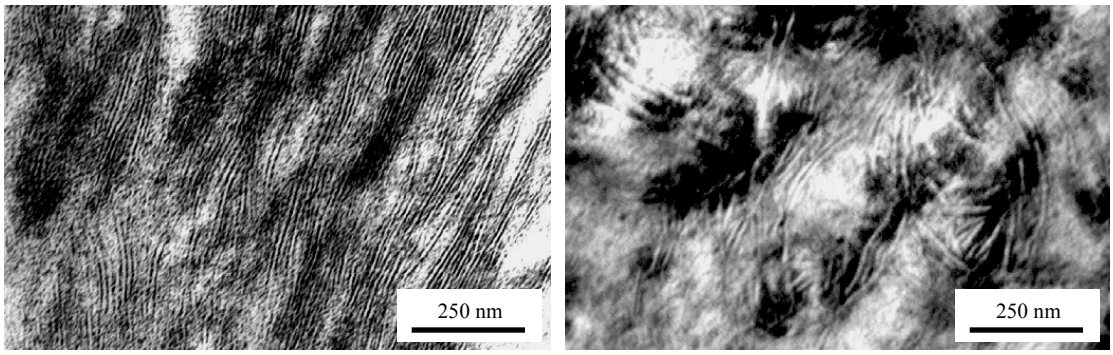

(a) (b)

Figure 5.16 TEM micrographs of (a) pure PE and (b) a PE / EOC blend melt-processed at 170°C.

The dark areas are the EOC-rich regions. It can be seen that the PE crystals penetrate into the EOC-rich regions. From this observation, it was inferred that at least some of the PE and the EOC were mixed in the melt-phase at the time of crystallisation. As explained in a previous publication [92], and part one of this report, thermal analysis revealed that in the solid state the material comprised essentially pure domains of amorphous EOC and amorphous PE, since there were no significant differences between the glass transition temperatures of the components in the pure materials and the corresponding transitions in the blend samples.

5.3.1 Orientation

The orientation function *f* describes the orientation of the crystalline axis relative to some reference direction in the sample. The orientation function is defined as

$$f_x = \frac{3\overline{\cos^2 x} - 1}{2} \tag{5.21}$$

where $\overline{\cos^2 x}$ designates the average cosine squared value of the angle *x* between the reference direction in the sample and the *x* crystallographic direction.

Stein [93] has set up a generalized model for uniaxial crystal orientation of polyethylene unit cell in the coordinate system as shown in Figure 5.17.

The Z-axis of the X, Y, Z cartesian coordinate system is taken as the stretching direction. The angles α, β, and ε are measured between the Z-axis and the a, b, and c crystallographic axes, respectively.

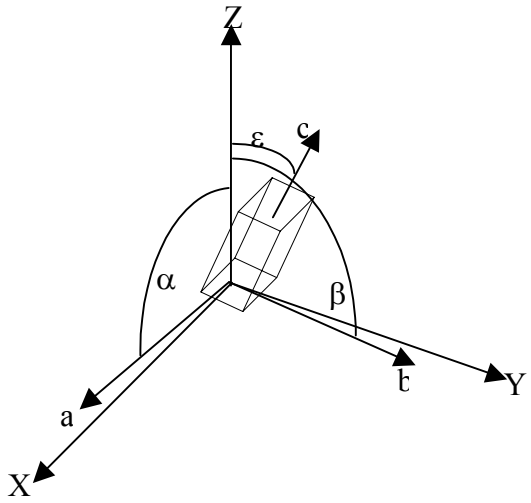

Figure 5.17 The coordinate system used for describing the orientation of polyethylene crystal.

Since the three axes are perpendicular for the orthorhombic unit cell,

$$\overline{\cos^2\alpha} + \overline{\cos^2\beta} + \overline{\cos^2\varepsilon} = 1 \tag{5.22}$$

and therefore

$$f_\alpha + f_\beta + f_\varepsilon = 0 \tag{5.23}$$

where the three orientation functions are defined as:

$$f_\alpha = \frac{3\overline{\cos^2\alpha} - 1}{2} \tag{5.24}$$

$$f_{\beta} = \frac{3\overline{\cos^2 \beta} - 1}{2} \tag{5.25}$$

$$f_{\varepsilon} = \frac{3\overline{\cos^2 \varepsilon} - 1}{2} \tag{5.26}$$

Thus for this model, the three orientation functions are not independent and only two of them are required to characterize the orientation.

Crystalline orientation was determined by the measured intensity I_{meas} in counts per second at each azimuthal angle, ψ, where the azimuthal angle is defined as the angle between the stretching direction and the plane of measurement of θ_{hkl}. The measured intensity must be corrected for absorption [94], polarization and background before it can be used to evaluate $\overline{\cos^2 \phi_{hkl}}$. The equation used for correction of the measured intensity is

$$I(\psi) = (I_{meas} - I_{background}) K_{polarization} K_{absorption} \tag{5.27}$$

Where $I_{background}$ is background intensity

$$K_{polarization} = \frac{2}{1 + \cos^2(2\theta_{hkl})} \tag{5.28}$$

$$K_{absorption} = \frac{\mu t(\sec 2\theta_{hkl} - 1)}{1 - \exp[-\mu t(\sec 2\theta_{hkl} - 1)]} \tag{5.29}$$

where μ is the linear absorption coefficient and t is the thickness of the sample film.

For a system that is oriented uniaxially,

$$\overline{\cos^2 \psi_{hkl}} = \frac{\int_0^{90} I(\psi) \cos^2 \psi \sin \psi d\psi}{\int_0^{90} I(\psi) \sin \psi d\psi} \quad (5.30)$$

Equation (5.30) can be used to evaluate $\overline{\cos^2 \psi_{hkl}}$ by multiplying the corrected intensities by the appropiate values of the sine and cosine function and plotting the results against the azimuthal angle. The area under the curves can be calculated by numerical integration by using the trapezium rule.

5.3.2 Effect of copolymer upon PE crystal orientation

Azimuthal scans for the (200) and (020) crystal plane of the orthorhombic PE crystals are displayed in Figure 5.18. The crystallinity and orientation values calculated for the PE samples are listed in Table 5.2.

Table 5.2. Orientation from X-ray data, peak melting point, Tm, and crystallinity, C, from DSC for the sheet extrusion PE compounds[a]

EOC content (vol%)	f_α	f_β	f_ε	C (wt%)	Tm (°C)
0	0.067	-0.211	0.143	58.0	133.6
	(0.007)	(0.007)	(0.016)	(0.70)	(0.14)
5	0.100	-0.234	0.135	57.2	133.9
	(0.004)	(0.006)	(0.010)	(1.27)	(1.60)
10	0.096	-0.237	0.141	57.4	133.5
	(0.004)	(0.002)	(0.002)	(1.54)	(0.89)

[a]numbers in parenthesis are the standard deviations from three replicate determinations

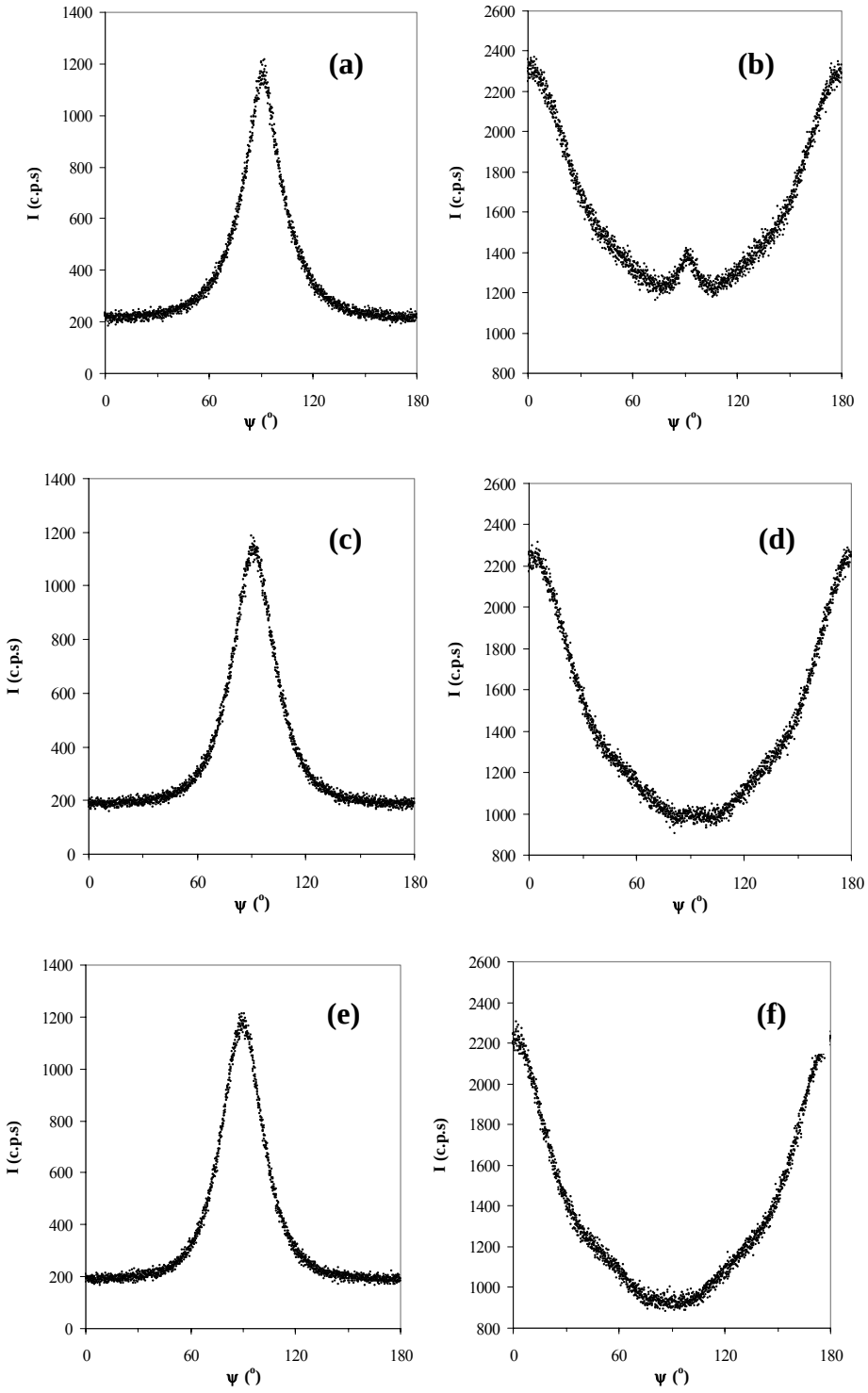

Figure 5.18 Azimuthal angle scans for specimens in reflection mode: (a) PE (020) plane, (b) PE (200), (c) 5 vol% EOC (020) plane, (d) 5 vol% EOC (200), (e) 10 vol% EOC (020) plane, and (f) 10 vol% EOC (200) vol%.

Melting temperature and heat of fusion data reveal that the presence of the copolymer in the blends did not significantly affect the crystal size or crystallinity, respectively, of the PE crystalline phase. The X-ray analysis in Table 5.2 characterises the overall, i.e. average, preferred orientation of the PE crystals that arises from the crystallisation of the oriented PE melt. The melt was oriented, principally uniaxially, by the flow through the coat hanger die and in the nip of the chill rollers. Overall, the b-axis has a negative orientation function with respect to the machine direction, indicating a most probable orientation perpendicular to the machine direction. The b-axis direction is the growth direction of the PE orthorhombic lamellar crystals and hence this result places the lamellae in orientations perpendicular to the machine direction. Conversely, the a and c-axes have positive orientation functions indicating most probable orientations towards the machine direction; the higher orientation function for the c-axis indicates a higher probability of the c-axis being aligned towards the machine direction than for the a-axis with the machine direction. The orientation functions show little difference in the average orientation of the PE crystals upon addition of the EOC elastomer.

Further information concerning the influence of EOC upon PE crystal formation in the sheets may be gleaned through inspection of the azimuth angle scans. The azimuth angle scan of the (200) planes in the pure PE specimen shows a general decrease in scattering intensity as the specimens were rotated from $\psi = 0$ to 90^{o}, indicating a preferred orientation of the normal to the (200) plane, i.e. the a-crystallographic axis, towards the machine direction. Additionally, however, there is an increase in scattering intensity around the ψ angle of 90°. It is inferred from this observation that there is a discrete fraction of crystals oriented for which the normals to the (200) planes lie in the plane of the incident / diffracted beam plane when the sample is turned to 90° around the normal direction. That is, with the a-crystallographic direction towards the transverse direction. The azimuth angle scan for the (020) plane shows a maximum at $\psi = 90^{o}$ that indicates a preferred orientation of the b-axis in the transverse direction. The (020) scan does not show a discontinuity in the intensity profile, however. This could be because the anticipated decrease in the scattering by the (020) plane of the second fraction of crystals coincides with the maximum in the scattering in the first set, and hence is obscured. The bimodal crystal

orientation is also evident from the azimuth angle scan for the (110) plane. The orientation of the first set of (110) planes corresponds to maxima in the curves at ψ = 70 and 110°; for the second set, the maximum is at ψ = 90°. These results suggest the presence of a bimodal crystal orientation in the pure PE samples. This may be a consequence of the row-nucleation mechanism whereby crystals form perpendicular to one another.

The precise mechanism of formation is not agreed upon at present, but is thought to be caused by a second population of crystals being nucleated around the regions of the initial crystal formation. The rise in intensity at 90°, Ψ, is less pronounced in the samples containing 5% of EOC and is largely suppressed in the sample containing 10% EOC. Apparently, the presence of EOC in the extruded samples suppresses the formation of the second fraction of crystals resulting in a single population of crystals with a common most favoured orientation.

Yu and Wilkes [56] studied the influence of PE molecular weight distribution (MWD) upon the crystal orientation in extruded films of polyethylenes that had the same average molecular weight. It was reported that a stacked lamellar morphology was obtained through extrusion of a PE sample with a relatively narrow MWD whilst a fibril nucleated morphology resulted in the films of the PE sample with the broader MWD. This difference was attributed to the longer relaxation time of the samples with the broader MWD. Presumably, the melt orientation persists longer after exit from the extruder die in the sample with longer relaxation times resulting in crystallisation of the oriented melt and subsequent fibril nucleation.

The rheological data of PE and EOC were obtained using a Haake RT20 25 mm parallel plate rheometer; nineteen increments in the frequency of the oscillation were made over the range 0.06 to 64.3 rad.s^{-1}. Measurements were made at 443 K under a constant stress of 250 Pa. Zero shear rate complex viscosity, η^*_0, was obtained from Carreau's constitutive equation:

$$\eta^*_\omega = \eta^*_0\left(1+(\tau\omega)^a\right)^{(n-1)/a} \tag{5.31}$$

where η^*_ω is the complex viscosity at ω, τ is the average relaxation time, a is the non-Newtonian exponent (slope of the viscosity curve in the pseudoplastic region at $\dot{\gamma} \to \infty$), and n is a fitting constant; η^*_0, τ, and n were found from the un-weighted least sum-of-squares method for the fit of the η^*_ω values experimentally determined through rheometry upon the model containing ω as the independent variable.

$$ss_{\min} = \sum_{j=1}^{n} \Delta y_j^2 \tag{5.32}$$

where ss_{min} is the minimum sum of squares of n residuals, Δy, $\Delta y_j = \eta^{*'}_{\omega} - \eta^*_{\omega}$, η^*_ω is the experimental value, and $\eta^{*'}_\omega$ is the corresponding value calculated from the model for datum j. The Solver program in the Microsoft Excel '97 spreadsheet software was used to accomplish this task.

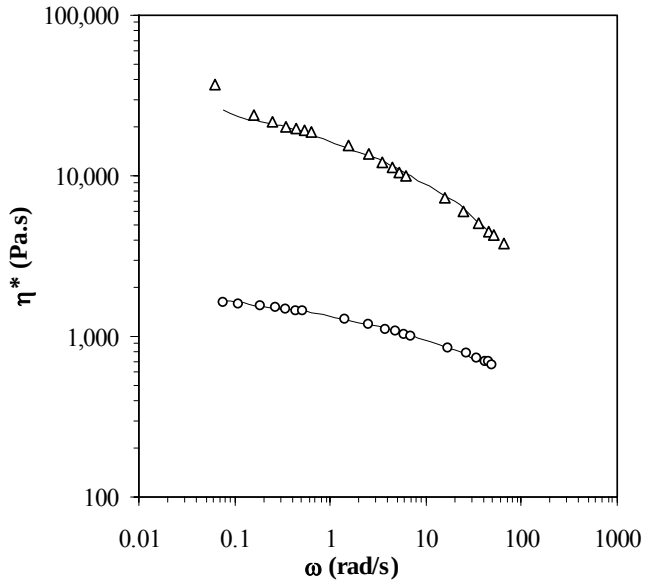

Figure 5.19 Dynamic shear modulus, η^*, versus angular velocity, ω, for (Δ) EOC and ($\bigcirc$) PE; curves are the least sums of squares fits of Carreau equation.

The complex viscosity versus angular velocity curves for the PE and EOC are shown in Figure 5.19; the best-fit values of the Carreau equation to these data are shown in Table 5.3. These data indicate the higher melt viscosity and longer average

relaxation time of the EOC in comparison with the PE. In this work, we may speculate that since the EOC has higher melt viscosity, a longer average relaxation time, and is at least partially miscible with the PE melt, a disproportionately large level of stress may be taken upon the EOC chains in the flowing melt relative to the PE chains. This may result in preferential orientation of the EOC and hence reduced orientation of the PE under melt-flow. It might be that the low crystallinity, around 10 wt% at most, and low crystallisation temperature, around 40^{o}C, and hence low surface energy of the EOC precludes the EOC from nucleating the second fraction of PE crystals, thereby preventing the row-nucleation of the PE crystals. Consequently, the bimodality of the PE crystal orientation in the pure PE is suppressed through the presence of the EOC in the melt.

Table 5.3 Curve fitting parameters of Carreau equation

Resin	**η^*_0 (Pa.s)**	**τ (s)**	**a**	**a^{-1}**
EOC	122,000	5.9	0.19	5.3
PE	1,600	2.8	1.89	0.5

5.3.3 Fracture toughness studies

The fracture toughness of the materials was studied using the essential work of fracture method. This method was based on the assumption that [73]

$$w_f = w_e + \beta w_p l \tag{5.33}$$

where β is the shape factor, l is the ligament length and w_f, w_e, and w_p are the specific total, essential, and non-essential work of fracture, respectively. A linear plot of w_f versus l was used to determine w_e and βw_p under plane stress conditions.

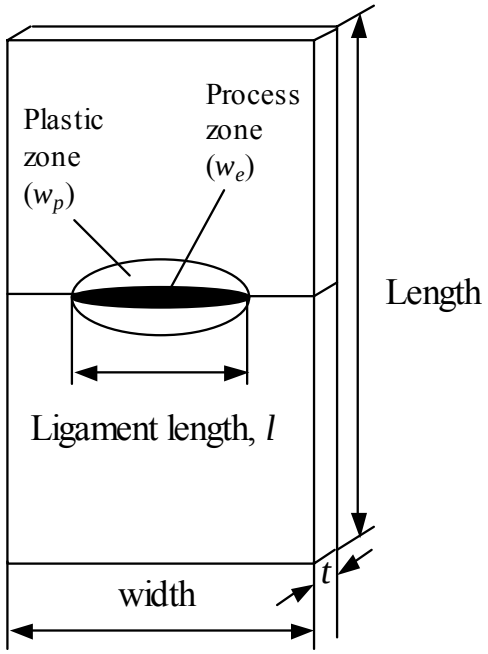

Figure 5.20 The DENT samples used for the essential work of fracture test.

The intercept of the plot is the essential work of fracture. That is when the least sum of squares fit to the experimental data is extrapolated to zero ligament length. Linearity of the plot is associated with plane stress conditions. The slope of the plot is related to the non-essential work of fracture. As illustrated in Figure 5.20, this analysis allows characterisation of the energy absorbed in the 'process zone' involved with the cracking process and the 'plastic zone' that surrounds the process zone, rather than giving an ill-defined overall energy consumption value.

Figure 5.21 and 5.22 show plots of specific fracture energy versus ligament length for the specimens in which the crack propagated in TD and MD, respectively. The linearity of the plots indicates that the samples tested were deformed under plane stress conditions over the range of ligament lengths that was employed.

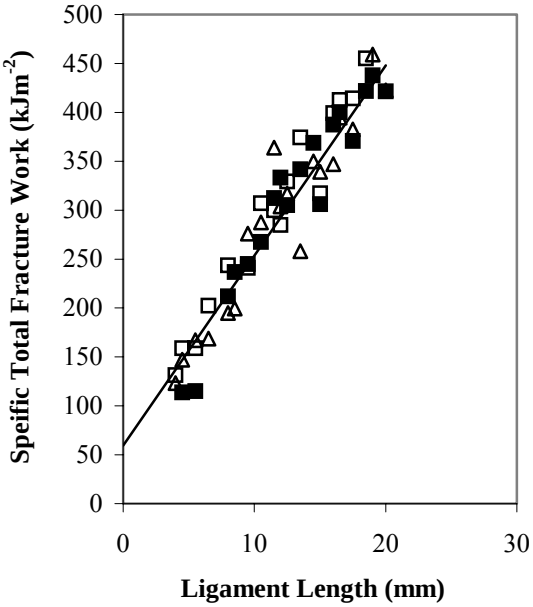

Figure 5.21 Crack propagation in TD: (□) PE pure, (■) PE / EOC 5 vol%, and (Δ) PE / EOC 10 vol%.

Data for the analysis of fracture of sheet samples, obtained from the gradients of the plots and the energy-axis intercepts, are documented in Table 5.4. The plane stress fracture toughness for crack propagation in the MD was strongly influenced by EOC content while for crack propagation in the TD, EOC had no influence.

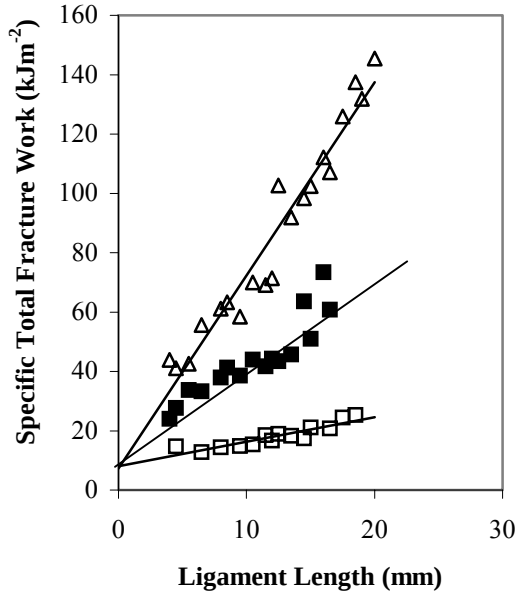

Figure 5.22 Crack propagation in MD: (□) PE pure, (■) PE / EOC 5 vol%, and (Δ) PE / EOC 10 vol%.

Specifically, the presence of partially miscible EOC affected the non-essential work of fracture *(w_p)* while the essential work of fracture *(w_e)* was little affected by EOC when the crack propagated in the MD.

Table 5.4 Tensile test and plane stress fracture toughness data obtained from extruded sheets for crack propagation in the machine direction (MD) and transverse direction (TD)[a]

EOC content (vol%)	Crack propagation direction	Tensile strength[b] (MPa)	Breaking strain[b] (%)	w_e (kJm^{-2})	βw_e (kJm^{-3})
0	MD	12.8	305	7.9	0.9
		(1.05)	(78)		
	TD	26.2	344	59.2	20.9
		(0.85)	(39)		
5	MD	12.4	379	8.3	2.4
		(1.97)	(78)		
	TD	28.1	275	46.2	20.5
		(0.85)	(19)		
10	MD	12.9	407	7.4	5.6
		(3.05)	(69)		
	TD	27	284	59.5	19.4
		(0.59)	(21)		

[a] numbers in parenthesis are the standard deviations from ten replicate determinations

[b] note the tensile data relevant for the crack propagation in MD is from the samples tensile tested in TD and vice versa for crack propagation in the TD

The orientation of the PE in the MD dominated the crack processes travelling in the TD. This was related to higher tensile strength in the MD, as shown in Table 5.4, which was a consequence of the orientation process, with the tensile strength in the direction of orientation being around double that in the perpendicular direction. This is because the energy absorbed, i.e. the fracture toughness, is the product of the tensile force and the sample extension. However, the orientation led to enhanced crack propagation in the MD, associated with reduced tensile strength in the transverse

direction. The presence of the interlocked EOC-rich and PE domains resulted in greater energy dissipation through the non-essential work of fracture.

5.4 Part 4: The Effect of Compounding Upon Fracture Toughness of PE / ECB and PE / EOC Blends

In the previous sections, it was presented that the PE / copolymer blends exhibit characteristics of partially miscible blends. The final solid-state morphology being determined through the stages of dissolution, phase separation, and subsequent domain coarsening that takes place during melt-processing. Apparently, the length-scale, or coarseness, of the morphology is affected by the processing conditions, most notably temperature and storage time in the melt after cessation of melt-flow. To further investigate these phenomena, and to determine their influence upon the fracture toughness, a series of PE / copolymer blends were prepared under several conditions of temperature, shear history, and storage time in the melt. In this part of the work, pure PE, PE / EOC, and PE / ECB blends (85:15 wt%) were prepared through two different processing regimes. In the first case, samples were prepared through single screw extrusion at barrel temperatures of 170 or 220ºC. For the second batch of sample, the materials were passed through a twin screw extruder first and then through a single screw extruder. All samples were subsequently compression moulded to make sheets at 170^{o}C for 3 or 15 minutes. The extrusion conditions were chosen to confer a relatively gentle shear history, using only a single screw extruder that is most often used for shaping operations, whilst the twin-screw extruder conferred a relatively intensive shear history typically found during compounding. Two compression times were used, i.e. 3 or 15 minutes to allow for a broad range of storage time in the melt after cessation of melt-flow. The effects of processing conditions on the fracture toughness of the blends and their morphology were thus investigated.

5.4.1 Morphology of polymer blends

Phase morphology is one of the most important factors that influence the properties of the polymer blends. Phase morphology, in this instance, refers to the size and shape of domains in the polymer blends. The compressed specimens were sectioned and the stubs etched with permanganic acid reagent before being viewed using a scanning electron microscopy (SEM), after vapour deposition of gold. The following figures show examples of the SEM micrographs of the blends where etching with permanganic acid for 18 hours at room temperature has preferentially removed the copolymer-rich material from the sectioned surfaces.

Figure 5.23 shows SEM micrographs of the PE / EOC blends after compression moulding at 170^{o}C for the samples that passed only the single screw extruder, at barrel temperature 170^{o}C or 220^{o}C; each sample was compression moulded for 3 and 15 minutes.

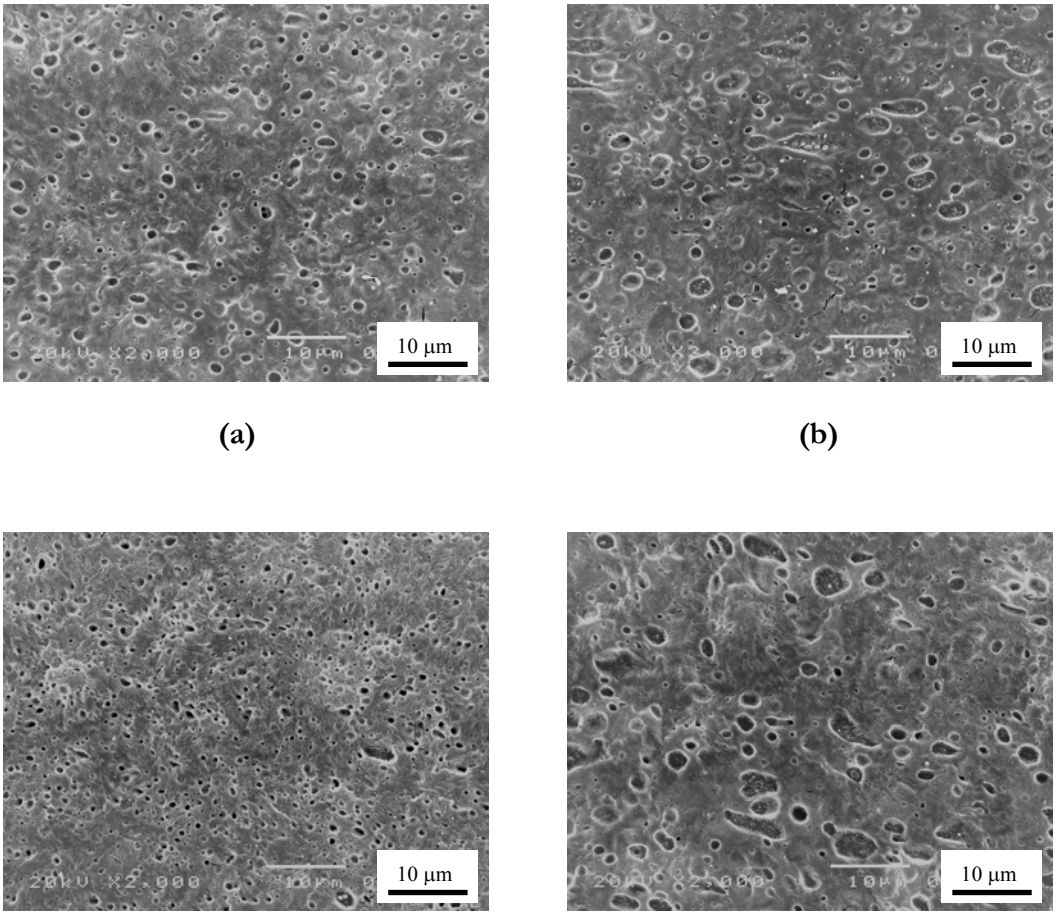

(a) **(b)**

(c) **(d)**

Figure 5.23 SEM micrographs of PE / EOC blends after compression moulding at 170°C from single screw extrusion only, at barrel temperature 170°C (a) compressed 3 min (b) compressed 15 min and at barrel temperature 220°C (c) compressed 3 min (d) compressed 15 min.

Figure 5.24 shows micrographs of the PE / EOC blends that also passed through the twin-screw extruder prior to single-screw extrusion and compression moulding.

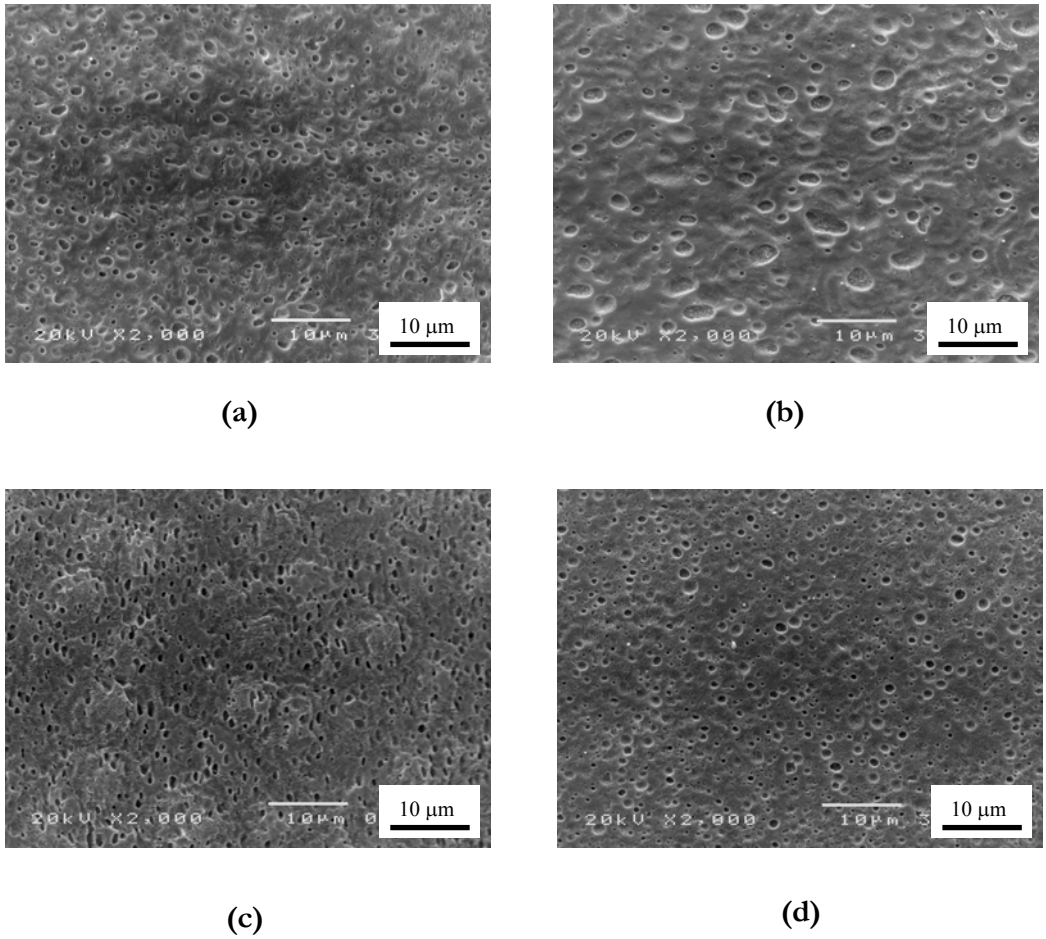

Figure 5.24 SEM micrographs of PE / EOC blends after compression moulding at 170°C following twin-screw extrusion and single-screw extrusion, at barrel temperature 170°C (a) compressed 3 min (b) compressed 15 min and at barrel temperature 220°C (c) compressed 3 min (d) compressed 15 min.

Figure 5.25 displays the corresponding micrographs for the PE samples that contained ECB copolymer, where the samples were simply extruded using the single-screw extruder before being compression moulded for 3 or 15 minutes. Figure 5.26 comprises images of the ECB containing samples that were passed through the twin-screw extruder during the first step of the processing.

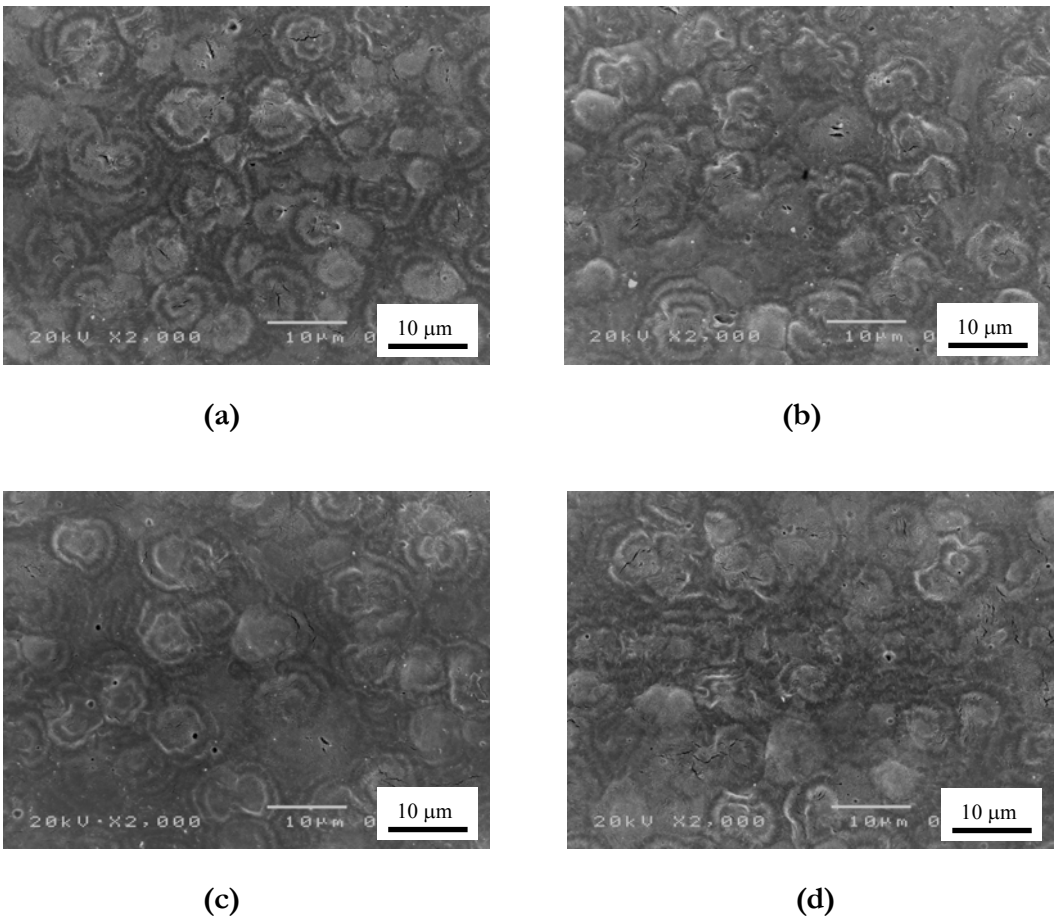

Figure 5.25 SEM micrographs of PE / ECB blends after compression moulding at 170^{o}C from single screw extrusion only, at barrel temperature 170^{o}C (a) compressed 3 min (b) compressed 15 min and at barrel temperature 220^{o}C (c) compressed 3 min (d) compressed 15 min.

From the micrographs it is immediately apparent that the ECB and EOC copolymers give markedly different morphologies for all processing conditions. The EOC formulations always show etched regions that are the signature of domains

comprising material of low crystallinity that was oxidised by the etchant, leaving holes with approximately circular sections. In the case of the ECB containing blends, holes of the type seen for the EOC containing samples are absent.

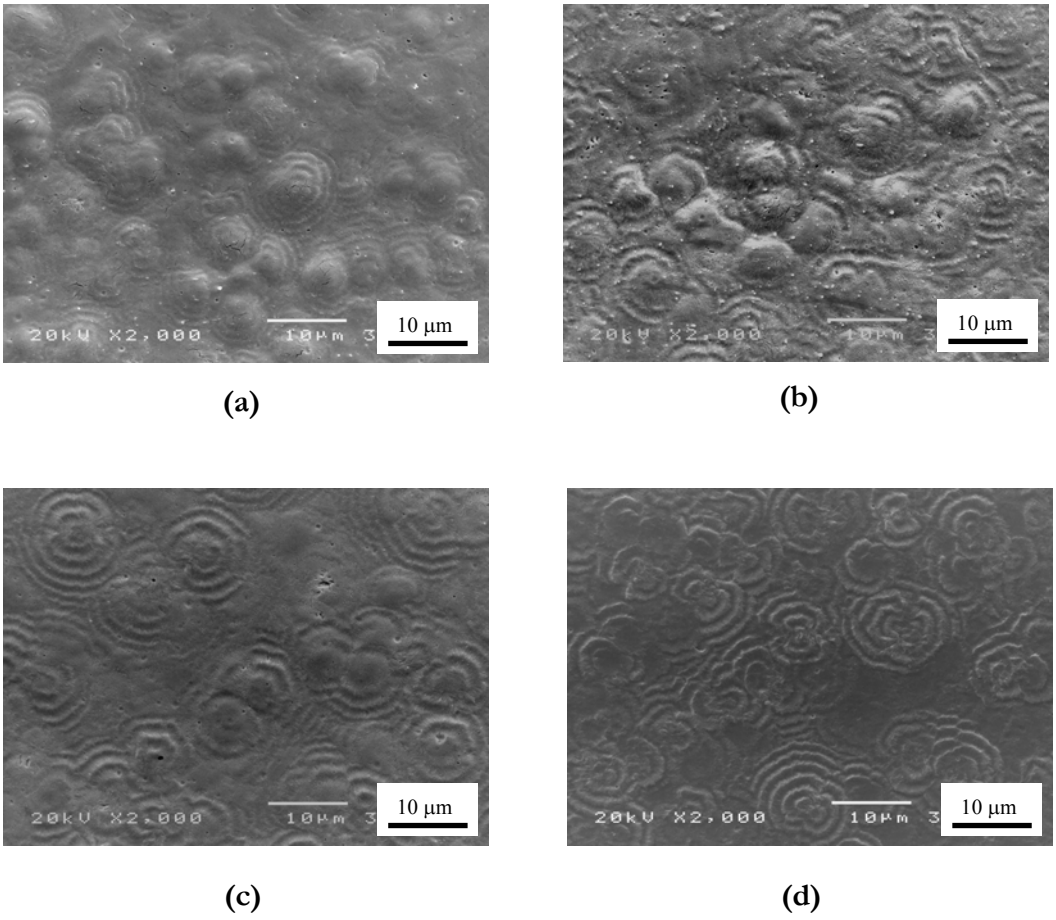

Figure 5.26 SEM micrographs of PE / ECB blends after compression moulding at 170°C after twin screw extrusion and single screw extrusion at barrel temperature 170°C (a) compressed 3 min (b) compressed 15 min and at barrel temperature 220°C (c) compressed 3 min (d) compressed 15 min.

When the copolymer is ECB, the banded spherulitic morphology of the PE majority phase is clearly visible; the PE spherulites are typically around 10 µm in diameter. The smallest length-scale of features resolvable in these micrographs is around 200 nm. This corresponds to the size of the lamellar bundles, that is the

morphological features in the PE spherulites that contain around ten lamellar crystals within each of them. All samples prepared through compression moulding had similarly spherulitic PE morphologies, but in the case of the EOC samples, the PE semi-crystalline texture is obscured by the superimposed EOC-rich domains.

Table 5.5 Number average diameter (D_n) of PE / EOC blends[a]

Sample	Extruder type	Barrel temp. (°C)	Compress. time (minutes)	D_n (μm)
PE / EOC	Single screw only	170	3	0.96 (0.24)
PE / EOC	Single screw only	170	15	1.32 (0.38)
PE / EOC	Single screw only	220	3	0.44 (0.14)
PE / EOC	Single screw only	220	15	1.25 (0.41)
PE / EOC	Twin screw and single screw	170	3	1.02 (0.23)
PE / EOC	Twin screw and single screw	170	15	1.44 (0.40)
PE / EOC	Twin screw and single screw	220	3	0.76 (0.23)
PE / EOC	Twin screw and single screw	220	15	1.01 (0.24)

[a]Numbers in parenthesis are the standard deviations.

The number average diameter (D_n) of the dispersed particles of PE / EOC blends are shown in Table 5.5. Apparently, the number average diameter is larger when the compression moulding time was longer. This is the consequence of the coalescence of dispersed phase in the melt-state state during storage. Through the process of Ostwald ripening where small droplets are consumed in the formation larger domains, of raduius, r. It is a statistical process whereby the domains grow in linear proportion to the cubed root of time, t.

$$r_t^3 = r_0^3 + kt \tag{5.34}$$

Where k is a rate constant and r_0 is the initial particle diameter at the start of the ripening process. The increase in domain size with storage time in the melt is

indicative of a two-phase melt with non-zero interfacial tension between the co-existing phases. The driving force for enlargement of the minority phase is the reduction in interfacial area between the domains of differing composition. A reduced interfacial area enhances the stability of the system because the total interfacial energy, that is the product of the interfacial tension and the interfacial area, is proportionally decreased. Additionally, the dispersed particle size depends upon the extrusion temperature with smaller domains being associated with the higher temperature. The inferences from the characterisation in the previous sections was that the PE / EOC system has limited miscibility. Whilst a single phase melt was never found at compositions greater than 10 wt% of copolymer below the degradation point of the polymers, compatibly was enhanced at elevated temperatures; it was suggested that there may be a virtual upper critical solution temperature at very high temperatures that is inaccessible due to the limited stabilities of the constituent polymers. Apparently, the result of this phenomenon is that melt processing at the higher temperature leads to finer domain morphologies. Comparison of the domain sizes for samples that only differed in the extrusion regime, that is whether the single screw extruder was used alone or in conjunction with the twin-screw extruder, does not reveal any significant difference between the processing methods.

The relaxation temperatures determined using the DMTA are documented in Table 5.6. The γ-relaxation temperature of the pure PE is around –112°C and is not significantly altered when either copolymer is present in the blend under any of the processing conditions. The β-relaxations were weak in all cases, possible due to the high crystallinity of the PE. The implication of these observations is that in the solidified mouldings the polymers reside as phase separated amorphous PE and amorphous copolymer.

Table 5.6 Temperature of PE γ-relaxation in the samples processed by single screw extrusion, SS, and by both single-screw and twin-screw extrusion, TS

Sample	Barrel Temp. (°C)	Compress. Time (min)	γ-relaxation-SS (°C)	γ-relaxation-TS (°C)
Pure PE	170	3	-114.2	-112.2
Pure PE	170	15	-110.8	-112.2
Pure PE	220	3	-111.5	-112.3
Pure PE	220	15	-111.9	-109.4
PE / EOC	170	3	-111.4	-111.9
PE / EOC	170	15	-112.9	-114.5
PE / EOC	220	3	-111.8	-110.2
PE / EOC	220	15	-112.8	-113.6
PE / ECB	170	3	-112.4	-111.6
PE / ECB	170	15	-111.4	-113.6
PE / ECB	220	3	-111.9	-113.2
PE / ECB	220	15	-113.1	-110.2

The DSC data, listed in Table 5.7, reveal that in each case the PE in the blends crystallises in much the same way as the pure PE, having essentially the same crystallinity and slightly lower melting point, regardless of the type of copolymer used, indicating the copolymer does not greatly affect the formation of crystals in the PE. Thus, there is little evidence for mixing of the constituent polymers at the molecular level in the solidified samples. The extensive branching of the copolymers preclude their incorporation into the linear PE crystals, although the copolymer may affect the PE crystalline melting point through its presence as an impurity in the polymer melt. The ECB in the solidified blends then must reside as very small phase separated domains of comparable size, or finer, than the fibrillar texture of the crystalline PE phase. These ECB-rich domains do not coarsen, or coarsen relatively slowly, during storage in the melt. The etched regions of EOC material are clearly visible for every processing condition and therefore always forms domains coarser in length-scale than the fibrillar texture of the PE crystalline phase. The inference is that

the EOC was present in phase separated EOC-rich droplets in the melt, whereupon cooling to room temperature they became frozen-in to the solid-state morphology. Moreover, the size of the EOC-rich regions are dependent on processing temperature, extrusion procedure, and storage time in the melt.

Table 5.7 Melting temperature and degree of crystallinity of polymer blends processed through single screw extrusion only, SS, or single screw and twin-screw extrusion, TS[a]

Sample	Barrel Temp. (^{o}C)	Compress. time (min)	Melting Temp. - SS (^{o}C)	Crystallinity - SS (wt%)	Melting Temp. - TS (^{o}C)	Crystallinity - TS (wt%)
Pure PE	170	3	132.1 (1.81)	61.8 (1.51)	133.3 (0.27)	61.9 (0.47)
Pure PE	170	15	132.1 (1.26)	63.2 (0.46)	133.7 (0.14)	62.4 (0.98)
Pure PE	220	3	133.3 (0.84)	61.8 (0.07)	133.1 (0.41)	61.4 (1.28)
Pure PE	220	15	133.0 (0.60)	62.6 (0.41)	132.3 (0.91)	61.8 (0.80)
PE / EOC	170	3	131.8 (0.74)	62.9 (0.10)	131.9 (0.67)	62.2 (0.73)
PE / EOC	170	15	131.3 (1.11)	60.2 (0.83)	131.2 (0.82)	61.1 (1.04)
PE / EOC	220	3	132.5 (1.39)	62.9 (0.49)	132.2 (1.40)	62.2 (0.73)
PE / EOC	220	15	131.4 (0.78)	60.8 (0.44)	131.3 (1.99)	61.1 (0.15)
PE / ECB	170	3	130.7 (0.47)	61.7 (0.33)	131.9 (0.25)	61.6 (0.26)
PE / ECB	170	15	131.5 (0.57)	61.5 (0.42)	131.4 (1.23)	61.2 (0.62)
PE / ECB	220	3	131.4 (0.43)	59.7 (0.30)	130.9 (1.02)	59.7 (1.05)
PE / ECB	220	15	130.7 (0.67)	60.5 (0.58)	131.2 (0.78)	61.0 (0.75)

[a]Numbers in parenthesis are the standard deviations.

5.4.2 Fracture toughness

The essential work of fracture was used to determine the fracture toughness of the compression-moulded samples. The specimens used in this instance were of the single edge notched-type to facilitate their use in the MiniMat tester whilst filming the fracture process. Images were recorded using a video camera attached to a microscope that was placed above the test bed of the MiniMat. Images at certain times were captured from the videotapes for image analysis. The dimensions of the images were calibrated using the image of a linear scale captured under the same magnification as the fracture images. Examples of the fracture images are displayed in Figure 5.27, for

the blends prepared under various processing conditions. In the figure, the micrographs on the left hand side are of the EOC containing material, labelled (a), (b) and (c), whilst those on the right hand side are the PE / ECB formulations, that is (d), (e) and (f).

In each case, the CTOD increases with the thickness of the original razor incision. It is at around 10 s when the distance x increases as the crack begins to propagate through the specimen. At this point, the material at the crack tip thins and turns white, indicating the onset of yielding. The crack tip typically opens to an angle of between 148 and 150°, as demonstrated in Figure 5.28. Ahead of the crack tip is a whitened area of material that appears more diffuse for the EOC containing specimens than for those containing ECB. Yielded area as a function of time is shown in Figure 5.29. The area of the whitened region increases more rapidly for the EOC containing samples. It may be that the dispersed domains of EOC-rich material cause greater delocalisation of the yielding process away from the crack tip, thereby altering the appearance of specimen as it fractures. For the ECB formulations, the elastomer is phases separated from the PE, as indicated by the DMTA data, but resides in domains that are of comparable size or smaller than the PE crystalline fibrils. Apparently, this results in less stress induced whitening of the PE upon yielding ahead of the crack tip. There were no visual differences between the appearances of the specimens that were prepared under different processing temperatures or moulding time; only the type of copolymer affected the fracture images, as exemplified in Figure 5.27. In the case of pure PE, the crack became blunted when tested in the Minimat using the single edge notched tension specimen, resulting in a tensile deformation of the ligament with no crack propagation. The data obtained for PE in these tests were therefore not meaningful.

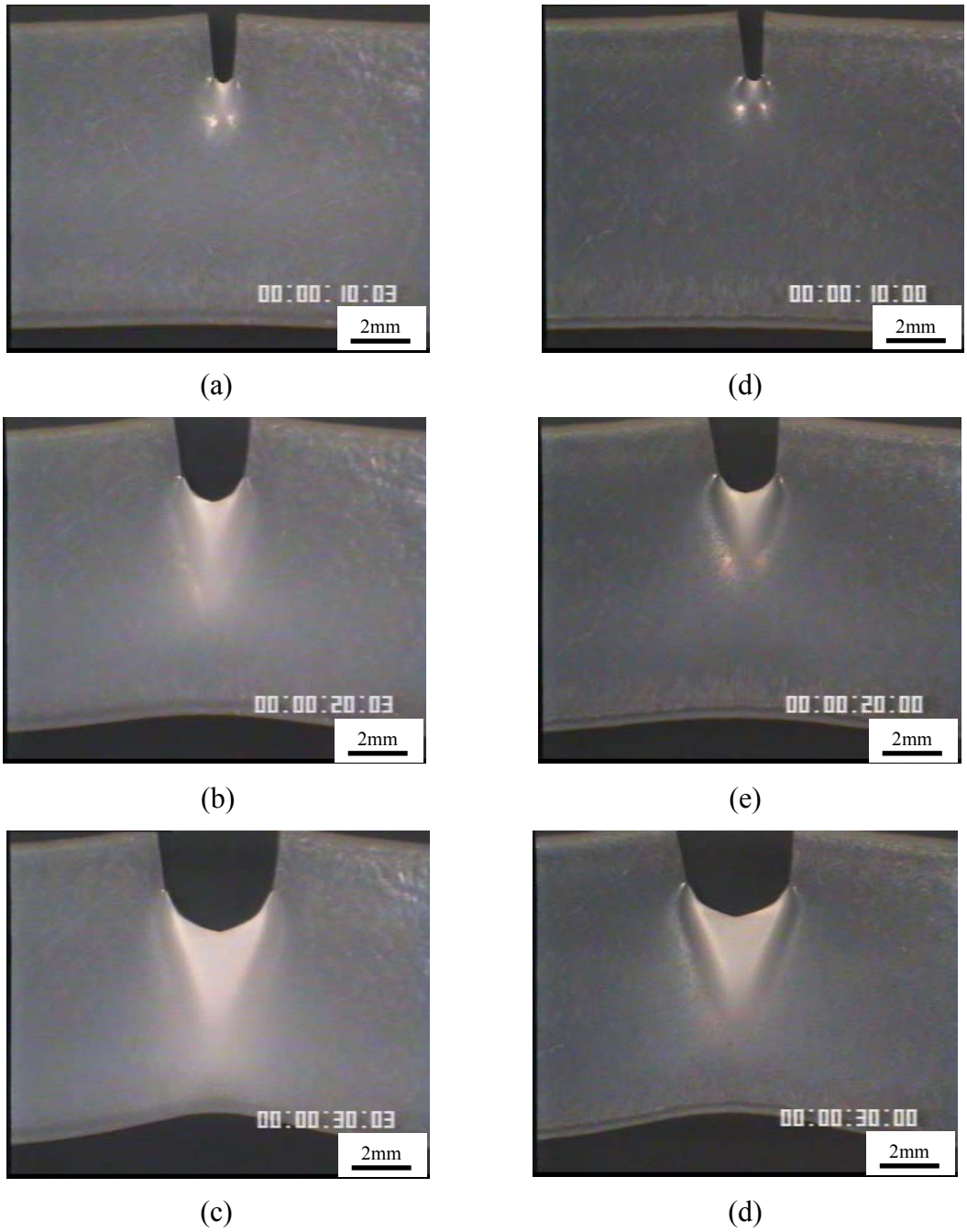

Figure 5.27 The video capture images of crack opening at various times for PE / EOC blends: (a), (b), and (c) and PE/ ECB blends: (d), (e), and (f). Both samples were extruded at barrel temperature 170^{o}C and compressed for 3 min.

From the Minimat tests upon the single edge notched tension specimens, the essential work of fracture was determined both as a function of ligament length and

test speed. Figure 5.30 contains typical essential work of fracture curves for the ECB and EOC containing materials for samples with various ligament lengths.

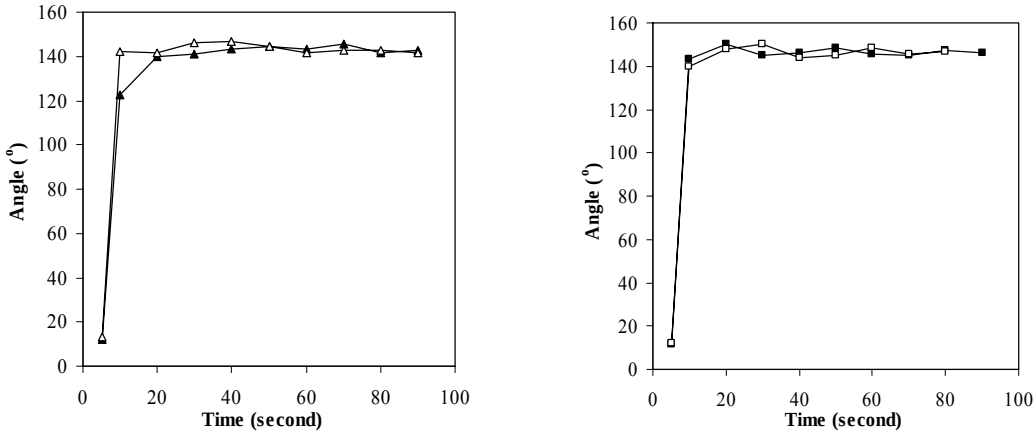

(a) (b)

Figure 5.28 Crack angle for blends extruded at 170°C: (a) EOC compounds moulded for (▲) 3 and (Δ) 15 min and (b) ECB compounds moulded for (■) 3 and (□) 15 min.

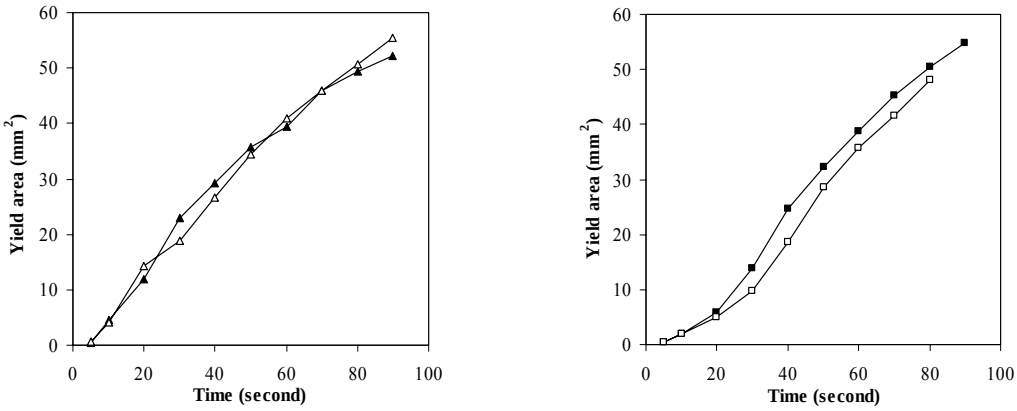

(a) (b)

Figure 5.29 Yield area for blends extruded 170°C: (a) EOC compounds moulded for (▲) 3 and (Δ) 15 min and (b) ECB compounds moulded for (■) 3 and (□) 15 min.

Essential work of fracture curves, determined as a function of test speed, are displayed in Figure 5.31.

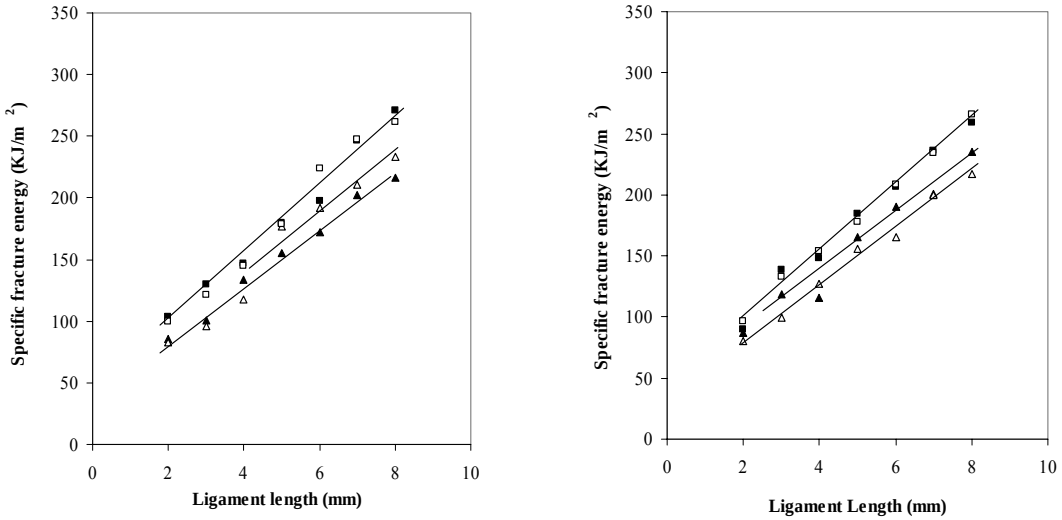

(a) (b)

Figure 5.30 Specific fracture energy for blends prepared using the single-screw extruder at (a) 170°C and (b) 230°C: ECB compounds moulded for (■) 3 and (□) 15 min and EOC compounds moulded for (▲) 3 and (Δ) 15 min.

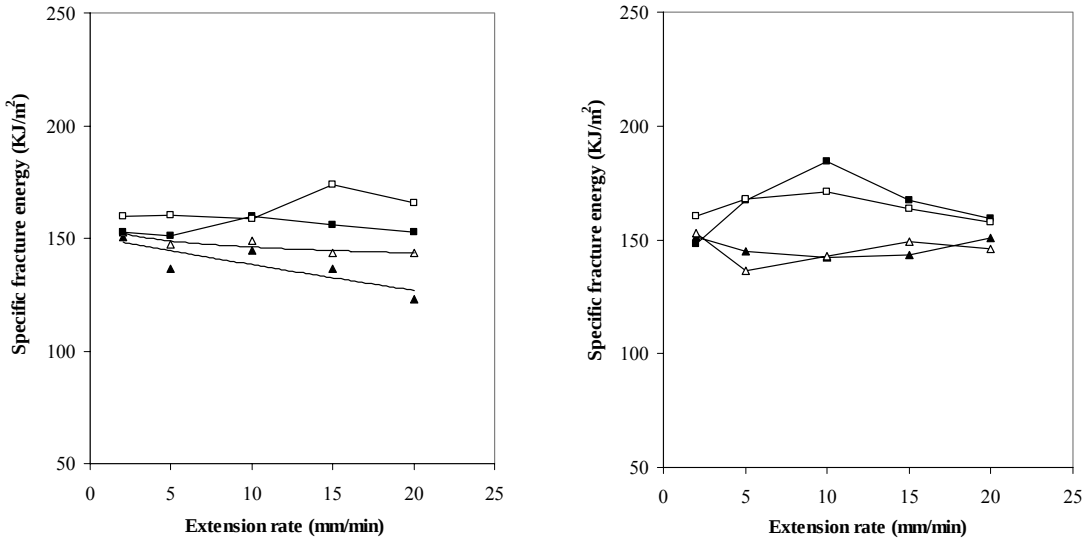

(a) (b)

Figure 5.31 Specific fracture energy for blends prepared using the single-screw extruder at (a) 170°C and (b) 230°C: ECB compounds moulded for (■) 3 and (□) 15 min and EOC compounds moulded for (▲) 3 and (Δ) 15 min.

The essential and non-essential work of fracture data, determined from varying the ligament length at constant test speed are summarised in Table 5.8 for the various formulations and processing conditions. In all cases, for every ligament length and test speed, the ECB containing samples had greater toughness than the PE / EOC materials.

Table 5.8 Essential work of fracture and non-essential work of fracture of polymer blends

Sample	Barrel Temp. (^oC)	Comp.time (minutes)	βw_p (kJm^{-3})	w_e (kJm^{-2})	βw_p (kJm^{-3})	w_e (kJm^{-2})
			Single Screw		Twin Screw	
PE / EOC	170	3	23	39	26	16
PE / EOC	170	15	27	24	25	30
PE / EOC	220	3	24	37	23	34
PE / EOC	220	15	23	33	24	32
PE / ECB	170	3	28	42	25	55
PE / ECB	170	15	29	37	26	55
PE / ECB	220	3	27	44	30	34
PE / ECB	220	15	27	44	26	44

Apparently, the microdispersion that results from the limited miscibility of EOC in the PE is less effective at toughening the matrix than the finer dispersion of the ECB-rich that is the result of greater melt-state compatibility between the PE and ECB in comparison with the PE / EOC compatibility. The fine length-scale morphology that is produced as the result of the greater compatibility of the components in the PE / ECB blend, in comparison with the compatibility in the PE / EOC system, provides greater plane stress fracture toughness in the sheet products. Moreover, the processing neither temperature nor the storage time in the melt had much effect upon the fracture toughness of the ECB formulations. This may be because the morphology was largely stable of the range of time and temperature used in sample preparation.

The dispersed domains of EOC-rich material confer relatively poorer fracture resistance, in comparison with the ECB. However, the larger dispersed EOC-domains,

which result from longer storage time in the melt or lower processing temperature, do tend to give slightly higher toughness than the smaller domains, as can be seen in Figure 5.30. There is, however, some scatter in the data when determining the essential work of fracture due to uncertainties in the extrapolation of the curves to zero ligament length.

CHAPTER 6
CONCLUSIONS

The thermomechanical history of polyolefin blends has a pronounced effect upon the morphology development, and therefore the physical properties of the materials. The effects of temperature and shear history differ depending upon the inherent mutual compatibility of the constituent polymers.

1. Melt flow during processing of the PE / EOC blend that is partial miscibility under quiescent conditions resulted in the formation of a fine length-scale morphology comprising intertwined PE lamellae and EOC domains. It may be inferred that the morphology resulted from the concurrent liquid-liquid and solid-liquid phase separation that occurred upon cessation of flow and cooling.

2. The PE / EOC system is partially miscible in the melt state, tending towards enhanced miscibility at higher temperatures. Moreover, prior processing conditions distinctly affect the domain coarsening in subsequent processing operations, even after up to six hours annealing in the melt-state under quiescent conditions. The complex, multi-layered phase morphology produced in the solid state during moulding, is the product of the partial miscibility in the melt state and the phase separation that takes place upon cooling and crystallisation. The resultant morphology has a marked bearing upon the toughness of the material under impact conditions at sub-ambient temperature. Coarser morphologies that are a consequence of higher elastomers contents and less compatibility of the blend components at lower temperature result in greater impact toughness at sub-ambient temperature.

3. The presence of the branched copolymer (EOC) affected the fracture of PE differently depending upon the state of the oriented test specimens. For crack

propagation in the TD, the orientation of the PE dominated the fracture process and hence the presence of EOC had little effect. For crack propagation in the MD, the branched copolymer increased the non-essential work of fracture, but had little effect upon the essential work of fracture.

4. The two types of branched copolymer investigated affect the fracture toughness of the PE / copolymer blends system. The influence of processing conditions upon the fracture toughness is dependent upon the mutual compatibility of the PE and the copolymer. The PE / ECB blend system has a finer length scale morphology that is a consequence of the greater compatibility than the PE / EOC blends system; the PE / ECB morphology is largely stable under the range of time and temperature used for specimen preparation. The consequence is that the PE / ECB blends is largely insensitive to melt processing conditions. The processing temperature and the storage time in the melt have little effect upon the morphology and fracture toughness of PE / ECB blends system, while these factors affect the morphology and fracture toughness of PE / EOC blends system because the domain morphology coarsens with decreasing processing temperature and increasing storage time in the melt.

It has been shown that the processing history has a pronounced effect upon the morphology development of polyolefin blends. The effects of shearing and temperature have a critical effect upon the morphology that forms through subsequent processes. Moreover, the key findings are that it is vital to understand the mechanism of morphology development since this has an important effect upon the morphology that is subsequently produced. This has particular relevance in polymer processing because polymer materials usually experience two to three stages of melt processing in the production of a finished article. Each step of the processing then must be considered to understand the morphology and properties of the finished article.

REFERENCES

1. Crist B. Comments on: Ambiguities in the interpretation of small angle neutron scattering from blends of linear and branched polyethylene. Polymer 1997;38(12): 3145-7.
2. Weimann PA, Jones TD, Hillmyer MA, Bates FS, Londono JD, Melnichenko Y, et al. Phase behaviour of isotactic polypropylene-poly(ethylene/ethylethylene) random copolymer blends. Macromolecules 1997;30(12):3650-7.
3. Rhee J, Crist B. Phase behaviour, morphology and mechanical properties of polyethylene-copolymer blends. J Polym Sci Polym Phys Ed 1994;32:159-69.
4. Olabisi O, Robeson LM, Shaw MT. Polymer-Polymer Miscibility. New York: Academic Press; 1979.
5. Chen ZJ, Wu RJ, Shaw MT, Weiss RA, Fernandez ML, Higgins JS. Rheo-optical behaviour of binary polymer blends: the effect of simple shear flow on phase behavior. Polym Eng and Sci 1995;35(1):92-9.
6. Horst R, Wolf BA. Phase diagrams calculated for sheared ternary polymer blends. Polymer 1997;38(18):4697-03.
7. Inoue T. Special seminar presentation at Mahidol University Thailand. December; (1998).
8. Higgins JS, Fruitwala H, Tomlins PE. Correlation of phase-separation behaviour in polymer blends with thermodynamic measurements in the one-phase region. Macromolecules 1989;22:3674-81.
9. Chen CY, Md W, Yunus ZW, Chiu HW, Kyu T. Phase separation behaviour in blends of isotactic polypropylene and ethylene-propylene diene terpolymer. Polymer 1997;38(17):4433-8.

10. Otsuka N, Yang Y, Saito H, Inoue T, Takemura Y. Phase behaviour and morphology development in a blend of isotactic polypropylene and hydrogenated poly(styrene-co-butadiene). Polymer 1998;39(8-9):1533- 8.
11. Hindawi IA, Higgins JS, Galambos AF, Weiss RA. Flow-induced mixing of blends of poly(ethylene-vinyl acetate) and solution chlorinated polyethylene. Macromolecules 1989;22:3674-81.
12. Kammer HW, Kummerloewe C, Kressler J, Melior JP. Shear-induced phase changes in polymer blends. Polymer 1991;32(8):1488-92.
13. Fernandez ML, Higgins JS, Richardson SM. Flow instabilities in polymer blends under shear. Polymer 1995;36(5):931-9.
14. Hindawi IA, Higgins JS, Wiss RA. Flow-induced mixing and demixing in polymer blends. Polymer 1992;33(12):2522-8.
15. Charrier JM. Polymer materials and processing : plastics, elastomers and composites. New York: Hanser Publishers; 1990.
16. McMillan FM. Polymer materials encyclopedia. United State of America: CRC Press Inc; 1996. p. 6424-6.
17. Ziegler K, Holzkamp E, Breil H, Martin H. The M.ovrddot.uhlheim low-pressure polyethylene process. Angew Chem (1955);67:541-7.
18. Pino P, Giannini U, Porri L. Encyclopedia of Polymer Science & Engineering, Ed.; Mark HF, Bikales NM, Overberger CG, Menges G, Kroschwitz SI. New York: Wiley; 1985. p. 147.
19. Pino P, Oschwald A, Ciardelli F, Carlini C, Chiellini E. In: Chien JCW, editor Coordination Polymerization of α-Olefins. New York: Elsevier;. p. 25,
20. Ultracki LA. Polymer alloys and blends: thermodynamics and rheology. New York: Vienna Hanser Publisher; 1989
21. Venables RA. Course note In: Polymer blends SCCH 665 Msc in Polymer Science. Mahidol University 1998.
22. Puig CC. On the cocrystallization phenomena in blends of high density polyethylene and low density polyethylene. Polymer Bulletin 1997;38:715-20.

23. Utracki LA, Dumoulin MM Editors. Polymer Topics Polyblends-1993 National Research Council Canada Industrial Materials Institute. Polym Eng Sci. 1995;35(1):128.
24. Kresge EN. Polymer Blends Ed.; Paul DR and Newman S. New York: Academic Press; 1978. p. 293-318.
25. Lohse DJ. The melt compatibility of blends of polypropylene and ethylene-propylene copolymers. Polym Eng and Sci 1986;26(21):1500-9.
26. Wignall GD, Child HR, Samuels RJ. Structural characterization of semicrystalline polymer blends by small-angle neutron scattering. Polymer (1982);23(7):957-64.
27. Barham PJ, Hill MJ, Keller A, Rosney CC. A phase separation in polyethylene melts. Journal of Materials Science Letters 1988;7(12):1271-5.
28. Mirabella FM Jr, Westphal SP, Fernando PL, Ford EA, Williams JG. Morphological explanation of the extraordinary fracture toughness of linear low-density polyethylenes. Journal of Polymer Science, Part B: Polymer Physics 1988;26(9):1995-2005.
29. Deblieck RAC, Mathot VBF. Morphology of heterogeneous ethylene-octene copolymers with very low densities (VLDPEs). Journal of Materials Science Letters (1988);7(12):1276-80.
30. Gedde UW. Polymer physics. London: Chapman & Hall; 1995.
31. Fredrickson GH, Liu AJ, Bates FS. Entropic corrections to the Flory-Huggins theory of polymer blends architectural and conformational effects. Macromolecules 1994;27:2503-11.
32. Bate FS, Schulz MF, Rosedale JH. Correlation of binary of binary polyolefin phase behaviour with statistical segment length asymmetry. Macromolecules 1992;25:5547-50.
33. Carriere CJ, Silvis HC. The effects of short-chain branching and comonomer type on the interfacial tension of polypropylene-polyolefin elastomer blends. J Appl Polym Sci 1997;66:1175-81.

34. Yamaguchi M, Miyata H, Nitta K. Compatibility of binary blends of polypropylene with ethylene-α-olefin copolymer. J Appl Polym Sci 1996;62:87-97.
35. Yamaguchi M; Nitta KH; Miyata H; Masuda T. Rheological properties for binary blends of i-PP and ethylene-1-hexene copolymer. J Appl Polym Sci 1997;63(4):467-74.
36. Chen CY, Md W, Yunus ZW, Chiu HW, Kyu T. Phase separation behaviour in blends of isotactic polypropylene and ethylene-propylene diene terpolymer.Polymer.1997;38(17):4433-38.
37. Yang Y, Otsuka N, Saito H, Inoue T, Takemura Y. Morphology and elastomeric properties of isotactic polypropylene / hydrogenated poly(styrene-co-butadiene) blends: a potential for a new thermoplastic elastomer. Polymer 1998;40(3):559-64.
38. Otsuka N, Yang Y, Saito H, Inoue T, Takemura Y. Phase behaviour and morphology development in a blend of isotactic polypropylene and hydrogenated poly(styrene-co-butadiene). Polymer 1998;39(8-9):1533-8.
39. Lee CH, Saito H, Inoue T. Morphology development in isotactic polypropylene / partially hydrogenated oligo(styrene-co-indene) blend. Macromolecules 1995;28(24):8096-101.
40. Mader D, Thomann Y, Suhm J, Mulhaup R. Influence of comonomer incorporation on morphology and thermal and mechanical properties of blends based upon isotactic metallocene-polypropene and random ethane / 1-butene copolymers. J Appl Polym Sci 1999;74(4):838-48.
41. Yamaguchi M. Effect of molecular structure in branched polyethylene on adhesion properties with polypropylene. J Appl Polym Sci (1998);70(3):457-63.
42. Morgan RL, Hill MJ, Barham PJ, Frye CJ. Liquid-liquid phase separation in ternary blends of linear polyethylene with two ethylene-butene copolymers. Polymer 1997;38(8):1903-09.

43. Graessley WW, Krishnamoorti R, Balsara NP, Fetters LJ, Lohse DJ, Schulz, DN, et al.. Effect of deuterium substitution on thermodynamic interactions in polymer blends. Macromolecules 1993;26(5):1137-43.
44. Rhee J, Crist B. Thermodynamics and phase separation in melt blends of polyethylene and model copolymers. Macromolecules 1991;24:5663-9.
45. Vanden ES, Mathot VBF, Koch MHJ, Reynaers H. Thermal behaviour and morphology of homogeneous ethylene-1-octene copolymers with high comonomer contents. Polymer 2000;41(13):4889-900.
46. Bensason S, Nazarenko S, Chum S, Hiltner A, Baer E. Elastomeric blends of homogeneous ethylene-octene copolymers. Polymer 1997;38(15):3913-9.
47. Miles IS, Rostami S. Multicomponent polymer systems. Great Britain: Longman Scientific & Technical; 1992.
48. Hindawi IA, Higgins JS, Wiss RA. Flow-induced mixing and demixing in polymer blends. Polymer 1992;33(12):2522-8.
49. Hindawi I, Higgins JS, Galambos AF, Wiess RA. Flow-induced mixing of blends of poly(ethylene-vinyl acetate) and solution chlorinated polyethylene. Macromolecule 1990;23:670-4.
50. Madbouly SA, Ohmomo M, Ougizawa T, Inoue T. Effect of the shear flow on the phase behaviour of polystyrene/ poly(vinyl methyl ether) blend. Polymer 1990;40:1465-72.
51. Madbouly SA, Ougizawa T, Inoue T. Phase behaviour under shear flow in PMMA/SAN blends effect of molecular weight and viscosity Macromolecules 1999;32:5631-6.
52. Katsaros JD, Malone MF, Winter HH. The effects of flow on miscibility in a blend of polystyrene and poly(vinyl methyl ether). Polym Eng and Sci 1989;29(20):1434-45.
53. Okamoto M, Inoue T. Phase separation mechanism and structure development in poly(butylene terepthalate) / polycarbonate blends. Polymer 1994;35(2):257-61.

54. Okamoto M, Shiomi K, Inoue T. LCST-type phase behaviour and structure development during melt processing in a polycarbonate / poly(styrene-co acrylinitrile) blend. Polymer 1995;36(1):87-91.
55. Sano H, Yui H, Li H, Inoue T. Regularly phase-separated structure in an injection-moulded blend of isotactic polypropylene and high density polypropylene. Polymer 1998;39(21):5265-7.
56. Yu TH, Wilkes GL. Orientation determination and morphological study of high density polyethylene (HDPE) extruded tubular films: effect of processing variables and molecular weight distribution. Polymer 1996;37(21):4675-87.
57. Godshall D, Wilkes G, Krishnaswamy RK, Sukhadia AM. Processing-structure-property investigation of blown HDPE films containing both machine and transverse direction oriented lamellar stacks. Polymer 2003;44(18):5397-06.
58. Mirabella FM Jr, Barley JS. Ostwald ripening in an immiscible hydrogenated polybutadiene and high-density polyethylene blend. Journal of Polymer Science, Part B: Polymer Physics 1994;32(13):2187-95.
59. Mirabella FM Jr. Phase separation and the kinetics of phase coarsening in commercial impact polypropylene copolymers. Journal of Polymer Science, Part B: Polymer Physics 1994;32(7):1205-15.
60. Hill MJ, Barham PJ. Ostwald ripening in polyethylene blends. Polymer 1995;36(17):3369-75.
61. Feng Y, Hay JN. Phase separation in a commercial block propylene-ethylene copolymer. Polymer 1998;39(21):5277-80.
62. Hesegawa H, Sakurai S, Takanka M, Hashimoto T. Small-angle neutron scattering studies on the miscibility of protonated polyisoprene/duterated polybutadiene blends. Macromolecules 1991;24:1813-19.
63. Tomura H, Saito H, Inoue T. Light scattering analysis of upper critical solution temperature behaviour in a poly(vinylidene fluoride) / poly(methyl methacrylate) blend. Macromolecules 1992;25:1611-4.
64. Svobode P, Kressler J, Chiba T, Inoue T. Light-scattering and TEM analyses of virtual upper critical solution temperature behavior in PCL/SAN blends. Macromolecules. 1994;27:1154-9.

65. Wignall GD, Londono JD, Lin JS, Alamo RG, Galandte MJ, Mandelkern L. Morphology of blends of linear and long chain branched polyethylene in the solid state: A study by SANS, SAXS, and DSC. Macromolecules 1995;28:3156-67.
66. Mirabella Jr FM, McFddin DC. Xe n.m.r. spectroscopic characterization of multiphase polypropylene copolymer. Polymer 1996;37(6):931-8.
67. Crist B, Nesarikar AR. Coarsening in polyethylene-copolymer blends Macromolecules 1995;28:890-6.
68. Rhee J, Crist B. Thermodynamics and phase separation in melt blends of polyethylene and model copolymers. Macromolecules 1991;24:5663-9.
69. Rana D, Kim HL, Kwag H, Rhee J, Cho K, Woo T, et al. Blends of ethylene 1 octene copolymer synthesized by Ziegler-Natta and metallocene catalysts. II Rheology and morphological behaviours. J Appl Polym Sci 2000;76:1950-64.
70. Wu J, Mai YW. The essential fracture work concept for toughness measurement of ductile polymers. Polym Eng Sci 1996;36(18) 2275-88.
71. Wells AA. Proc. Symposium on Crack propagation. Cranfield; 1961. p. 210.
72. Cotterell B, Reddel JK. The essential work of plane stress ductile fracture. International Journal of Fracture 1977;13(3):267-77.
73. Mai YW, Cotterell B. On the essential work of ductile fracture in polymers. International Journal of Fracture 1986;32(2):105-25.
74. Hashemi S. Plane-stress fracture of polycarbonate films. Journal of Materials Science 1993;28(22):6178-84.
75. Saleemi AS, Nairn JA. The plane-strain essential work of fracture as a measure of the fracture toughness of ductile polymers. Polym Eng Sci 1990;30(4):211-8.
76. Levita G, Parisi L, McLoughlin S. Essential work of fracture in polymer films. Journal of Materials Science 1996;31(6):1545-53.
77. Wildes G, Keskkula H, Paul DR. Fracture characterization of PC / ABS blends: effect of reactive compatibilization, ABS type and rubber concentration. Polymer 1999;40(25):7089-107.

78. Wu JS, Mai YW, Cotterell B. Fracture toughness and fracture mechanisms of poly(butylene terephthalate) / polycarbonate/impact modifier blend. Part I. Fracture properties. Journal of Materials Science 1993;28(12):3373-84.
79. Mai YW, Cotterell B. Effects of pre-strain on plane stress ductile fracture in α-brass. Journal of Materials Science 1980;15(9):2296-306.
80. Swei H, Crist B, Carr SH. The J integral fracture toughness and damage zone morphology in polyethylenes. Polymer 1991;32(8):1440-6.
81. Casellas JJ, Frontini PM, Carella JM. Fracture characterization of low-density polyethylenes by the essential work of fracture: changes induced by thermal treatments and testing temperature. J Appl Polym Sci 1999;74(4):781-96.
82. Pegoretti A, Marchi A, Ricco T. Determination of the fracture toughness of thermoformed polypropylene cups by the essential work method. Polym Eng Sci 1997;37(6):1045-52.
83. Yokoyama Y, Ricco T. Fracture toughness and material orientation of injection molded, rubber-modified polypropylene Application of essential work method. Plastics, Rubber and Composites Processing and Applications 1996;25(9):417-22.
84. Rhee J, Crist B. Phase behaviour, morphology, and mechanical properties of polyethylene-copolymer blends. Journal of Polymer Science, Part B: Polymer Physics 1994;32(1):159-69.
85. Morton-Jones, DH. Polymer Processing. London: Chapman and Hall; 1989. p. 71
86. Rauwendaal C. Polymer Extrusion: 2nd ed. Munich: Hanser Publishers; 1990. p. 181.
87. Nielson LE. Polymer rheology. New York: Marcel Dekker; 1977. p. 16.
88. Grulke EA. Polymer process engineering. New Jersey: PTR Prentice Hall; 1994. p. 577.
89. Bicerano J. Prediction of polymer properties. New York: Marcel Dekker; 1993. p. 286.
90. Bicerano J. Prediction of polymer properties. New York: Marcel Dekker; 1993. p. 66.
91. Crawford RJ. Plastics Engineering. 2nd ed. Oxford: Pergamon Press; 1987. p. 33.

92. Tabtiang A, Parchana B, Venables RA, Inoue T. Melt-flow-induced phase morphologies of a high-density polyethylene / poly(ethylene-co-1-octene) blend. Journal of Polymer Science, Part B: Polymer Physics 2001;39(3):380-9.
93. Stein RS. X-ray diffraction, birefringence and infrared dichroism of stretched polyethylene. II. Generalized uniaxial crystal orientation. Journal of Polymer Science 1958;31:327-34.
94. Samuels RJ. Structured polymer properties: the identification, interpretation, and application of crystalline polymer structure. New York: Wiley-Interscience; 1974.
95. Crawford RJ. Plastics Engineering: 2nd Ed. Oxford: Pergamon Press; 1987. p. 280.
96. Progelhof RC, Throne JL. Polymer engineering principles. Munich: Hanser Publishers; 1993. p. 129.
97. Dehoff RT. Quantitative microscopy. New York: McGraw-Hill; 1968. p. 131.
98. Wypych G. Fillers. Canada: ChemTec Publishing; 1993. p. 143.
99. Gedde UW. Polymer physics. London: Chapman and Hall; 1995. p. 21.
100. Rhee J, Crist B. Thermodynamics and phase separation in melt blends of polyethylene and model copolymers. Macromolecules. 1991;24:5663-9.
101. Olabisi O, Robeson LM, Shaw MT. Polymer-polymer miscibility. New York: Academic Press; 1979. p. 46.
102. Klein J, Fletcher DF, Lewis J. Dynamics of entangled star branched polymers. Faraday Symposia of the Chemical Society. 1983;18:159-71.
103. Bartels CR, Graessley WW, Crist B. Measurement of self-diffusion coefficient in polymer melts by a small-angle neutron scattering method. Journal of Polymer Science, Polymer Letters Edition 1983;21(6):495-9.
104. Voorhees PW. Ostwald ripening of two-phase mixtures. Annual Review of Materials Science 1992;22:197-215.
105. Ratke L, Voorhees PW. Growth and coarsening: Ripening in materials science. Berlin: Springer; 2002.

106. Mai YW, Cotterell B, Horlyck R, Vigna G. The essential work of plane stress ductile fracture of linear polyethylenes. Polym Eng and Sci 1987;27(11):804-9.
107. Hashemi S. Plane-stress fracture of polycarbonate films. Journal of Materials Science 1993;28(22):6178-84.
108. Chan WYF, Williams JG. Determination of the fracture toughness of polymeric films by the essential work method. Polymer 1994;35(8):1666-72.
109. Karger-Kocsis J, Czigany T. On the essential and non-essential work of fracture of biaxial-oriented filled PET film. Polymer 1996;37(12):2433-8.
110. Hashemi S. Fracture toughness evaluation of ductile polymeric films. Journal of Materials Science 1997;32(6):1563-73.
111. Wu J, Mai YW. The essential fracture work concept for toughness measurement of ductile polymers. Polym Eng Sci 1996;36(18):2275-88.
112. Maspoch ML, Santana OO, Grando J, Ferrer D, Martinez AB. The essential work of fracture of a thermoplastic elastomer. Polymer Bulletin (Berlin) 1997;39(2):249-55.
113. Karger-Kocsis J, Czigany T, Moskala EJ. Thickness dependence of work of fracture parameters of an amorphous copolyester. Polymer 1997;38(18):4587-93.
114. Karger-Kocsis J, Cziigany T, Moskala EJ. Deformation rate dependence of the essential and non-essential work of fracture parameters in an amorphous copolyester. Polymer 1998;39(17):3939-44.
115. Li WD, Li RKY, Tjong SC. Fracture toughness of elastomer-modified polypropylene. Polymer Testing 1998;16(6):563-74.

APPENDIX

APPENDIX A

X-ray Orientation function

The X-ray diffractogram of pure PE and PE / EOC sheet samples were obtained through WAXD studies.

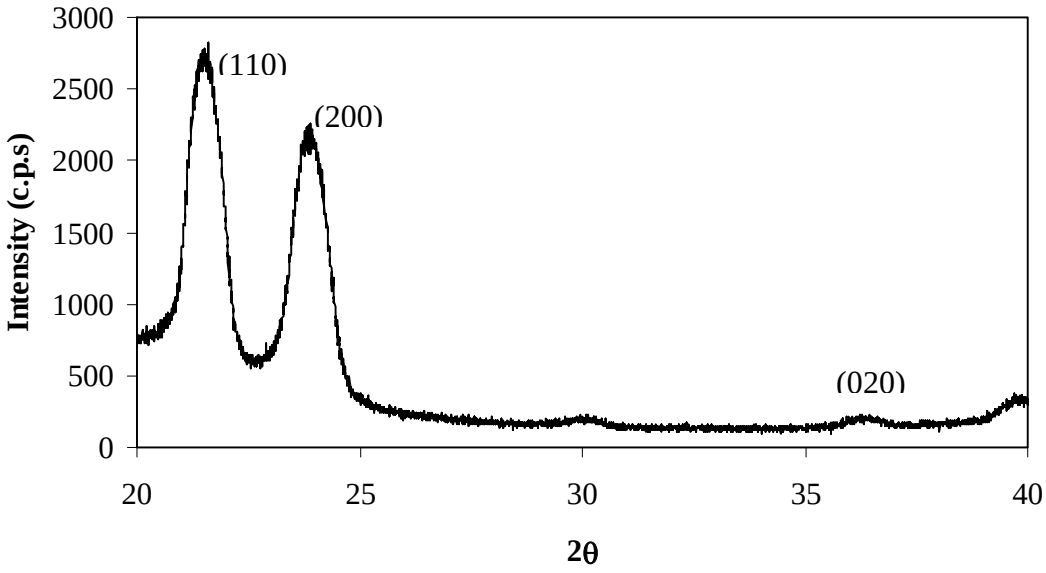

Figure A1 X-ray diffractogram of pure PE and PE /EOC sheet samples.

Table A1 Experimental and calculated data for determine orientation function of pure PE sheet samples at (200) crystal plane

Pure PE (200) crystal plane	Integration area of $I(\psi)\cos^2\psi \sin\psi$ (units)	Integration area of $I(\psi)\sin\psi$ (units)	$\cos^2\phi_{hkl}$
	51283.41	134685.73	0.3808
	49949.66	133234.46	0.3749
	52117.54	136974.26	0.3805
	51154.57	135923.56	0.3763
	52875.29	137404.46	0.3848
	49467.30	133004.81	0.3719

Table A2 Experimental and calculated data for determine orientation function of pure PE / EOC 5 vol% sheet samples at (200) crystal plane

PE / EOC 5 vol% (200) crystal plane	Integration area of $I(\psi)\cos^2\psi\sin\psi$ (units)	Integration area of $I(\psi)\sin\psi$ (units)	$\cos^2\phi_{hkl}$
	44839.07	112058.54	0.4001
	42994.63	108321.50	0.3969
	45778.04	113546.65	0.4032
	43363.18	109353.94	0.3965
	45160.03	112083.44	0.4029
	43425.26	108979.80	0.3985

Table A3 Experimental and calculated data for determine orientation function of pure PE / EOC 10 vol% sheet samples at (200) crystal plane

PE / EOC 10 vol% (200) crystal plane	Integration area of $I(\psi)\cos^2\psi\sin\psi$ (units)	Integration area of $I(\psi)\sin\psi$ (units)	$\cos^2\phi_{hkl}$
	41750.09	104456.61	0.3997
	41825.07	104553.12	0.4000
	43797.59	110740.04	0.3955
	43493.71	110427.65	0.3939
	43820.92	110379.88	0.3970
	43864.16	110536.14	0.3968

Table A4 Experimental and calculated data for determine orientation function of pure PE sheet samples at (020) crystal plane

Pure PE (020) crystal plane	Integration area of $I(\psi)\cos^2\psi\sin\psi$ (units)	Integration area of $I(\psi)\sin\psi$ (units)	$\cos^2\phi_{hkl}$
	27177.09	138037.40	0.1969
	28084.44	148566.63	0.1890
	27423.91	142489.96	0.1925
	27876.59	146703.42	0.1900
	26527.27	130290.94	0.2036
	29038.12	156321.33	0.1858

Table A5 Experimental and calculated data for determine orientation function of pure PE / EOC 5 vol% sheet samples at (020) crystal plane

PE / EOC 5 vol% (020) crystal plane	Integration area of $I(\psi)\cos^2\psi\sin\psi$ (units)	Integration area of $I(\psi)\sin\psi$ (units)	$\cos^2\phi_{hkl}$
	21532.46	118385.43	0.1819
	22541.00	129826.73	0.1736
	23472.12	129040.46	0.1819
	25126.55	145011.64	0.1733
	21523.09	120582.12	0.1785
	22459.62	128474.25	0.1748

Table A6 Experimental and calculated data for determine orientation function of pure PE / EOC 10 vol% sheet samples at (020) crystal plane

PE / EOC 10 vol% (020) crystal plane	Integration area of $I(\psi)\cos^2\psi\sin\psi$ (units)	Integration area of $I(\psi)\sin\psi$ (units)	$\cos^2\phi_{hkl}$
	22387.20	128874.27	0.1737
	22051.55	126020.79	0.1750
	23729.05	135602.77	0.1750
	23654.96	133243.26	0.1775
	23981.97	136594.91	0.1756
	23487.26	132933.71	0.1767

Table A7 Calculated data for determine orientation function of pure PE

Pure PE	$\cos^2\alpha$	$\cos^2\beta$	$\cos^2\varepsilon$	$f\alpha$	$f\beta$	$f\varepsilon$
	0.381	0.197	0.422	0.071	-0.205	0.134
	0.375	0.189	0.436	0.062	-0.216	0.154
	0.380	0.192	0.427	0.071	-0.211	0.141
	0.376	0.190	0.434	0.065	-0.215	0.150
	0.385	0.204	0.412	0.077	-0.195	0.117
	0.372	0.186	0.442	0.058	-0.221	0.163
Average	0.378	0.193	0.429	0.067	-0.211	0.143
Standard deaviation	0.005	0.006	0.011	0.007	0.010	0.016

Table A8 Calculated data for determine orientation function of PE / EOC 5 vol%

PE /EOC 5 vol%	$\cos^2\alpha$	$\cos^2\beta$	$\cos^2\varepsilon$	$f\alpha$	$f\beta$	$f\varepsilon$
	0.400	0.182	0.418	0.100	-0.227	0.127
	0.397	0.174	0.429	0.095	-0.240	0.144
	0.403	0.182	0.415	0.105	-0.227	0.122
	0.397	0.173	0.430	0.095	-0.240	0.145
	0.403	0.178	0.419	0.104	-0.232	0.128
	0.398	0.175	0.427	0.098	-0.238	0.140
Average	0.400	0.177	0.423	0.100	-0.234	0.134
Standard deaviation	0.003	0.004	0.007	0.004	0.006	0.010

Table A9 Calculated data for determine orientation function of PE / EOC 10 vol%

PE /EOC 10 vol%	$\cos^2\alpha$	$\cos^2\beta$	$\cos^2\varepsilon$	$f\alpha$	$f\beta$	$f\varepsilon$
	0.400	0.174	0.427	0.100	-0.239	0.140
	0.400	0.175	0.425	0.100	-0.238	0.137
	0.395	0.175	0.430	0.093	-0.238	0.144
	0.394	0.178	0.429	0.091	-0.234	0.143
	0.397	0.176	0.427	0.096	-0.237	0.141
	0.397	0.177	0.426	0.095	-0.235	0.140
Average	0.397	0.176	0.427	0.096	-0.237	0.141
Standard deaviation	0.002	0.001	0.002	0.004	0.002	0.002

APPENDIX B

DMA traces for pure PE, PE / EOC and PE / ECB blend samples at various processing conditions

Table B1 The DMA traces show the γ-relaxation in the samples processed by single screw extrusion at different barrel temperatures and compression times

Single screw extrusion only	
Barrel temperature 170°C	**Barrel temperature 220°C**
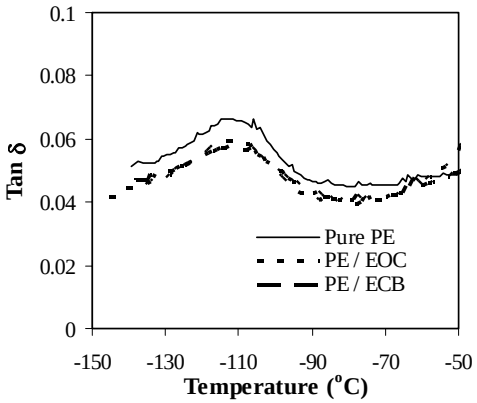	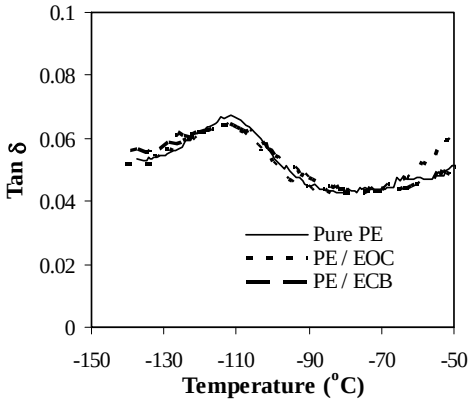
Compression time 3 minutes	Compression time 3 minutes
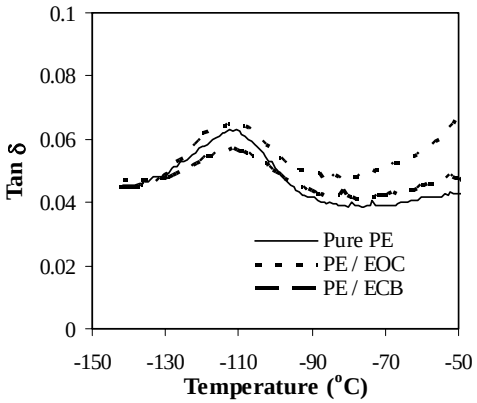	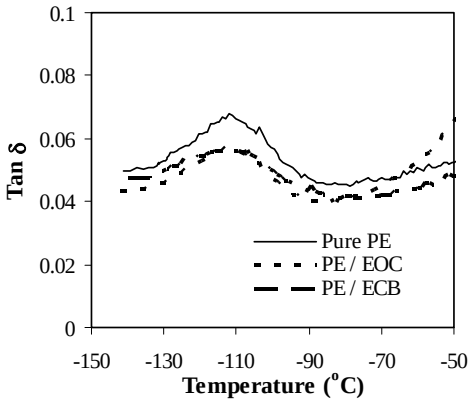
Compression time 15 minutes	Compression time 15 minutes

Table B2 The DMA traces show the γ-relaxation in the samples processed by both twin screw and single screw extrusion at different barrel temperatures and compression times

Twin screw extrusion and single screw extrusion	
Barrel temperature 170°C	**Barrel temperature 220°C**
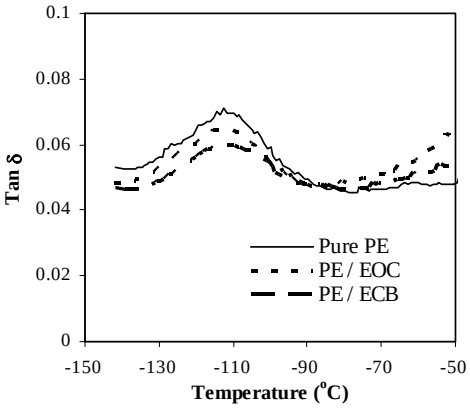	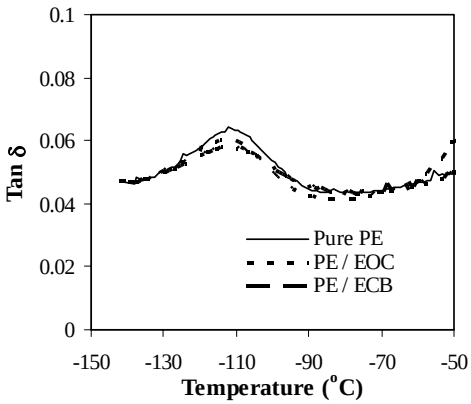
Compression time 3 minutes	Compression time 3 minutes
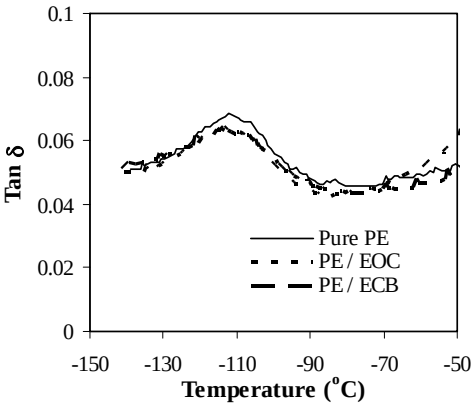	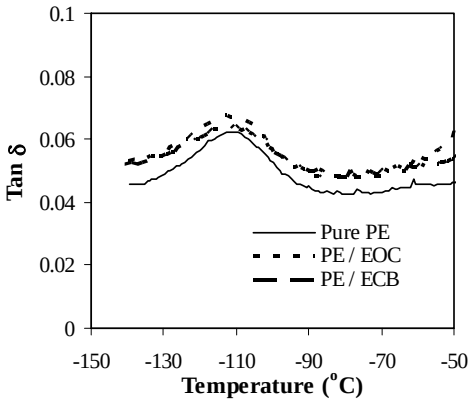
Compression time 15 minutes	Compression time 15 minutes

BIOGRAPHY

NAME Mr. Patcharapol Supatham

DATE OF BIRTH 8 February 1976

PLACE OF BIRTH Bangkok, Thailand

INSTITUTIONS ATTENED

Mahidol University, 1993-1997:
Bachelor of Science (Chemistry)

Mahidol University, 1998-2004:
Doctor of Philosophy (Polymer Science and Technology)

RESEARCH GRANTS

Young / New Scientist Development Scholarship,
Faculty of Science, Mahidol University;
2000-2001

Thailand Research Fund (TRF),
Golden Jubilee Ph.D. Program,
Grant No. PHD / 0179 / 2543;
2001-2004